Theoretical and Experimental Investigation of Solvatochromic and Photochromic Materials

By

Patrick Owen Harry Tuck

A thesis submitted to the Department of Chemistry in compliance with
the requirements for the degree Master of Science (Chemistry)

Lakehead

Thunder Bay, Ontario, Canada

December 2009

ABSTRACT

This thesis includes a study of solvatochromic molecules in the liquid and gas phases, and a study of photochromic molecules in the solid phase. The solvatochromic molecules studied are Nile Red, Betaine 30 and its penta tert-butyl substituted analog Betaine 45, 4-DMABN and its derivatives, as well as N-phenyl-benzohydroxamic acid and its derivatives. The photochromic molecule of study was the spiropyran molecule commonly known as $6\text{-}NO_2\text{-}BIPS$, which was investigated in polymer media.

Calculation of the change in electronic dipole moment from the ground to the first excited state of Nile Red was accomplished by experimental and theoretical methods. Nile Red possessed a structured absorption band with two maxima, which caused a dilemma as to which absorption maximum to pair with the emission maximum for the purpose of calculating Stokes Shift. For this reason, the average $\Delta\mu$ was found to be 2.38 D $\pm$ 0.76 D, when using an absorption maxima that red-shifts like the emission maxima, and 2.81 D $\pm$ 0.96 D when using a maxima that is stationary. A Configuration Interaction Singles (CIS) and Time-Dependent Density Functional Theory (TD-DFT) study using a polarized continuum solvent model to study the effects of solvation, geometry, excitations and their relationship with each other was also carried out. The calculated $\Delta\mu$ value from HF and CIS techniques was found to be 2.24 D in acetonitrile, which is comparable to that found from our experimental investigation.

A TD-DFT study using a polarizable continuum solvent model was perfomed on Betaine 30. Several correlation plots of the experimental vs. Theoretical E_T^N (our work)

were made and evaluated. It was found that TD-DFT excitation energies were overestimated in non-polar solvents and underestimated in the more polar solvents. The inclusion of explicit solvation was found to improve the plot of Experimental vs. Theoretical E_T^N such that a conversion equation

$$E_T^N{}_{\text{Experimental}} = (0.832)\, E_T^N{}_{\text{Theoretical}} + 0.029 \quad \text{with and } r_2 = .954 \text{ be made.}$$

A TD-DFT study on the first three excitation energies of 4-aminobenzontrile, 4-(N,N)-dimethylaminobenzontrile (DMABN), its ethyne analog (DMABE) and a fluorinated ethyne analog (DMABFE) was made to gain insight into why DMABN exhibits dual fluorescence while the others do not. The excited state energies were monitored indirectly using TD-DFT in gas phase and in cyclohexane and acetonitrile well as simulated in the solvents cyclohexane and acetonitrile. A lowering of the second lowest lying excited state was found to surpass the lowest lying excited state, which provides evidence that fluorescence could occur from two different states. A reversal of states was observed for one of the four molecules, as observed experimentally, but this rationale could not explain why Nile Red exhibits dual fluorescence.

A TD-DFT study of four *para-N*-substituted *N*-phenylbenzohydroxamic acids was carried out to determine the effects of substitution and solvation on conformation (cis/trans), absorption and pK_A. The study successfully characterized the effects of substitution, conformation, deprotonation and solvation on the excitation energies using TD-DFT. PK_A values were also reported, where the inclusion of explicit solvation was found to moderately improve them relative to experimental data.

A kinetic study on the ring-closure of 6-NO_2-BIPS to its colourless spiropyran form was studied in polystyrene, poly tert-butyl styrene, polymethyl methacrylate, poly n-butyl methacrylate, polyvinyl acetate and polycarbonate. Physical properties of the polymers such as glass transition temperature (T_g), free volume and polarity all affected the rate of decoloration. The T_g and free volume was also found to affect absorption maxima, causing a blue-shift to the λ_{max} of 6-NO_2-BIPs in polymers with lower T_g values and as polarity increased. The addition of the plasticizer dibutyl phthalate (DBP) to the polymer resulted in an increased decoloration rate by decreasing T_g. Several other plasticizers were investigated in polycarbonate exclusively and all were found to increase the rate of decoloration. However, a link between the structure of the plasticizer and its effect on the rate of discoloration could not be established.

Table of Contents

DEDICATED TO BODDINGTON, MY PET RABBIT (2001-2008)

ACKNOWLEDGEMENTS

List of Abbreviations

6-NO$_2$-BIPS:1',3'-Dihydro-1',3',3'-trimethyl-6-nitrospiro[2*H*-1-benzopyran-2,2'-(2*H*)-indole]

AcN: Acetonitrile

B3LYP: Becke 3-parameter Exchange-Correlation Functional with the Lee, Yang and Parr Correlation functional

B-O: Born-Oppenheimer

BzBP: Benzyl Butyl Phthalate

CIS: Configuration Interaction Singles

CT: Charge Transfer

DBP: Dibutyl Phthalate:

DE: Dielectric Enrichment

DEA: Diethyl Adipate

DEP: Diethyl Phthalate

DFT: Density Functional Theory

DMABN: 4-(N, N)-Dimethylaminobenzonitrile

DMP: Dimethyl Phthalate

Dn-OP: Di-n-octyl-phthalate

EtOAc: Ethyl Acetate

EtOH: Ethanol

GTO: Gaussian Type Orbital

-H: Hydrogen as Substituent (unsubstituted)

HA: Hydroxamic Acid functional group

HF: Hartree-Fock

HOMO: Highest Occupied Molecular Orbital

HOMO-n: Occupied Molecular Orbital that is n Orbitals lower in Energy than the HOMO

KS: Kohn-Sham

lbs: Large Basis Set [6-311++(d,p)] in Chapters 4 and 6, [6-311++(fd,2p)] for Chapter 7

LE: Locally Excited

LSDA: Local Spin Density Approximation

LUMO: Lowest Unoccupied Molecular Orbital

LUMO+n: Unoccupied Molecular Orbital that is N Orbitals Higher in Energy from the LUMO

MC: Merocyanine

-Me: Methyl as Substituent

MeOH: Methanol

MP: Moller-Plesset

-NO$_2$: Nitro as Substituent

NR: Nile Red

-OMe: Methoxy as Substituent

PBE0: Perdew, Burke and Erzenhoff Zero-parameter Hybrid Exchange-Correlation Functional

PBHA: *N*-phenylbenzohydroxamic Acid

PC: Polycarbonate

PCM: Polarizable Continuum Model

PICT: Planarized Intramolecular Charge Transfer

PMMA: Polymethyl Methacrylate

Pn-BMA: Poly n-butyl Methacrylate

PS: Polystyrene

PTBS: Poly tert-butyl Styrene

PVAc: Polyvinyl Acetate

RICT: Rehybridization Intramolecular Charge Transfer

SAS: Solvent-Accessible Surface

sbs: Small basis set [(6-31+G(d)]

SCF: Self-Consistent Field

SES: Solvent-Excluding Surface

SP: Spiroyran

STO: Slater Type Orbital

TD-DFT: Time-Dependent Density Functional Theory

TICT: Twisted Intramolecular Charge Transfer

TMS: Tetramethylsilane

WICT: Wagging Intramolecular Charge Transfer

List of Tables

Note

The architecture of this thesis is different from a traditional thesis. Chapters 3 through 8 are presented in the format of manuscripts that have or will be submitted to peer-reviewed journals. For this reason each of these chapters possesses their own abstract, introduction and references. Hopefully, the redundancies between these chapters do not cause any difficulty in the overall readability in the thesis.

Chapter 1

General Introduction

1.1 Solvatochromism and Photochromism

In condensed media, the absorption and emission spectra of a molecule may change as a consequence of its chemical surrounding, temperature, pressure or an external electric field.[1] A general term for the study of these external factors is perichromism, in which *peri* is from the Greek meaning "around". When molecules absorb and/or emit in the visible region, the effects of perichromism can be quite colorful. For example, a color dye may appear green in cyclohexane, purple in methanol and blue in water. Since the changes in absorption and emission spectra are due to changing the chemical surrounding of the dye, this phenomenon is known as solvatochromism. The largest theme that encompasses every chapter of this thesis is the study of the chemical environment (perichromism) on the electronic spectra of solute molecules.

Solvatochromism is the effect of a solvent on the electronic transition between the ground state and an excited state of a solute molecule. To account for this, two pieces of information are required. The first piece of information is the character of the solvent, which can be described by geometry, point dipole charge, polarizability, density and hydrogen bonding ability. The second is the character of the ground and excited states, which allows for the understanding of the nature of the transition occurring (eg. $\pi^* \leftarrow \pi$ or $\pi^* \leftarrow n$). However, often discrepancies in the characterization of the excited state or the type of transition are reported in the literature. Such is the case for the molecules studied in this thesis, in which large discrepancies regarding the description

of the excited state exist, or no known description has been reported. The main purpose of this thesis is to elucidate the properties of the excited state, with emphasis on the dipole moment, since it is the main contributor to non-specific interactions between solute and solvent and can drastically change the transition energy. However, the possibility of polarizability and hydrogen bonding is considered.

Nile Red is the first molecule of study and has been pursued since it was first developed and studied in 1985.[2] Nile Red is a fluorescent dye which has absorption and emission spectra that red-shift with increasing the surrounding polarity. For this reason it has been a valuable probe for lipid environments, such as cellular membranes using fluorescence microscopy.[3-7] Another feature of Nile Red is that it exhibits dual fluorescence, which is in contradiction to Kasha's rule, which states that only one emission maximum is observed because all excitations relax non-radiatively to the lowest lying excited state before fluorescing back to the ground state.[8] Nile Red also possesses two excitation maxima, but whether these transitions are between two separate electronic states, vibronic in nature, or arise due to two conformers in equilibrium remains unclear.

Betaine 30 could be considered the prime example of solvatochromism. The difference in vector magnitude of the dipole moment between the ground (15 Debye) and its first excited state (-6D) is 9 D, which makes it extremely sensitive to the polarity of a solvent.[9] The consequences of this sensitivity can be seen in the color of the various solutions of Betaine 30; red in methanol, violet in ethanol, green in acetone and yellow

in anisole.[10] For this reason, the transition energy of Betaine 30 has been determined in over 400 solvents, and an empirical solvent polarity scale has been developed. However, although the excited state dipole moment has been determined experimentally and theoretically,[11] no TD-DFT investigation of the excitation of Betaine 30 has been done. Its sheer size makes it expensive in terms of computer time.

4-(N,N)-Dimethylaminobenzonitrile was the first molecule found to exhibit dual emission (like Nile Red) from two low lying excited states states.[12] It has been studied rigorously both experimentally and theoretically. Thus far the best explanation for dual fluorescence is that there are two low lying excited states close in energy from which transitions can occur. These two excited states possess different geometries and charge distributions, as one excitation has a large charge transfer associated with its transition while the other does not. At this point in time, neither of these excited states has been described with confidence regarding their geometries or their excited state dipole moments. Another interesting fact is that dual fluorescence is not observed for 4-aminobenzonitrile or 4-dimethylaminobenzoethyne, which raises questions as to what role substitution, geometry and solvent play in dual fluorescence.[13-16]

N-phenylbenzohydroxamic acids (PBHAs) have excellent chelating ability in basic media.[17-19] PBHAs also have a high barrier of rotation around the C-N bond, and therefore an equilibrium between *cis* and *trans* conformers exists.[18, 20-22] The *trans* conformer shows significantly different absorption spectra in solution from the *cis*, which makes it a powerful tool for identification. In solution where the *trans*

conformation is the dominant species for the unsubstituted N-phenylbenzohydroxamic acids as determined experimentally by UV/VIS spectroscopy. To our knowledge, no study on the effects of solvation and substitution on the electronic spectra of *para-N*-substituted *N*-phenylbenzohydroxamic acids have been done.

The chapter regarding the photochromic molecule 1',3'-Dihydro-1',3',3'-trimethyl-6-nitrospiro[2*H*-1-benzopyran-2,2'-(2*H*)-indole], commonly named 6-NO$_2$-BIPS , deserves its own section. 6-NO$_2$-BIPS is a photochromic molecule as it can undergo photochemically, a reversible ring-opening reaction from one chemical structure to another. The ring-closed species is a spiropyran, while the ring open species is a merocyanine. The spiro bond breaks (by light) to form a structure with two full charges (zwitterionic) separated by conjugation.[23,24] The two species are significantly different in structure, thus their absorption spectra are also significantly different. The spiropyran structure absorbs in the ultraviolet and the merocyanine absorbs in the visible. For this reason, 6-NO$_2$-BIPS is a viable molecular switch, can be used for optical storage, and can be made into optical lenses as reading eye glasses or sunglasses.[25] The downside of 6-NO$_2$-BIPS is that it has poor fatigue resistance and a slow rate of ring-closure. The problem of fatigue resistance has been researched and improved by making the photochromic molecule a pendant group on the the polymer backbone.[26] However, the slow rate of ring-closure remains a problem. For example, several conformers of the ring-open MC exist. In addition, ring-closure is more inhibited by the polymer matrix due to restricted motions. Therefore the physical properties of the polymer matrices

5

surrounding the merocyanine play an important role. Chapter 8 relates the effects of physical properties of polymers on the ring closure kinetics of merocyanine.

1.2 References

1 P. Suppan and N. Ghoneim, *Solvatochromism*, Royal Society of Chemistry, Cambridge, 1997

2 P. Greenspan and S. D. Fowler, *J. of Lipid Research*, 1985, 26, 781-789

3 J. T. Hjelle, B. T. Golinska, D. C. Waters, K. R. Steidley, D. R. McCarroll, T. Pavlina, S. L. Smith, J. K. Lloyd and J. W. Dobbie, *Peritoneal Dialysis International*, 1991, 11, 207-212

4 K. Liu, T. G. Maddaford, B. Ramjiawan, M. J. B. Kutryk and G. N. Pierce, *Molecular and Cellular Biochemistry*, 1991, 108, 39-48

5 P. Greenspan and R. L. Gutman, *Electrophoresis*, 1993, 14, 65-68

6 L. L. Castell and R. Mann, *Aquaculture*, 1994, 119, 89-100

7 P. M. Gocze and D. A. Freeman, *Cytometry*, 1994, 17, 151-158

8 M. Kasha, *Discuss. Faraday Soc.*, 1950, 9, 14

9 E. Lippert, *Z. Naturforschung*, 1955, 10A, 541

10 C. Reichardt, *Solvents and Solvent Effects in Organic Chemistry*, WILEY-WCH, Weinheim, 2003

11 P. G. Jasien and L. L. Weber, *J. of Mol. Structure: THEOCHEM* , 2001, 572, 203-212

12 E. Lippert, W. Luder and H. Boos, Advances in Molecular Spectroscopy

13 K. A. Zachariasse, T. Vonderhaar, A. Hebecker, U. Leinhos and W. Kuhnle, *Pure and Applied Chemistry*, 1993, 65, 1745-1750

14 K. A. Zachariasse, M. Grobys, T. vonderHaar, A. Hebecker, Y. V. Ilichev, O. Morawski, I. Ruckert and W. Kuhnle, *J. of Photochem: A*, 1997, 105, 373-383

15 W. Rettig and B. Zietz, *Chem. Phys. Lett.*, 2000, 317, 187-196

16 Z. R. Grabowski, K. Rotkiewicz and W. Rettig, *Chem. Rev.*, 2003, 103, 3899-4031

17 D. A. Brown and M. V. Chidambaram, *Metal Ions in Biological systems*, Marcel Dekker, New York, 1982

18 H. Kehl, *Chemistry and Biology of Hydroxamic Acids*, S. Karger AG, New York, 1982

19 Y. K. Agrawal and S. G. Tandon, *J. of Inorganic and Nuclear Chemistry*, 1974, 36, 869-873

20 D. P. Dissanayake and R. Senthilnithy, *J. of Mol. Structure: THEOCHEM*, 2009, 910, 93-98

21 R. Senthilnithy, H. D. Gunawardhana, M. D. P. De Costa and D. P. Dissanayake, *J. of Mol. Structure: THEOCHEM*, 2006, 761, 21-26

22 A. Niño, C. Muñoz-Caro and M. L. Senent, *J. of Mol. Structure: THEOCHEM*, 2000, 530, 291-300

23 E. Fischer and Y. Hirschberg, *J. Am. Chem. Soc.*, 1952, 4522

24 H. Durr and H. Bouas-Laurent, *Photochromism: Molecules and Systems*, Elsevier, Amsterdam, 2003

25 B. Lukyanov and M. Lukyanova, *Chem. Hetero. Comp.*, 2005, 41, 281-311

26 A. Radu, R. Byrne, N. Alhashimy, M. Fusaro, S. Scarmagnani and D. Diamond, *J. of Photochem: A*, 2009, 206, 109-115

Chapter 2

Methods

2.1 UV/VIS Spectroscopy

Spectroscopy allows one to study the transitions in a molecule due to the interactions with electromagnetic radiation whether it be absorption, emission or scattering. Electronic transitions require a considerable amount of energy and are typically found in the ultraviolet to visible range of the spectrum. UV/VIS spectroscopy studies the electronic transitions of a molecule from the ground to excited states.[1]

A spectrometer consists of four essential parts: the light source, monochromator, sample holder, and the detector. In this thesis, the spectrometer used was a Perkin Elmer Lambda 11 spectrometer. Details regarding these four essential parts will be given.

The light source of the spectrometer consisted of two separate lamps. The first lamp is a tungsten-halogen lamp which radiates in the visible region and the second lamp is a deuterium lamp which emits in the ultraviolet region. However, scanning the sample without filtering the light can only give you the absorption in reference to a blank, since the detector is non-specific to the wavelength of incoming light. Therefore to get more information, such as λ_{max}, the wavelength-dependence absorption is required. For this a monochromator is required.

A monochromator possesses a diffraction grating that diffracts the light of different wavelengths into different directions, so that only light of a selected wavelength passes through the sample. The selected wavelength can then go on

through the sample and to the detector. The bandpass (accuracy) of this instrument was 2nm.

Solution samples used for Chapter 3 were always carried out in 1 cm x 1 cm x 4 cm high quartz crystal cuvette, positioned in a fashion so that the pathlength was 1 cm. Both glass and plastic cuvettes were unsuitable because both absorb light in the near UV range. In addition, the solvents used may damage the integrity of a plastic cuvette. For Chapter 8 measuring the absorbance of 6-NO$_2$-BIPS in polymer media, a special sample holder was designed to hold polymer thin films on quartz slides that possess the same wall thickness as a regular quartz cuvette.

The detector was a non-specific photomultiplier tube that will detect any light that hits it. No adjustments were made to this part of the instrument.

2.2 Fluorescence Spectroscopy

Fluorescence spectroscopy is almost the same technique as UV/VIS spectroscopy. UV/VIS spectroscopy measures the excitation energy from the ground to the excited state, while fluorescence spectroscopy measures the energy change from a relaxed excited state to the ground state. The major differences between the two techniques are detailed hereunder[1].

The instrument used for excitation and emission spectra was a Perkin Elmer LB-50 luminescence spectrometer. The luminescence spectrometer (fluorometer) is similar to a UV/VIS spectrometer in the sense that it possesses a light source, a sample and a

detector. However there are some key differences between the two instruments. For one, rather than two light sources, only a Xenon Arc (discharge) is used. Secondly, the detector is set at a ninety degree angle to prevent interference between the unabsorbed light and the emitted light. A final difference is that a second diffraction grating monochromator (the "emission") is placed between the sample and the detector. The second monochromator allows for the determination of the emission maximum. This is done by having the first monochromator isolate the excitation wavelength and hold it constant while the second emission monochromator is used to scan through the wavelengths.

This technique was used in chapters 3 and 4 for determining the excitation and emission maxima of Nile Red in binary solvent mixtures.

2.3 Computational Methods

Electronic transitions (absorption and emission) can also be studied computationally by *ab initio* methods. *Ab initio* means no empirical data is necessary. These techniques include Hartree-Fock(HF), Møller-Plesset (MP) and Density Functional(DFT) theories[2]. These theories are powerful, with the ability to compute an eigenfunction, for which physical observables can be extracted. The solvation shell of a molecule can be studied using the polarizable continuum model. HF is used in chapter 4 of this thesis, while DFT is used in chapters 4-7. All calculations were made using the Gaussian software G03 and G09.[3,4] In this section, the theory and underlying assumptions of computational chemistry are discussed.

$$\hat{H}\psi=E\psi \tag{2-1}$$

The energy of a molecule can be determined from the Schrodinger equation (2-1), where the Hamiltonian operator $\hat{H}$ extracts the energy from the eigenfunction known as the wavefunction. The usual Hamiltonian operator is comprised of 5 terms (Equation 2-2), accounting for the sum of kinetic and potential energies of each subatomic particle in the molecule. These terms include two kinetic energy terms (one for nuclei, one for electrons) and three potential (interaction) energy terms. While there is an exact solution for the Schrödinger equation of the hydrogen atom, such is not the case for a molecule. There is no exact solution for three or more particles in motion. Thus a number of assumptions need to be used.

2.3.1 Born -Oppenheimer approximation

$$\hat{H} = \sum_i \frac{\hbar^2}{2m_e} \nabla_i^2 - \sum_k \frac{\hbar^2}{2m_k} \nabla_k^2 - \sum_i \sum_k \frac{e^2 Z_k}{r_{ik}} \nabla_k^2 + \sum_{i<j} \frac{e^2}{r_{ij}} + \sum_{k<l} \frac{e^2 Z_k Z_l}{r_{kl}} \tag{2-2}$$

To solve the many-body problems, the nuclei are assumed to be stationary. The consequence is the removal of the term corresponding to nuclear kinetic motion while the term corresponding to nuclear-nuclear repulsion becomes a constant. This assumption is known as the Born-Oppenheimer approximation, and still allows one to solve the Schrodinger with integrity. Nuclear motion is considerably slower than that of electrons (a proton or neutron is 1800 times more massive than an electron).

The Born-Oppenheimer (B-O) approximation allows computational chemistry to associate energy with molecular structure. The B-O approximation also leads to the

concept of a potential energy surface (PES), where the energy is plotted against the nuclear geometry of a molecule. It is the B-O approximation which allows a "search" for molecular geometries of low energy, a process referred to as geometry optimization. The molecular geometries that are lowest in energy are the most important since they will be the most abundant (a Boltzmann distribution) and can then be useful for predicting physical properties such as equilibrium constants, like pK_A.

A geometry optimization in computational chemistry requires three pieces of information. These are: a first guess at the nuclear geometery, the number of electrons (i.e. charge) and the multiplicity. From the information provided, the energy (E) and first derivative of the energy with respect to the nuclear geometry ($\delta E/\delta R$) can be calculated. A slight geometry change is then administered to the molecule, at which point E and $\delta E/\delta R$ are calculated again. The energy is dependent on many geometric degrees of freedom, and an algorithm facilitates geometry optimization. The most common algorithm is the Berny algorithm, and it uses the forces acting on the atoms and the second derivative of the energy to predict what geometrical change will result in a lowering of the energy. The algorithm continues to change the geometry until $\delta E/\delta R$ becomes close to zero and the geometry is a stationary point.[2] A stationary point that increases in energy as a result of any geometry change is a local minimum. Furthermore, of these minima, the one that is the lowest in energy is the absolute minimum. A stationary point that is a maximum along a geometric coordinate that separates two minima is a saddle point (transition state).

2.3.2 The Mean-Field Approximation and the Hartree-Fock Self Consistent Field (HF-SCF) Method

Another problem is the electron-electron repulsion term in equation (2-2), and a second approximation is required. This problem is overcome by assuming that each electron is described by a one electron function (orbital). This assumption is a mean-field approximation because each electron "feels" the average of electrons. A negative consequence of invoking this mean field approximation is that HF theory completely neglects instantaneous electron-electron interactions. However, a positive consequence is that one can find the energies of each molecular orbital (ϕ_i). The molecular orbital is described as a linear combination of atomic orbitals (equation 2-3). These atomic orbitals are basis functions (χ_r), and are desbribed in more detail in section 2.3.4. The molecular orbital is defined as a sum of all basis functions weighted by coefficients c_{ri} such that the contribution of each basis function may vary.

$$\phi_i = \Sigma_r c_{ri} \chi_r \tag{2-3}$$

The values of these coefficients that weight each basis function are unknown and are solved by the self consistent field (SCF) method. The SCF method uses the variational principle, which states that the calculated energy will always be higher than the exact energy, and allows one to get the coefficients from the Roothan matrix equation:

$$FC = SC\varepsilon \tag{2-4}$$

14

Where F is the Fock matrix, C is the coefficient matrix, S is the overlap matrix and ε is the energy. The Fock Matrix elements are obtained from the Fock operator. For example, the Fock matrix elements are obtained from the basis functions r and s:

$$F_{rs} = \langle \chi_r | \hat{F} | \chi_s \rangle \qquad (2\text{-}5)$$

where $\hat{F}$ is the one-electron Fock operator:

$$\hat{F}(1) = \hat{H}^{core} + \sum_{j=1}^{n}(2\langle \chi_r(1) | \hat{J} | \chi_s(1) \rangle - \langle \chi_r(1) | \hat{K} | \chi_s(1) \rangle) \qquad (2\text{-}6)$$

Where $\hat{H}^{core}$ is the one electron core Hamiltonian for basis functions r and s:

$$\hat{H}^{core}(1) = -\frac{1}{2}\nabla_{(1)}^2 - \sum_{nuclei} \frac{Z_{nuclei}}{r_{(1)nuclei}} \qquad (2\text{-}7)$$

and $\hat{J}$ and $\hat{K}$ are the coulomb and exchange operators, respectively. These operators then operate on an arbitrary function f(1) and lead to equations (2-10) and (2-11):

$$\hat{J}(1)f(1) = f(1) \int |\phi_j(2)|^2 \frac{1}{r_{12}} dv_2$$

$$\hat{K}(1)f(1) = f(1) \int \frac{\phi_j(2)f(2)}{r_{12}} dv_2$$

$$\langle \chi_r(1) | \hat{J} | \chi_s(1) \rangle = \sum_{t=1}^{b}\sum_{u=1}^{b} c_{tj}^* c_{uj}(rs|tu) \qquad (2\text{-}10)$$

$$\langle \chi_r(1) | \hat{K} | \chi_s(1) \rangle = \sum_{t=1}^{b}\sum_{u=1}^{b} c_{tj}^* c_{uj}(ru|ts) \qquad (2\text{-}11)$$

where (rs|tu) is the 2-electron repulsion integral,

$$(rs|tu) = \frac{\int\int \chi_r^*(1)\chi_s(1)\chi_t^*(2)\chi_u(2)}{r_{12}} dv_1 dv_2 \qquad (2\text{-}12)$$

$(ru|ts)$ is a similar repulsion integral, but with basis functions u and s exchanged. When you substitute equations (2-10) and (2-11) into (2-6) you get equation (2-13), which is more practical for carrying out the SCF method.

$$F_{rs} = H_{rs}^{core} + \sum_{t=1}^{b}\sum_{u=1}^{b} P_{tu}\left[(rs|tu) - \frac{1}{2}(ru|ts)\right] \qquad (2\text{-}13)$$

P_{tu} are the density matrix elements that are obtained from the coefficients:

$$P_{tu} \equiv 2\sum_{j=1}^{n/2} c_{tj}^* c_{uj} \qquad (2\text{-}14)$$

Looking back at equation (2-4), we have defined the Fock matrix but not the overlap matrix. It is just a matrix that accounts for every overlap of basis functions between each other:

$$S_{rs} = \langle \chi_r | \chi_s \rangle \qquad (2\text{-}15)$$

Once the matrix elements have all been determined, the secular equation can be set up to obtain a guess of the orbitals energies ε:

$$\begin{bmatrix} F_{11} - S_{11}\varepsilon_i & \cdots & F_{1N} - S_{1N}\varepsilon_i \\ \vdots & \ddots & \vdots \\ F_{N1} - S_{N1}\varepsilon_i & \cdots & F_{NN} - S_{NN}\varepsilon_i \end{bmatrix} = 0 \qquad (2\text{-}16)$$

Finding the roots of the determinant will give the energies ε_1 through ε_N for an N sized matrix. N is related to the total number of basis functions. Substituting one of those roots back in to the Roothaan equation and setting it to zero, you will get new and improved coefficients that weight your basis functions such that your guessed energy is

16

closer to the exact energy. These improved coefficients can be further improved by finding new Fock matrix elements from the updated density matrix elements and solving the secular equation a second time. Iteration is continued until the coefficients of generation n are sufficiently close to the coefficients of generation n-1.

2.3.3 An Extension of Hartree-Fock: Configuration Interaction

At this point, the Hartree-Fock SCF method for the ground state can obtain the optimal weightings (coefficients) of each molecular orbital such that the energy is minimized taking a determinant of the Roothaan Equation. However, one determinant is not accurate enough in describing molecules that have two electronic configurations that are close or equal in energy, or for excited states.

For the description of an excited state, a promoted electron requires the linear combination of two or more determinants, since there are a number of possible configurations. This inclusion of several determinants to account for several configurations of excited states is called Configuration Interaction. The first determinant corresponds to the ground state (HF) configuration, while the others correspond to determinants of possible excited state configurations. For an excited state, the linear combination of these configurations can be expressed as:

$$\Psi = a_0 \psi_{HF} + \sum_i^{occ.} \sum_r^{virt.} a_i^r \psi_i^r + \sum_{i<}^{occ.} \sum_{r<}^{virt.} a_{ij}^{rs} \psi_{ij}^{rs} + \cdots \tag{2-17}$$

Where i and j are occupied molecular orbitals and r and s are virtual (unoccupied) orbitals in the HF ground state reference wavefunction. The energies can

be determined taking the determinant of the secular equation, equation (2-16), and finding the roots. The "resonance" matrix element is then:

$$H_{nm} = \langle \psi_n | \hat{H} | \psi_m \rangle \qquad (2\text{-}18)$$

Where m and n are configurations that cannot be equal (m≠n). Since there are a plethora of virtual orbitals and therefore even many possible configurations, only accounting for configurations pertaining to single electron excitations is called Configuration Interaction Singles (CIS).

2.3.5 Density Functional Theory (DFT) and its extension Time Dependent-DFT

Density Functional Theory is analogous to HF theory, however rather than manipulating the wavefunction, you manipulate the electron density. Electron density is related to the wavefunction because it is the probability of finding an electron at a given position, and the electron can be described by its wavefunction.

$$\rho = \langle \psi | \psi \rangle \qquad (2\text{-}19)$$

One difference is that the electron density is a physical observable, while the wavefunction is not. In 1964, Hohenberg and Kohn proved two theorems which allowed for the construction of a Hamiltonian operator for the electron density, which parallels the Hamiltonian for the wavefunction. These are the Hohenberg-Kohn existence theorem and the Hohenberg-Kohn variational theorem.[5] The existence theorem proved that a many-particle system of N electrons with 3N spatial coordinates can be reduced to 3 spatial coordinates (x, y, z) by using a functional. It is called a functional (function of

a function) because the energy is a function of the electron density which is in turn a function of electron position. The existence theorem was proven by solving the functional for a uniform electron gas in an external positive potential distributed over all space. The second theorem showed that the electron density followed a variational theorem like that of HF theory. Optimization of the orbital coefficients could be achieved by evaluating the expectation value of the energy, which is always greater than the exact energy. The energy functional of a molecule is partitioned into the kinetic energies of non interacting electrons and nuclei, as well as the potential energies between each of them, similar to the HF Hamiltonian. With the application of the Born-Oppenheimer approximation, the expression accounting for the energy terms is:

$$E[\rho(r)] = T_{ni}[\rho(r)] + V_{ne}[\rho(r)] + V_{ee}[\rho(r)] + \Delta T[\rho(r)] + \Delta V_{ee}[\rho(r)] \qquad (2\text{-}20)$$

The terms are the kinetic energy of the electrons (non-interacting), the potential energy between electrons and nuclei, potential energy for classical electron-electron repulsion, potential energy correction for the kinetic energy of interacting electrons (corrects term 1) and lastly, the correction to the electron-electron repulsion energy (corrects term 3). Unlike HF, these five terms account for every interaction in a many body system, and for this reason DFT is a complete theory. Expanding the first three terms in equation (2-20), and condensing the last two:

$$E[\rho(r)] = \sum_i^N \left(\langle \phi_i | -\frac{1}{2}\nabla_i^2 | \phi_i \rangle - \langle \phi_i | \sum_k^{nuclei} \frac{Z_k}{r_i - r_k} | \phi_i \rangle \right)$$

$$+ \sum_i^N \langle \phi_i | \frac{1}{2} \int \frac{\rho(r)}{|r_i - r|} dr | \phi_i \rangle + E_{xc}[\rho(r)] \qquad (2\text{-}21)$$

19

where ϕ_i are Kohn-Sham orbitals, N is the number of electrons and ρ is the electron density which is an exact eigenfunction (analogous to the wavefunction) expressed as:

$$\rho = \sum_{i=1}^{N} \langle \phi_i | \phi_i \rangle \qquad (2\text{-}22)$$

As mentioned earlier, the Kohn-Sham variational theorem proves that the energy from the trial electron density will always be higher than the actual energy.[6]

To optimize the orbitals that minimize the energy, Density Functional Theory uses the Kohn-Sham (KS) equation that finds the weightings of each contributing orbital in a SCF fashion.[6] This is expressed as

$$h_i^{KS} \phi_i = \varepsilon_i \phi_i \qquad (2\text{-}23)$$

h_i^{KS} is the one-electron Kohn-Sham (KS) operator. The KS operator is defined as:

$$h_i^{KS} = \frac{1}{2} \nabla_i^2 - \sum_k^{nuclei} \frac{z_k}{r_i - r_k} + \int \frac{\rho(r')}{|r_i - r'|} dr' + V_{XC} \qquad (2\text{-}24)$$

where V_{XC} is the functional derivative for the exchange-correlation energy:

$$V_{XC} = \frac{\delta E_{XC}}{\delta \rho} \qquad (2\text{-}25)$$

For DFT, no approximations are made to account for all the electron-electron interactions, which contrasts with HF which uses the mean-field approximation. However, the operator required for the exchange-correlation energy [bolded in equation (2-21)], must be approximated. It can only be found precisely for a uniform free electron gas.

This final term is the most problematic because the Hohenberg-Kohn existence theorem only proves that one exists. The exact functional for a many-body system cannot be determined, so the exchange-correlation energy functional(s) that account for all non-classical electron-electron interactions are formulated, and take on the form

$$E_{XC}[\rho(r)] = \int \rho(r)\varepsilon_{XC}[\rho(r)]dr \qquad (2\text{-}26)$$

where ε_{XC} is the exchange-correlation energy density functional. The most basic ε_{XC} is that of the local spin density approximation (LSDA).[7] More modern functionals combine the LSDA functional with generalized gradient corrected functionals (GGAs) that add Hartree-Fock exchange (Hybrid functionals). The amount of HF exchange can be varied. In this thesis, two (B3LYP and PBE0) hybrid functionals are used.[3, 8, 9]

B3LYP, is a three parameter exchange functional combined with two correlation functionals, taking on the form:

$$E_{xc}^{B3LYP} = E_{xc}^{LDA} + a_0\left(E_x^{HF} - E_x^{LDA}\right) + a_x\left(E_x^{B3} - E_x^{LDA}\right) + a_c\left(E_c^{LYP} - E_c^{LDA}\right) \qquad (2\text{-}27)$$

where $a_0=0.2$, $a_x=0.72$, $a_c=0.81$, which are fitting parameters optimized from empirical data. This exchange functional uses three fractions of the exchange in the exchange energy functionals, specifically the Hartree-Fock exchange functional , the LSDA exchange functional , and a gradient density functional designed by Becke.[6] In combination with these exchange functional. The two correlation functionals used are the LSDA correlation energy density functional and the generalized gradient functional developed by Lee, Yang and Parr.

The PBE0 functional also uses both HF and DFT exchange:

$$E_{xc}^{PBE0} = E_{xc}^{PBE0} + 0.25\left(E_x^{HF} - E_x^{PBe0}\right) \qquad (2\text{-}28)$$

Where E_{xc}^{PBE0} and E_x^{PBE0} are the GGA exchange-correlation and exchange functionals of Perdew, Burke and Erzenhoff.[7] PBE0 uses 25% HF exchange, which was rationalized from arguments in perturbation theory. PBE0 does not use empirical data as did B3LYP and is considered parameter-free.

At this point, the formulation of the Hamiltonian using the electron density has been shown to account for all interactions. This allows for a good determination of the ground state energy. For determining the energy of the excited state Time-Dependent Density Functional Theory (TD-DFT) was introduced by Runge and Gross in 1984.[10] This formulation allowed for the determination of absorption spectra, and uses perturbation theory to find the excitation energy. Perturbation theory is applied by selecting the density at t=0 to be the ground state density, followed by the addition of a small external potential for time t. For an added small external potential, the Hamiltonian responds in a linear fashion since the ground state Hamiltonian is known, and the new "perturbed" Hamiltonian can be written as:

$$H(r,t) = H(r,t) + \partial V^{ext}(r,t) \qquad (2\text{-}29)$$

Where $H(r,t)$ is the initial Kohn-Sham Hamiltonian and $\delta V^{ext}(r,t)$ is the external potential. The perturbed time dependent Kohn-Sham Hamiltonian can then be written as the sum of the terms:

$$H_{KS}[\rho](t) = H_{KS}[\rho] + \delta V_H[\rho](t) + \delta V_{XC}[\rho](t) + \delta V^{ext}(t) \qquad (2\text{-}30)$$

The Hartree and exchange-correlation potentials respond to the external potential linearly, and can be expanded as:

$$\partial V_H[\rho](r) = \frac{1}{|r-r|} \partial \rho(r) \qquad (2\text{-}31)$$

$$\partial V_{XC}[\rho](r) = f_{XC}(rt,\ rt)\, \partial \rho(r) \qquad (2\text{-}32)$$

δV^{eff} is the sum of the three potentials (Hartree, exchange-correlation and external(arbitrary and thus known) that have arisen due to the perturbation in equation (2-30). The linear response to the density $\delta[\rho]$ then takes the form:

$$\partial[\rho](r,t) = \chi_{KS}(rt,rt)\delta V^{eff}[\rho](rt) \qquad (2\text{-}33)$$

χ_{KS} is the density response function that can be expressed as:

$$\chi_{KS}(rt,rt) = \partial \sum_{jk}^{\infty} (f_k - f_j) \frac{\phi_j(rt)\phi_j^*(rt)\phi_k(rt)\phi_k^*(rt)}{\omega - (j-k) + i\eta} \qquad (2\text{-}34)$$

where ϕ_j, ε_j f_j are the ground state orbitals, eigenvalues and occupation number and ω is some given weight between zero and a half. ϕ_j, ε_j and f_j are the excited state orbitals, eigenvalues and occupation number. Inserting equation (2-33) into the equation (2-34), you get the TD-DFT Dyson equation:

$$\chi(r_1t_1, r_2t_2) = \chi_{KS}(r_1t_1, r_2t_2) + \chi_{KS}(r_1t_1, r_2t_2)\left(\frac{1}{|r_2-r_1|} + f_{XC}(r_2t_2, r_1t_1)\right)\chi(r_1t_1, r_2t_2) \quad (2\text{-}35)$$

The kernel f_{xc} is problematic but can be approximated from the f_{xc} of a uniform free electron gas. The excitation energies can be then extracted from the poles of this equation using a Green's function. The functional used in the TD-DFT calculations were the same as those used for geometry optimization, specifically TD-B3LYP in chapters 4-6 and TD-PBE0 in chapter 7.

2.3.4 Basis Sets

HF and DFT require basis functions that describe a molecular orbital. These basis functions are known collectively as basis sets and are comprised of a linear combination of atomic orbitals. The original basis functions were hydrogenic types, or Slater type orbitals (STO). Their usage requires equation (2-12) to be solved numerically, which is computationally expensive. A fix to this problem is to change the orbitals from having a radial decay (e^{-r}) to having a Gaussian decay (e^{-r^2}), which can be solved analytically. A Gaussian type orbital (GTO) then takes the form:

$$\varphi(x,y,z;\alpha,i,j,k) = (\frac{2\alpha}{\pi})^{3/4} \left[\frac{(2\alpha)^{i+j+k}i!j!k!}{(2i)!(2j)!(2k)!}\right]^{1/2} x^i y^j z^j e^{-\alpha(x^2+y^2+z^2)} \qquad (2\text{-}36)$$

where α controls the Gaussian width and I,j,k are integers that characterize the symmetry of the orbital that would normally be dictated angular momentum. For example if i+j+k=0, then the GTO would look like an s orbital, while if the sum was equal to i+j+k=1 it would look like a p orbital. One Gaussian orbital is not accurate enough to reproduce the radial decay, so a linear combination of GTOs used form an accurate description of an STO:

$$\varphi_{STO}(x, y, z; \{\alpha\}, i, j, k) = \sum_{a=1}^{m} c_a \varphi_{GTO}(x, y, z; \alpha_a, i, j, k) \qquad (2\text{-}37)$$

where m is the number of primitive Gaussian functions used and c_a are the coefficients that weight each Gaussian. When coefficients are allowed to be negative, certain primitive Gaussians can contribute to the overall STO function by contracting it. Increasing the number of Gaussians used to describe your STO, makes equation (2-12) become increasingly difficult. It is common to find a compromise between using the smallest basis set possible (to minimize computer time) without losing a good description of the wavefunction (accuracy). This is can be done by evaluating the effect of a basis set on the geometry of a molecule, as in chapters 4-7.

A basis set can be improved further by having multiple basis functions to describe each orbital. When two basis functions are used, it is called a double-zeta basis set, which is used in chapters 4-7. A triple-zeta basis set uses three basis functions per orbital and is used in Chapters 4, 6 and 7.

Basis sets can be further modified by having different Gaussians for the valence orbitals, because they are involved in bonding and therefore require flexibility. A split-valence basis set, takes on the form X-YZG for a double-zeta basis set. The X is the number of primitive Gaussians used for the core electrons while the Y and Z explain how many primitive Gaussians are used for each contracted basis function. In this thesis, the most common basis set is the 6-31+G(d), which means it is a double-zeta basis set with 6 primitive Gaussians to describe the core electrons, 3 primitive Gaussians to describe

the first contracted valence basis function and 1 primitive Gaussian to describe the second contracted valence basis function.

Polarization and diffuse functions are present in the basis set 6-31+G(d) denoted by the "(d)" and + respectively. The polarization function is used to allow for more asymmetry while the diffuse functions improve the description of the electron density far from the nuclei.

2.3.5 Polarizable Continuum Model

The optimizations and excitations of molecules in chapters 4-7 were carried out with a surrounding polarizable continuum to simulate solvation. Solvation is a collective term for non-specific and specific interactions between a surrounding cluster of molecules (solvent) and a specific molecule (solute). The Polarizable Continuum Model (PCM) is a model that accounts for the non-specific interactions between solvent and solute, and is an additional potential added to the overall Hamiltonian of the solute.[11] The effective Hamiltonian that accounts for both solute and solvent can then be written as:

$$\hat{H}^{eff} = \hat{H}^{solute} + \hat{H}^{solvent} + \hat{H}^{int} \tag{2-38}$$

which is made up of the solute and solvent Hamiltonians and the interaction between the two. However, the geometry of the solvent is irrelevant since it is a continuum and thus the effective Hamiltonian is simplified to being just the solute Hamiltonian and the

interaction Hamiltonian between the solute and the continuum. Thus to solve for the interaction term, a definition of the continuum is required.

The continuum ("solvent") is a continuous electric field that represents the average over all degrees of freedom. The electrostatic interaction of the solute in the continuum is described by the Poisson equation:

$$-\nabla^2 V(\vec{r}) = 4\pi \rho_m(\vec{r})$$
(2-39)

Where ρ_m the charge distribution and V(r) is is the sum of solute and reaction field electrostatic potentials:

$$V(\vec{r}) = V_M(\vec{r}) + V_R(\vec{r})$$
(2-40)

where V_M the electrostatic potential generated within the solute and V_R is the reaction field potential that is generated by the polarization of the continuum. The solute is placed within a cavity of this continuum, which is chosen arbitrarily. The cavity was arbitrarily made by summing the overlapping van der waals radii of the atoms in the molecule. There are two surfaces between the solute and the continuum, specifically the solvent-accessible (cavity) surface (SAS) and solvent-excluding surface (SES). These two surfaces mimic reality in that some vacant space near a molecule cannot be penetrated by a solvent molecule.

On the cavity surface of the continuum is a set of very small surface areas called tesserae, which have a density $\sigma(s)$ that polarize to the density of the solute $\sigma(r)$. The charge of each tesserae is variable, and the distribution of charge q_k is optimized in a

self-consistent manner such that the electrostatic interaction between the continuum and the solute is a minimum. Thus the reaction field potential can be expressed as:

$$V_R(\vec{r}) = \sum_k \frac{q_k}{|\vec{r} - \vec{s}_k|} \tag{2-41}$$

The polarization vector $\vec{P}_i(\vec{r})$ of the continuum that generated the reaction field potential is dependent on the dielectric constant, which can be arbitrarily selected to mimic the polarity of a solvent:

$$\vec{P}_i(\vec{r}) = -\frac{\varepsilon_i - 1}{4\pi} \nabla \vec{V}_R(\vec{r}) \tag{2-42}$$

ε_i is the dielectric constant of the region i. A continuum solvent can thus be created by choosing a dielectric constant value which provides the magnitude of charges on the tesserae. The solvent density is related to how many tesserae are to be used on the continuum surface.

The PCM model does not account for specific interactions such as hydrogen bonding. To include such an interaction, explicit solvation can be used. An actual solvent molecule is coordinated to the solute molecule and optimized at a QM level of theory. The solvent-solute dimer also is put in a continuum cavity to account for non-specific interactions of the dimer. This explicit solvation approach is used in chapters 5 and 7, for improving the excitation energies of Betaine 30 and the hydroxamic acids which are capable of hydrogen bonding in protic solvents.

2.3.6 References

1 D. A. Skoog, F. J. Holler and T. A. Nieman, *Principles of Instrumental Analysis*, Thomson Brooks/Cole, Salt Lake City, USA, 1997

2 C. J. Cramer, *Essentials of Computational Chemistry: Theories and Models*, Wiley, West Sussex, 2004

3 M. J. Frisch, G. W. Trucks, H. B. Schlegel, G. E. Scuseria, M. A. Robb, J. R. Cheeseman, J. A. Montgomery, T. V. Jr., K. N. Kudin, J. C. Burant, J. M. Millam, S. S. Iyengar, J. Tomasi, V. Barone, B. Mennucci, M. Cossi, G. Scalmani, N. Rega, G. A. Petersson, H. Nakatsuji, M. Hada, M. Ehara, K. Toyota, R. Fukuda, J. Hasegawa, M. Ishida, T. Nakajima, Y. Honda, O. Kitao, H. Nakai, M. Klene, X. Li, J. E. Knox, H. P. Hratchian, J. B. Cross, V. Bakken, C. Adamo, J. Jaramillo, R. Gomperts, R. E. Stratmann, O. Yazyev, A. J. Austin, R. Cammi, C. Pomelli, J. W. Ochterski, P. Y. Ayala, K. Morokuma, G. A. Voth, P. Salvador, J. J. Dannenberg, V. G. Zakrzewski, S. Dapprich, A. D. Daniels, M. C. Strain, O. Farkas, D. K. Malick, A. D. Rabuck, K. Raghavachari, J. B. Foresman, J. V. Ortiz, Q. Cui, A. G. Baboul, S. Clifford, J. Cioslowski, B. B. Stefanov, G. Liu, A. Liashenko, P. Piskorz, I. Komaromi, R. L. Martin, D. J. Fox, T. Keith, M. A. Al-Laham, C. Y. Peng, A. Nanayakkara, M. Challacombe, P. M. W. Gill, B. Johnson, W. Chen, M. W. Wong, C. Gonzalez and a. J. A. Pople, Gaussian 03 (Revision D.01), Gaussian, Inc., Wallingford, CT, 2004

4 M. J. Frisch, G. W. Trucks, H. B. Schlegel, G. E. Scuseria, M. A. Robb, J. R. Cheeseman, J. A. Montgomery, T. V. Jr., K. N. Kudin, J. C. Burant, J. M. Millam, S. S. Iyengar, J. Tomasi, V. Barone, B. Mennucci, M. Cossi, G. Scalmani, N. Rega, G. A. Petersson, H. Nakatsuji, M. Hada, M. Ehara, K. Toyota, R. Fukuda, J. Hasegawa, M. Ishida, T. Nakajima, Y. Honda, O. Kitao, H. Nakai, M. Klene, X. Li, J. E. Knox, H. P. Hratchian, J. B. Cross, V. Bakken, C. Adamo, J. Jaramillo, R. Gomperts, R. E. Stratmann, O. Yazyev, A. J. Austin, R. Cammi, C. Pomelli, J. W. Ochterski, P. Y. Ayala, K. Morokuma, G. A. Voth, P. Salvador, J. J. Dannenberg, V. G. Zakrzewski, S. Dapprich, A. D. Daniels, M. C. Strain, O. Farkas, D. K. Malick, A. D. Rabuck, K. Raghavachari, J. B. Foresman, J. V. Ortiz, Q. Cui, A. G. Baboul, S. Clifford, J. Cioslowski, B. B. Stefanov, G. Liu, A. Liashenko, P. Piskorz, I. Komaromi, R. L. Martin, D. J. Fox, T. Keith, M. A. Al-Laham, C. Y. Peng, A. Nanayakkara, M. Challacombe,

P. M. W. Gill, B. Johnson, W. Chen, M. W. Wong, C. Gonzalez and a. J. A. Pople, Gaussian 09 (A1), Gaussian, Inc., Wallingford, CT, 2009

5 W. Sham and P. Hohenberg, *Phys. Rev. A J1 - PRA*, 1964, 136, B864–B871

6 W. Kohn and L. J. Sham, *Phys. Rev.*, 1965, 140, A1133–A1138

7 J. C. Slater, *The Self-Consistent Field for Molecular and Solids, Quantum Theory of Molecular and Solids*, McGraw-Hill, New York, 1974

8 A. D. Becke, *Physical Review A*, 1988, 38, 3098-3100

9 J. P. Perdew, K. Burke and Y. Wang, *Physical Review B*, 1996, 54, 16533 LP - 16539

10 E. Runge and E. K. U. Gross, *Phys. Rev. Lett.*, 1984, 52, 997-1000

11 S. Mierts, E. Scrocco and J. Tomasi, *Chemical Physics*, 1981, 55, 117-129

Chapter 3

An *Ab Initio* and TD-DFT study of Solvent Effect Contributions to the Electronic Spectrum of Nile Red[1]

[1]P.O.Tuck, M.Rappon, R.C.Mawhinney, Phys. Chem. Chem. Phys., 2009, 11, 4471–4480

3.1 Introduction

Nile Red (*Figure 3-1*) is a lipophilic fluorescent dye that exhibits a large red shift in both its absorption and emission spectra as solvent polarity is increased.[1] This solvent effect, known as solvatochromism, is attributed to the difference in ground and excited state dipole moments.[2] Conceptually, when the ground state has the larger dipole moment it will be preferentially stabilized by a more polar solvent, which will increase the transition energy gap and induce a blue-shift in the spectrum. In contrast, when the excited state has the larger dipole moment it will be stabilized by a more polar solvent and the transition energy decreases, which is observed as a red-shift in the spectrum. The former is negative solvatochromism whereas the latter is positive solvatochromism.[3] The sensitivity of Nile Red (NR) to its surrounding environment has made it a valuable tool as a fluorescence probe in studying polymers,[1] ionic liquids,[4] liquid crystals,[5] Langmuir-Blodgett films,[6] cavities of cyclodextrins[7,8] and zeolite structures.[9] Commercial applications of Nile Red utilize both its fluorescence and sensitivity.[10, 11] The solvent sensitivity of NR is due to a significant increase in dipole moment from the ground to the excited state, which is a consequence of a large charge transfer between the donor (diethyl amino) and acceptor (carbonyl oxygen) moieties of NR (see Figure 3-1). Therefore, from the perspective of application, an accurate determination of the dipole moments in NR is of considerable interest.

Figure 3-1: Nile Red

The determination of the ground and excited state dipole moments has been attempted and the values obtained exhibit considerable discrepancies. Dutt et al. were first to report a value of 11.6 D for the change in electric dipole moment, obtained by reorientation dynamics.[12] Ohta, Dutta and Komada investigated Nile Red in non-polar and polar solvents as well as in polymer thin films and reported a change in dipole of 6.8 D.[1,6] Foreman, Golini and Williams reported ground and excited state dipole values of 8.9 D and 14.4 D using a solvatochromic approach and 8.4 D and 13.4 D using a thermochromic approach.[13] Another thermochromic investigation, by Ghoneim in 2000, reported ground and excited state dipole moments of 7 D and 14.5 D, respectively, in 2-methyl tetrahydrofuran.[14] More recently, Kawski and Bojarksi addressed the discrepancy by attributing it to approaches which assume the polarizability (α) of the solute to be zero.[15] Another oversimplification is the incorporation of the Onsager model in which it is assumed that all solvents form a spherical cavity around the solute, despite the rod-like structure of NR (Figure 3-1).

Geometry change as a consequence of solvent polarity is another important aspect to be addressed since dual fluorescence in Nile Red has been reported in methanol/water binary mixtures.[12] Hydrogen bonding may play a role in such cases, which can cause a shift in the absorption and or fluorescence peak depending on how

33

the solvent interacts with the dye, as discussed by Rappon and Gillson.[16] Exciplex formation has been proposed as a possible mechanism for dual fluorescence, but past studies have shown that it is not a necessary criterion[17, 18] and recent results show that even in non-protic solvents, dual fluorescence in NR is observed.[19] Also, the second peak is independent of solute concentration, which eliminates the possibility of excimer formation and leaves only the possibility that two accessible conformers of NR exist on the first excited state PES. Related to this is the difficulty in describing the changes in structural parameters for such a complex molecule, which limits a straight-forward mapping of the PES.[20] Most literature reports attribute the two minima on the first excited state PES as being due to a rotation of the diethylamino group from the plane of the ring system to a twisted orientation. This concept of a twisted excited state geometry is referred to as a Twisted Intramolecular Charge Transfer (TICT) state.[21,22] Accompanying the TICT state is a significant increase in the excited state dipole moment. An alternative proposal, and independent from the TICT hypothesis, is a Wagging Intramolecular Charge Transfer (WICT) state in which dual fluorescence is explained through rehybridization (pyramidalization) of the diethylamino nitrogen as the major geometry change that affects the PES.[23] Previous semi-empirical-ZINDO/S calculations by Foreman, Golini and Williams showed that varying the twist angle lowered one excited state with a large dipole moment beyond another with a significantly smaller dipole, supporting the TICT proposal.[13] However, Pessine et al. predicted dipole moments for the first four excited states of NR using a CIS/CEP-31g model chemistry and found that a planar geometry for the first excited state exhibited a

larger dipole moment (12.95 D) than the corresponding twisted geometry (7.92 D), contradicting the TICT proposal.[24]

Although Nile Red has been extensively researched, several issues are yet to be resolved and fully elucidated. This paper reports a Time Dependent-Density Functional Theory (TD-DFT) and a CIS study of NR using an all electron basis set to explore the relationship between solvation, geometry and electronic transitions. The dipole moments and polarizabilities of NR are reported. Insight regarding the TICT state is given through an evaluation of the donor and acceptor twist angle potential energy curve. Another issue that is addressed is the most stable conformation of the diethylamino group in the ground state.

3.2 Computational

All calculations were carried out using the Gaussian 03 program.[25] Gas phase and solvated ground state optimized geometries were obtained using both Density Functional Theory and Hartree-Fock Theory. The hybrid DFT functional used throughout this paper was the Becke 3-parameter exchange functional[26] combined with the Lee Yang and Parr correlation functional.[27] A split valence 6-31+G(d)[28] basis set was used, with polarization and diffuse functions added to allow for asymmetry and a better description of electron density far from the nuclei. Configuration interaction singles (CIS) was employed for HF excitation energies and was also used to optimize the first excited state.[29] Time Dependent-Density Functional Theory using the B3LYP functional (referred to throughout as TD-B3LYP) was employed for excitation energies using B3LYP optimized ground state geometries.

The Polarized Continuum Model (PCM) was used to simulate the non-specific solvation of NR.[30] The PCM model is an improvement on the Onsager cavity model since the solute cavity is described by the sum of interlocking atomic spheres generated from their Van der Waals radii. Since this model only accounts for the electrostatic interaction between the solvent and solute molecules, protic solvents were excluded from this study. Acetonitrile/Benzene binary mixtures were selected for this study, since NR can be inspected over a large polarity range and are experimentally miscible. By varying the dielectric constants and solvent radii, eight solvents were mimicked: benzene, acetonitrile and six acetonitrile/benzene mixtures of known mole ratios (see Table 3-1). For benzene and acetonitrile the default values were used while for the binary mixtures the dielectric constants and solvent radii employed were based on a mole fraction weighted average of the benzene and acetonitrile values. While literature reports show that the dependence of the dielectric constant on the mole fraction of acetonitrile for these mixtures deviates slightly from linearity,[31] there are no equivalent assessments of the other two parameters required for the chosen solvent model and so it is necessary to use the linear approximation in this study.

3.3 Results and Discussion

3.3.1 Predominant Conformation of Nile Red

Before pursuing our investigation into the effects of solvent on the electronic spectrum, it was necessary to first determine the global minimum. Several conformers of Nile Red were optimized and are displayed in Figure 3-2. Only the gas phase and acetonitrile results are included here since they correspond to the lower and upper

36

bounds of our study (ε=0-37). Included in Figure 3-2 are the relative energies, twist angles and pyramidalization values used to characterize the conformation of the donor in relation to the ring system, and the $S_0 \rightarrow S_1$ excitation energies. The twist angle (see Figure 3-1 for atom numbering scheme) is defined as the average of the two dihedral angles $\phi_{C5-C6-N19-C20}$ and $\phi_{C1-C6-N19-C23}$. Pyramidalization is defined as the deviation from planarity of the three atoms attached to the nitrogen ($180° - |\phi_{C6-N19-C20-C23}|$).

Conformer D was found to be most stable. This conformer has one ethyl group lying above the ring system plane and the other one below with the diethylamino group slightly twisted out of plane (6.3°) but with negligible nitrogen pyramidalization (0.2°). Conformer B is the second most stable conformer, lying 2.97kJ/mol above conformer D. In this conformer both ethyl groups are above the plane of the ring system with a twist angle of almost zero (0.5°) and a nitrogen pyramidalization of 1.9°. Conformers A and C are, respectively, 12.49 and 10.08kJ/mol less stable than conformer D. Conformer C has one ethyl group lying in the plane of the ring system and the other lying above it, with a twist angle of -6.6° and a nitrogen pyramidalization of 20.5° while conformer A has one ethyl group in the plane of the ring system and the other below the ring, with a twist angle of 11.6° and a nitrogen pyramidalization of 19°. Earlier work by Pessine et al. found several minima at the AM1 level of theory, with a global minimum reminiscent of our conformer B.[18] None of the other conformers were reported and thus we cannot compare fully to our findings. However, optimization of this global minimum at the HF/CEP-31g level of theory produced a structure with twist angles of 0.2°, suggesting it is the same structure as our conformer B. The electronic excitation energies of all four

conformers are nearly the same, deviating by no more than 2 nm. The energetic

ordering of the four conformers remains almost identical, although conformers A and C

are now approximately isoenergetic and have nearly the same twist angle and nitrogen

pyramidalization. Solvation induces some geometric changes, but nothing overly

drastic. These changes will be discussed in detail in 3.3.3C. Similarly, there is a change in

electronic excitation energies, to be discussed in detail in 3.3.3B, but all four conformers

continue to have nearly identical $S_0 \rightarrow S_1$ excitation energies. These results indicate that

conformer D is the global minimum under all conditions considered in this study and will

be used exclusively for the remainder of our investigation.

3.3.2 Method Assessment

The adequacy of the approach used in this study is addressed in Table 3-1. The

experimental λ_{max} values for NR range from 536 nm in benzene to 549 nm in

acetonitrile.[19] In general, both CIS and TD-B3LYP overestimate the excitation energy,

with TD-B3LYP closest to experiment. Most importantly, though, is that both methods

reproduce the experimental trend of red shifts with increasing solvent polarity. The CIS

values in benzene and acetonitrile are 321 nm and 328 nm, respectively, whereas the

TD-B3LYP values in benzene and acetonitrile are 502 nm and 516 nm, respectively. The

large inaccuracy of excitation energy by CIS has been well documented, where it

typically overestimates the energy of large molecules by 0.5-2 eV (1.52 eV when

comparing CIS acetonitrile predicted value to experiment).[32] TD-B3LYP was found to

overestimate the energy by 0.14-0.31 eV, which is a considerable improvement from

CIS.

Conformer A
Energy / KJ/mol
-Gas Phase*: 12.49
-Acetonitrile*: 10.79
Twist Angle / °
-Gas Phase: 11.6
-Acetonitrile: 4.4
Pyramidalization / °
-Gas Phase: 19.0
-Acetonitrile: 16.3
TD-B3LYP
-Gas Phase: 461nm
-Acetonitrile: 513nm

Conformer B
Energy / KJ/mol
-Gas Phase*: 2.97
-Acetonitrile*: 3.47
Twist Angle / °
-Gas Phase: 0.5
-Acetonitrile: 1.4
Pyramidalization / °
-Gas Phase: 1.9
-Acetonitrile: 2.4
TD-B3LYP
-Gas Phase: 462nm
-Acetonitrile: 515nm
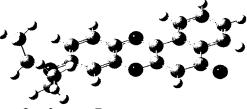
Conformer C
Energy (KJ/mol)
-Gas Phase*: 10.08
-Acetonitrile*: 10.79
Twist Angle / °
-Gas Phase: -6.6
-Acetonitrile: -5.0
Pyramidalization/ °
-Gas Phase: 20.5
-Acetonitrile: 16.9
TD-B3LYP
-Gas Phase: 461nm
-Acetonitrile: 513nm

Conformer D
Energy (KJ/mol)
-Gas Phase*: 0.00
-Acetonitrile*: 0.00(-57.91)†
Twist Angle / °
-Gas Phase: 6.3
-Acetonitrile: 3.7
Pyramidalization/ °
-Gas Phase: 0.2
-Acetonitrile: 0.5
TD-B3LYP
-Gas Phase: 463nm
-Acetonitrile: 516nm

Figure 3-2: NR conformers Optimized structures (rB3LYP/6-31+G(d)) with twist angle and pyramidalization gas phase geometries. TD-B3LYP excitation energies in gas phase and acetonitrile are also shown from their respective geometries.[* relative to conformer D, † relative to gas phase energy]

The experimental range of 13 nm is reproduced by TD-B3LYP while the CIS range of 7 nm is approximately one-half that from experiment. TD-B3LYP also succeeds in reproducing the slight increase in transition energy in the dielectric range of $\varepsilon=23$-37. The use of a larger basis set 6-311++G(d,p) (not shown) was found to decrease the TD-B3LYP excitation energies by 2 nm and the CIS transition energies by 1-2 nm in every case. The smaller basis set is assumed to be sufficient for the remainder of the study. Despite the poor performance of the HF based method, we still included the results in the remainder of this study since geometry optimization of the first excited state was only possible within the CIS ansatz.

3.3.3 Effect of solvation on the absorption spectra of Nile Red

The direct and indirect consequences of solvation on the absorption spectra are illustrated in Figure 3-3. The absorption spectra displayed were created from the calculated excitation maxima using the G03 default half-width at half height of 2685.83cm^{-1}. The four excitation spectra shown in Figure 3-3 correspond to (A) unsolvated geometry/unsolvated excitation, (B) unsolvated geometry/ solvated excitation, (C) solvated excitation/unsolvated excitation and (D) solvated geometry/ solvated excitation. This was done to partition the effects of geometry change on excitation from those of solvation on the electronic transition. Spectra B and D, which correspond to excitations in the presence of acetonitrile as solvent, show a large red-shift in the excitation maxima in comparison to spectra A and C which correspond to excitations in the gas phase. The presence of a solvent field also changes the geometry which in turn brings a small red-shift of its own. This is noted when comparing spectra A

and C, which correspond to excitation energies without the presence of a solvent field. In spectrum A, the gas phase optimized geometry was used while in spectrum C the acetonitrile optimized geometry was used.

Table 3-1: Effect of Solvent Polarity on NR absorption Maxima for TD-B3LYP Functional and CIS using a 6-31+G(d) basis set. Experimental values are shown for comparison.

Solvent (ε)	$\lambda_{max\text{-}B3LYP}$*	$\lambda_{max\text{-}CIS}$*	$\lambda_{max\text{-}exp't.}$‡
Gas Phase (0)	463	302	N/A
Benzene (2.247)	502	321	536
Binary Mixture 1 (4.52)	511	325	538
Binary Mixture 2 (12.50)	518	328	549
Binary Mixture 3 (20.51)	518	329	550
Binary Mixture 4 (22.53)	518	329	550
Binary Mixture 5 (28.08)	517	328	550
Binary Mixture 6 (33.17)	517	328	550
Acetonitrile (36.64)	516	328	549

*Excitation energies calculated using geometries optimized in the corresponding solvent

‡ The preparation of Nile Red in solution was carried out with concentrations of 1µM. Binary Mixtures were prepared by combining benzene with acetonitrile of known volume ratio.

The same effect can be observed on going from B to D. This solvent induced geometry change also causes a red-shift in the excitation maxima, but to a much smaller extent. Thus, the red-shift in the electronic spectra of NR is a result of the effect of the solvent on both the electronic transition through an electrostatic stabilization of the excited state and a solvent induced geometry change. Solvatochromism itself has been extensively reviewed by Reichardt, most notably on the study of Betaine 30.[2] The partitioning of the solvent effects into an indirect geometry effect and a direct field effect is relatively new[33] and can potentially provide more insight into the cause of solvatochromism in NR. These two effects of the solvent field are now examined individually by holding one constant.

3.3.3 A) Effect of solvent polarity on the electronic transitions

Figure 3-4 displays plots of changes in the calculated λ_{max} for a fixed geometry as the solvent field is varied. In Figure 3-4(a), the CIS excitation energies for the first three excitations at the HF optimized gas phase geometry are presented and in Figure 3-4(b) the TD-B3LYP results at the B3LYP optimized gas phase geometry are given. Focusing first on the CIS results, one notes that the $S_0 \rightarrow S_1$ transition, which is characterized as a HOMO$\rightarrow$LUMO transition, experiences a red-shift of 21 nm as the solvent polarity is increased, from 302nm in the gas phase to 323 nm in acetonitrile. The majority of the red-shift occurs between ε=0-4.5 followed by a small increase in transition energy in the dielectric range of ε=4.5-37. The $S_0 \rightarrow S_2$ transition undergoes a small red-shift with increasing polarity and is characterized by a mixture of configurations with a slight predominance of the HOMO-5$\rightarrow$LUMO transition. The $S_0 \rightarrow S_3$ transition is one that

blue shifts with increasing solvent polarity and corresponds to a lone pair from the

carbonyl group being excited into the LUMO. Moving to the TD-B3LYP results, one

notes that the $S_0 \rightarrow S_1$ transition undergoes a red-shift with increasing solvent polarity,
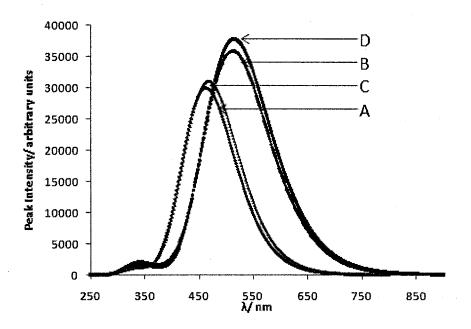
Figure 3-3: Partitioning the effects of solvent polarity and geometry on excitation energy of NR. The red (A) spectrum represents the gas phase geometry of NR with gas phase TD-B3LYP energy calculations. The green (B) spectrum represents the gas phase geometry of NR with a solvated (acetonitrile, $\varepsilon=37$) TD-B3LYP energy calculation. The orange (C) spectrum represents the solvated (acetonitrile, $\varepsilon=37$) geometry of NR with a gas phase TD-B3LYP energy calculation. The blue (D) spectrum represents the solvated (acetonitrile, $\varepsilon=37$) geometry of NR with a solvated (acetonitrile, $\varepsilon=37$) TD-B3LYP energy calculation.

similar to the CIS findings, and again the majority of the solvatochromic shift occurs in the lower polarity range, between ε=0-10. This suggests that there is a limit to how much stability a polar solvent can induce and is in agreement with the experimental results (see *Table 3-1*) which show that the red shift associated with the first UV/VIS absorption band of NR experiences little red shifting in the high solvent polarity range. The B3LYP molecular orbitals involved in the first three electronic transitions of Nile Red are displayed in *Figure 3-5*. Consistent with the CIS findings, the TD-B3LYP $S_0 \rightarrow S_1$ transition is a HOMO$\rightarrow$LUMO transition corresponding to a $\pi^* \leftarrow \pi$ transition. The TD-B3LYP $S_0 \rightarrow S_2$ transition is predominantly a HOMO-2 $\rightarrow$LUMO transition and shows a pronounced blue shift with an increase in solvent polarity while the $S_0 \rightarrow S_3$ transition is predominantly a HOMO-1$\rightarrow$LUMO transition and undergoes a small red-shift. As a result, the two states cross at a dielectric value of approximately 5, reversing the order of the two states. From this point forward, theTD-B3LYP S_2 label corresponds to the HOMO-2$\rightarrow$LUMO excitation of NR, despite it becoming higher in energy than the HOMO-1$\rightarrow$LUMO transition at higher solvent polarity.

As revealed in Figure 3-5, nearly all orbitals are stabilized by the increase in solvent polarity. This HOMO-2 orbital energy is affected the most, followed by the LUMO, LUMO+1 and HOMO-4 orbital energies. The HOMO orbital energy is unaffected and the HOMO-1 orbital is only very slightly stabilized. This variability in orbital energy stabilization is not uncommon[34-36] and only recently has a systematic understanding of the effects been considered.[37] The red shift in the $S_0 \rightarrow S_1$ transition can be rationalized as a result of the LUMO orbital energy being stabilized preferentially by the more

(a)

(b)
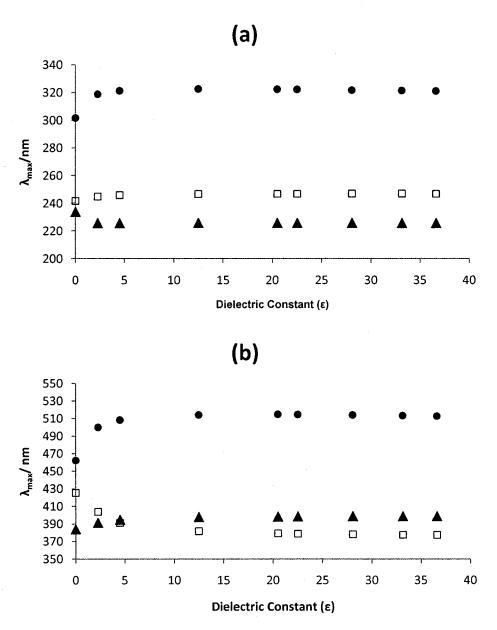
Figure 3-4: (a) Effect of solvent polarity on the spectroscopic shift (CIS) of the first three electronic excitations of Nile Red. Initial geometry used was that in the gas phase optimized at the HF/6-31+G(d) level of theory. (b) Effect of solvent polarity on the spectroscopic shift (TD-B3LYP) of the first three electronic excitations of Nile Red. Initial geometry used was that in the gas phase optimized at the B3LYP/6-31+G(d) level of theory. ●$S_0 \rightarrow S_1$; □ $S_0 \rightarrow S_2$; ▲$S_0 \rightarrow S_3$

Gas Phase · Benzene · Acetonitrile

LUMO+1
-0.041a.u. · -0.043a.u. · -0.048a.u.

LUMO
-0.099a.u. · -0.103a.u. · -0.108a.u.

HOMO
-0.202a.u. · -0.202a.u. · -0.202a.u.

HOMO-1
-0.240a.u. · -0.240a.u. · -0.242a.u.

HOMO-2
-0.244a.u. · -0.251a.u. · -0.262a.u.

HOMO-4
-0.261a.u. · -0.262a.u. · -0.266a.u.
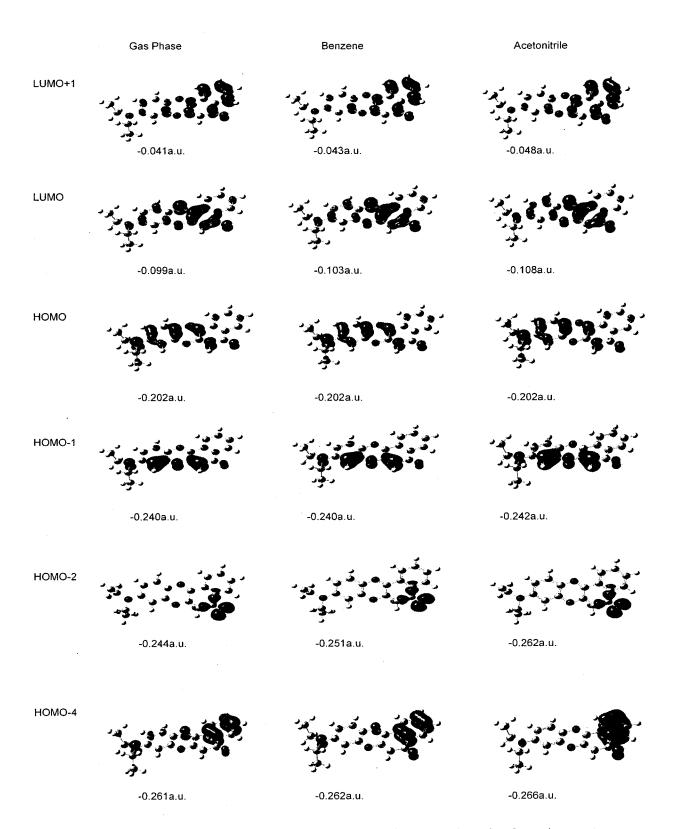
Figure 3-5: Kohn-Sham orbitals (isodensity=0.05) involved in the first three TD-B3LYP/6-31+G(d) excitations of Nile Red in the gas phase, benzene and acetonitrile.

polar solvent field. Since the $S_0 \rightarrow S_2$ transition is predominantly a HOMO-2$\rightarrow$LUMO transition and the HOMO-2 orbital is stabilized twice as much as the LUMO by a polar solvent like acetonitrile, the electronic transition is accompanied by a blue shift with an increase in solvent polarity.On the other hand, since the $S_0 \rightarrow S_3$ transition is predominantly a HOMO-1$\rightarrow$LUMO transition and the HOMO-1 is slightly stabilized by a polar solvent, a small red-shift is observed.

3.3.3 B) Effect of solvent polarity on ground state geometry

In Figure 3-3 it was shown that the effect of solvent polarity on the excitation spectra of NR is twofold, and one of these effects is geometric in origin. The structures obtained from a geometry optimization in each solvent polarity (ε=0-37) at both the HF and B3LYP levels have a diethylamino group that is almost in plane with the fused ring system. The changes in selected structural parameters of NR due to the change in solvent polarity are shown in Figure 3-6. The twist angle (see 3.3.1 for definition) for the optimized structure in the gas phase was found to be 7.5° for HF and 6.3° for B3LYP. As seen in Figure 3-6(a), an increase in solvent polarity decreases the twist angle monotonically to 5.2° and 3.8° for HF and B3LYP, respectively. Although both methods show the same trend, B3LYP predicts a larger twist angle. The decrease in the twist angle of the diethylamino group as the dielectric constant of the solvent increases is reinforced in Figure 3-7, which displays B3LYP energy scans of this twist angle in the gas phase, benzene and acetonitrile. The barrier to rotation of the diethylamino group increased by approximately 20 kJ/mol as the solvent dielectric constant increases from 0 to 37. Another interesting feature revealed in the energy scan of NR is that, in benzene,
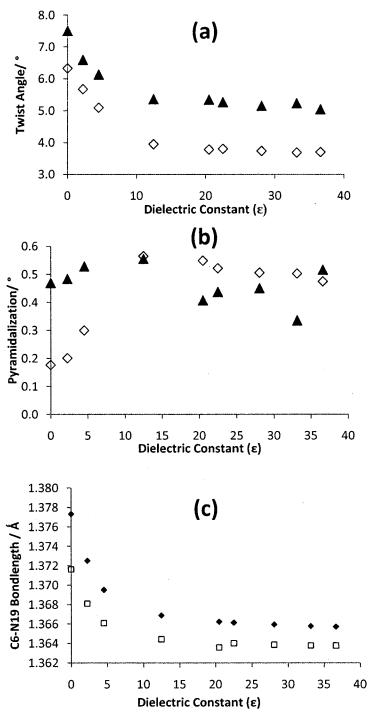
Figure 3-6: (a) Effect of Dielectric Constant on the NR Twist Angle for B3LYP and HF optimized ground state geometries (b) Effect of Dielectric Constant on the NR Pyramidalization Angle for B3LYP and HF optimized ground state geometries.(c) Effect of Dielectric Constant on the NR C6-N19 Bond Length (Å) for B3LYP and HF optimized ground state geometries. ◇B3LYP; ▲HF

48
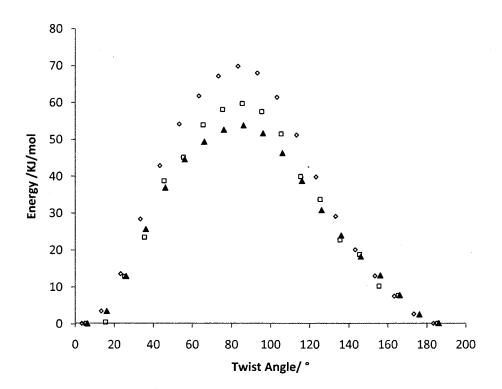
Figure 3-7: B3LYP energy curves of NR in ▲gas phase, ☐Benzene and ◇Acetonitrile. Twist angle is varied from optimized structure and incremented at 10 degrees for 18 steps. Energy plotted (kcal/mol) is relative to the optimized structure.

the twist angle is very flexible close to planarity, with basically no significant increase in energy up to a twist angle of 16°.

The change in the pyramidalization of the diethylamino nitrogen (see 3.3.1 for definition), which is a measure of the degree of nitrogen lone pair delocalization is presented in Figure 3-6(b) as the solvent polarity is increased. The overall change in pyramidalization is very small, with all values close to 0°, suggesting that solvent polarity has no affect on the delocalization of the lone pair into the neighbouring extended π-system in the ground state. In the B3LYP case, there appears to be an initial quadratic relationship (ε=0-10) between pyramidalization and solvent polarity, which then switches to a sinusoidal-like relationship for higher solvent polarities (ε=10-36). In the HF case, a sinusoidal-like relationship is seen over the whole solvent polarity range.

Related to both the twist angle and pyramidalization is the C-N bond length between the diethylamino group and the ring system, labeled C_6-N_{19} in Figure 3-1. The effect of solvent polarity on this parameter is given in Figure 3-6(c). An increase in solvent polarity results in a contraction of the C-N bond at both the B3LYP and HF levels of theory, consistent with a decrease in twist angle that results in a better overlap between the lone pair and extended π-system. The net change in bond length is 0.007 Å at the HF level and 0.012 Å at the B3LYP level. Gas phase optimized values of 1.372 Å and 1.377 Å for HF and B3LYP, respectively, infer significant C-N double bond character and correspond to an already present good overlap between the lone pair and the extended π-system. Previous studies reported slightly longer C-N bond lengths in NR of

50

1.40 Å (AM1) and 1.39 Å (HF/CEP-31g).[24] These distances corresponded to our conformer B, which has a slightly greater nitrogen pyramidalization (see Figure 3-2) that would suggest less overlap.

3.3.3 C) Effect of solvent induced geometry change on excitation energy
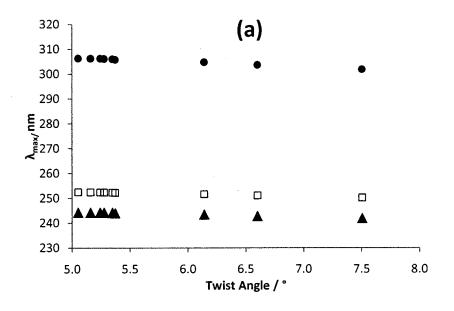
The effect of the resulting geometry changes due to solvation on the excitation energy are now considered through non-solvated CIS and TD-B3LYP energy calculations of the first three excited states of NR using the nine HF and nine B3LYP optimized structures from 3.3.3 B), which correspond to the global minimum in each solvent. The results are presented in Figure 3-8.
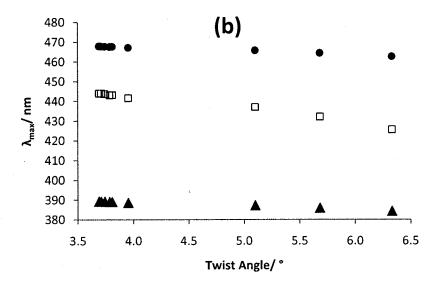
The effect of the solvent induced change in twist angle on the CIS excitation energies are given in Figure 3-8(a). The results indicate that there is little to no change in absorbance maxima, with the largest shift, of only 4nm, corresponding to the $S_0 \rightarrow S_1$ transition. The $S_0 \rightarrow S_3$ transition, nominally a $\pi^* \leftarrow n$ transition, is completely insensitive to this geometry change. As expected from our earlier assessment of TD-B3LYP as the more sensitive method, the same plot, but of the TD-B3LYP excitation energies for the B3LYP solvent induced change in twist angle, shown in Figure 3-8(b), indicates that all three transitions exhibit a linear blue shift. The $S_0 \rightarrow S_2$ transition shows the largest sensitivity, with a blue shift of 22 nm. Recalling that a large twist angle corresponds to a low solvent polarity, it would infer that the effect of the solvent induced geometry change is a red-shift in the excitation maxima as the solvent polarity increases. In 3.3.3 A) it was shown that the $S_0 \rightarrow S_2$ transition experiences a blue shift
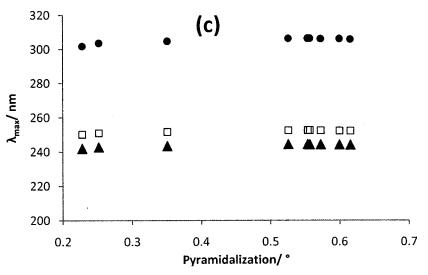
due to the large stabilization of the HOMO-2 orbital with increased solvent polarity. The aforementioned solvent induced geometric red-shift is overpowered by the direct influence of the solvent polarity on the transition energy.
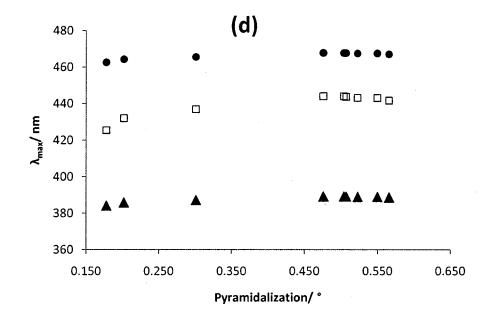
The effects of solvent induced changes on the nitrogen pyramidalization for the excitation energies can be seen in Figures 3-8(c) and 3-8(d), respectively, for CIS and TD-B3LYP. The CIS results show a very minor red-shift of between 2 nm and 4 nm with increasing nitrogen pyramidalization for all three excitations. Again, the TD-B3LYP results exhibit a greater sensitivity, with a red-shift of between 4 nm and 16nm with increasing nitrogen pyramidalization. This red-shift is most prominent for the $S_0 \rightarrow S_2$ transition, which experiences a red shift of 22 nm when pyramidalization is increased from 0.15 to 0.65. However, since the relationship between the nitrogen pyramidalization and solvent polarity is a minor issue, one cannot comment further.
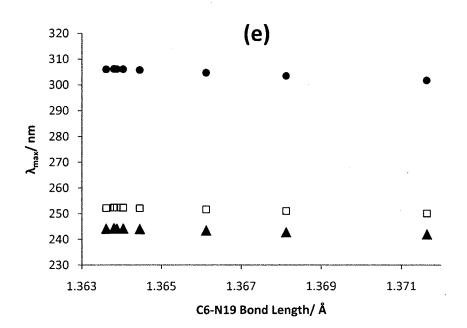
As noted in 3.3.3 B, the twist angle and C-N bond distance are intimately related. Thus, as shown in Figures 3-8(e) for CIS and 3-8(f) for TD-B3LYP, which plots the effect of the solvent induced change in C-N bond length on the three excitation energies, the effect of C-N bond expansion is a red shift in the electronic transition energies. Again, the TD-B3LYP results are more sensitive to changes and the $S_0 \rightarrow S_2$ transition experiences the largest shift at this level of theory.

(d)

(e)
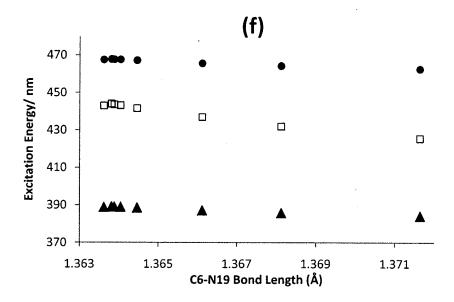
Figure 3-8: (a) Effect of twist angle on the first three CIS excitations of NR. Geometries were optimized at the HF/6-31+G(d) level of theory. (b) Effect of twist angle on the first three excitations of NR. Geometries were optimized at the B3LYP/6-31+G(d) level of theory.(c) Effect of pyramidalization angle on the CIS excitations of NR from HF optimized ground state geometries.(d) Effect of pyramidalization angle on the TD-B3LYP excitations of NR from B3LYP optimized ground state geometries.(e) Effect of C6-N19 bond length on the CIS excitations of NR from HF optimized ground state geometries.(f) Effect of C6-N19 bond length on the TD-B3LYP excitations of NR from B3LYP optimized ground state geometries.● $S_0 \rightarrow S_1$; □ $S_0 \rightarrow S_2$; ▲ $S_0 \rightarrow S_3$

3.3.3 D) Effect of Solvent on the Oscillator strength, Dipole Moment and Polarizability

Changes in oscillator strength, dipole moment and polarizability due to changes in the solvent field dielectric for the $S_0 \rightarrow S_1$ transition in Nile Red are presented in Table 3-2. As mentioned earlier, this transition corresponds to a HOMO$\rightarrow$LUMO transition and experiences a red shift with an increase in solvent polarity. Another feature of this transition is an increase in oscillator strength with increasing dielectric, as seen in Table 3-2. The increase, from 0.74 to 0.96 for TD-B3LYP and from 1.28 to 1.45 for CIS, occurs over a small dielectric range (ε=0-10). Thereafter it remains constant except at the highest dielectric values, where it decreases slightly. The magnitude of the dipole moment of NR (illustrated in Figure 3-9) is also affected by the solvent field, which indicates that the polarizability is non-zero. The B3LYP predicted value in the gas phase is found to be 9.28 D, which is 6 D smaller than the dipole moment of 15.11 D predicted for NR in acetonitrile. Similarly, the HF predicted value in the gas phase is 8.03 D, which is ca. 3 D smaller than the dipole moment of 11.04 D predicted for NR in acetonitrile. As highlighted in the Introduction, there have been several experimental determinations of the ground state dipole moment of NR. Briefly, from thermochromic studies in two different solvents (acetone and 2-methyl tetrahydrofuran) values of 8.4 D and 7 D were obtained,[13,14] while using the Lippert method, which employs many solvents, a ground state dipole moment of 8.9 D was obtained.[13] Using the latter as the more robust value for a permanent dipole moment, one finds that the HF gas phase prediction underestimates the dipole moment by ca. 0.9 D and the corresponding B3LYP value overestimates the dipole moment by ca. 0.4 D. The last item to consider here is the

effect of solvent polarity on the polarizability. Both the B3LYP and HF calculated polarizabilities for the ground state of NR increase with the dielectric constant. The B3LYP polarizabilities exhibit a very large initial shift, from 332 a.u. to about 500 a.u. between $\varepsilon=0$ and $\varepsilon=10$ and then level off at around 520 a.u.. The HF results exhibit a similar trend but begin at 271 a.u. in the gas phase and end at 385 a.u. in acetonitrile. Kawksi et al.[15] suggested that the polarizability should not be neglected in commonly used approaches for determining the dipole moment, it would appear that even when the polarizability is included, one may need to consider its solvent field dependence as well. Krishtal et al. reported the influence of structure on the polarizability of methane sulfonic acid clusters that suggests polarizability can also be partitioned into a field effect and geometry change effect.[38]

Table 3-2: TD-DFT and CIS Oscillator strengths (HOMO→LUMO transition), Dipole Moments and Polarizabilities of NR optimized at B3LYP and HF levels of theory.

ε^*	B3LYP			HF		
	f	μ_g/ D	$<\alpha>$/ a.u.	f	μ_g / D	$<\alpha>$/ a.u.
0.00	0.74	9.28	331.71	1.28	8.03	271.02
2.25	0.95	11.47	401.24	1.44	9.34	314.60
4.52	0.96	13.00	451.30	1.45	10.13	344.37
12.50	0.96	14.41	498.15	1.45	10.76	371.34
20.51	0.95	14.80	511.34	1.45	10.92	378.84
22.53	0.95	14.85	513.11	1.44	10.94	379.76
28.08	0.94	14.98	517.08	1.44	10.99	382.30
33.17	0.94	15.06	520.20	1.44	11.03	383.83
36.64	0.93	15.11	521.82	1.43	11.04	384.64

*See Table 3-1 for solvent description
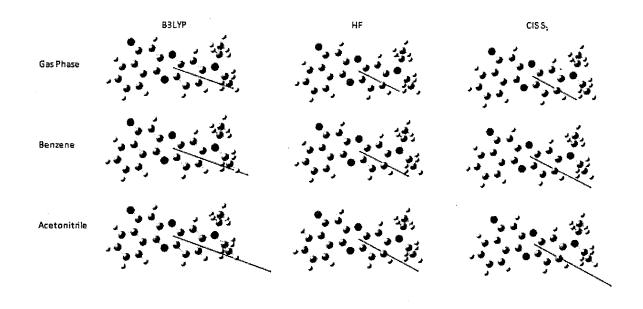
Figure 3-9: Visualization of the ground state B3LYP and HF and CIS excited state dipole moment vectors of NR in gas phase, benzene and acetonitrile.

3.3.4 Effect of solvation on the emission spectra of Nile Red

3.3.4 A) Effect of solvent polarity on the electronic transition

Using the CIS/6-31+G(d) optimized geometries for the first excited state of NR allows one to examine the effect of solvent polarity on the emission spectra. The CIS transition energies at both the ground and excited state optimized geometries are plotted against the change in solvent polarity in Figure 3-10. The previously noted CIS overestimation of the transition energies is observed here as well. In both states, the corresponding optimized geometry at that particular dielectric constant was used for assessing the transition energy. Gas phase (ε=0) and acetonitrile (ε=37) CIS emission energies were found to be 308 nm and 377 nm, respectively, and a more pronounced solvatochromic shift is observed in the emission spectra for larger solvent polarities, consistent with experimental findings[19] (included in supplementary data). In the gas phase, a difference of 6 nm is found between absorption and emission, indicating that the excited state geometry does not have a significant impact on the transition energy.

3.3.4 B) Effect of Solvent Polarity on the excited state Geometry

The solvent induced changes in the excited state geometry for selected geometric parameters are given in Figure 3-11 along with the corresponding changes in the ground state for comparison. The change in the twist angle of NR is given in Figure 3-11(a) and one sees that this parameter in the first excited state exhibits about the same solvent effect as in the ground state. Therefore, the twist angle does not seem to be a
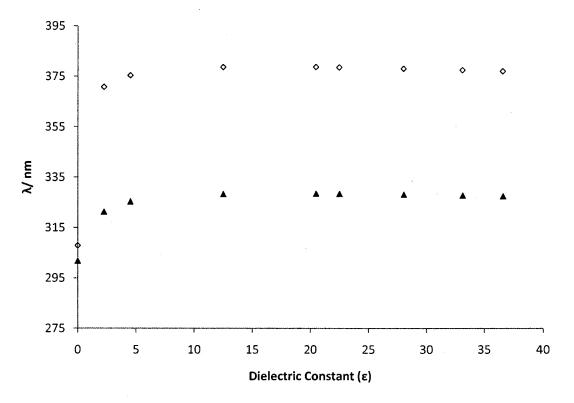
Figure 3-10: Effect of Solvent polarity on the absorption and emission spectra of

NR (CIS and TD-CIS. $\diamondsuit S_1 \rightarrow S_0$; ▲ $S_0 \rightarrow S_1$

factor in the increased excited state solvatochromic effect. The effect of solvent polarity on the pyramidalization of the first excited state is explored in Figure 3-11(b). The nitrogen pyramidalization in the first excited state follows a quadratic rise between $\epsilon=0$ and $\epsilon=10$ and then appears to exhibit a sinusoidal change upon increasing solvent polarity. The near 0° values obtained suggest that there is very little pyramidalization in the ground or first excited state and that the hybridization of the diethylamino nitrogen can be readily described as sp^2. The most significant geometric difference between the ground and excited state occurs for the C-N bond (Figure 3-11(c)). This bond distance in the first excited state of NR is longer than in the ground state, but the difference seems to be about 0.01 Å regardless of solvent polarity.

3.3.4 C) Effect of Solvent polarity on the First Excited State Dipole Moment

The CIS predicted dipole moment for the first excited state is compared with the respective ground state dipole moment in Table 3-3. Except for the gas phase value, all excited state dipole moments are larger than the corresponding ground state values. This would generally confer a red-shift with increasing solvent polarity as the earlier results demonstrated. The odd prediction of the gas phase first excited state dipole moment being less than that of the ground state value could be attributed to the poor accuracy of the CIS method. The overall change in dipole moment ($\Delta\mu=1$—2.4 D) for solvated NR appears to be considerably underestimated in comparison to values found in literature. Most findings for NR have the $\Delta\mu$ anywhere from 3 D to 11.6 D. A theoretical paper by Golini and Williams found a locally excited state of NR having a dipole moment (1.6 D) considerably less than its ground state (5.9D),[13] suggesting that
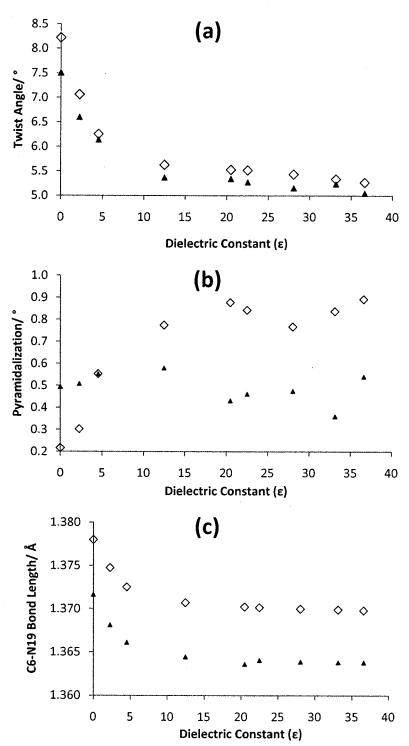
Figure 3-11: (a) Effect of Solvent Polarity on the Twist Angle of NR at CIS and HF optimized state geometries. (b) : Effect of Solvent Polarity on the Pyramidalization of NR at CIS and HF optimized state geometries. (c) Effect of Solvent Polarity on the NR C6-N19 Bond Length (Å) for CIS and HF optimized state geometries. ◇S_1; ▲ S_0

we may have located a locally excited state and further studies on the excited state properties are needed, especially in light of the difference in findings between HF and B3LYP. Also, it should be noted that the optimized excited state geometries of NR were not confirmed to be minima since no frequency analysis was performed due to program limitations.[25]

Table 3-3: Ground and Excited state Dipole Moments of Nile Red solvated in solvent with corresponding polarity.

ϵ^*	HF S_0 μ_g/ D	CIS S_1 μ_e/ D	$\Delta\mu$ / D
0.00	8.03	7.51	-0.52
2.25	9.34	10.33	0.99
4.52	10.13	11.58	1.46
12.50	10.76	12.71	1.94
20.51	10.92	13.02	2.10
22.53	10.94	13.06	2.12
28.08	10.99	13.17	2.18
33.17	11.03	13.25	2.22
36.64	11.04	13.29	2.24

*See Table 3-1 for solvent description

3.4 Conclusions

CIS and TD-B3LYP calculations of the excited states of Nile Red in PCM modeled solvents of various polarities were found to successfully reproduce trends observed in the experimental excitation and emission spectra.

The successful partition of the effect of polarity into a direct effect on the excitation energy and an indirect geometry induced effect on the transition energy provided further insight to the sensitive nature of these electronic transitions in NR. The twist angle about the diethylamino group and planar ring system as well as the related

C-N bond length were found to sufficiently describe the geometric change occurring with increased solvent polarity. The relationship between pyramidalization and excitation energy was negligible and this structural parameter appears to have little effect on the absorption spectrum of NR. The TD-B3LYP calculated excitation energies were found to be more accurate than those from CIS, which seriously overestimated the transition energies. However, both approaches show similar trends, but with the TD-B3LYP results more sensitive to the effects of non-specific solvation. The first excited state of NR was optimized using CIS, but the results suggest it is a locally excited state that exhibits a red shift in the emission spectra. No evidence of a Twisted Intramolecular Charge Transfer (TICT) state was found in this study. However, future experiments using TD-DFT excited state geometries could potentially resolve the matter with a systematic energy scan along the twist angle reaction coordinate.

3.5 References

1 A. K. Dutta, K. Kamada and K. Ohta, *J. Photochem. Photobiol., A*, 1996, 93, 57-64

2 C. Reichardt, *Solvents and Solvent Effects in Organic Chemistry*, WILEY-WCH, Weinheim, 2003

3 P. Suppan and N. Ghoneim, *Solvatochromism*, Royal Society of Chemistry, Cambridge, 1997

4 F. D'Anna, V. Frenna, S. La Marca, R. Noto, V. Pace and D. Spinelli, *Tetrahedron*, 2008, 64, 672-680

5 H. Tajalli, A. G. Gilani, M. S. Zakerhamidi and P. Tajalli, *Dyes Pigm.*, 2008, 78, 15-24

6 A. K. Dutta, K. Kamada and K. Ohta, *Chem. Phys. Lett.*, 1996, 258, 369-375

7 P. Hazra, D. Chakrabarty, A. Chakraborty and N. Sarkar, *Chem. Phys. Lett.*, 2004, 388, 150-157

8 V. J. P. Srivatsavoy, *J. of Lumin.*, 1999, 82, 17-23

9 N. Sarkar, K. Das, D. N. Nath and K. Bhattacharyya, *Langmuir*, 1994, 10, 326-329

10 K. E. Cooksey, J. B. Guckert, S. A. Williams and P. R. Callis, *J. of Microbiol. Methods*, 1987, 6, 333-345

11 G. J. Blanchard, *Chem. Phys.*, 1989, 138, 365-375

12 G. B. Dutt, S. Doraiswamy and N. Periasamy, *J. Chem. Phys.*, 1991, 94, 5360-5368

13 C. M. Golini, B. W. Williams and J. B. Foresman, *J. Fluoresc.*, 1998, 8, 395-404

14 N. Ghoneim, *Spectrochim. Acta, A.*, 2000, 56, 1003-1010

15 A. Kawski, P. Bojarski and B. Kuklinski, *Chem. Phys. Lett.*, 2008, 463, 410-412

16 M. Rappon and S. Gillson, *J. of Mol. Liq.*, 2006, 128, 108-114

17 H. Bischof, W. Baumann, N. Detzer and K. Rotkiewicz, *Chem. Phys. Lett.*, 1985, 116, 180-185

18 P. Suppan, *Chem. Phys. Lett.*, 1986, 128, 160-161

19 Manit Rappon and P. Tuck, unpublished results.

20 W. Rettig and B. Zietz, *Chem. Phys. Lett.*, 2000, 317, 187-196

21 Z. R. Grabowski, K. Rotkiewicz and W. Rettig, *Chem. Rev.*, 2003, 103, 3899-4032

22 W. Rettig and V. Bonacic-Koutecký, *Chem. Phys. Lett.*, 1979, 62, 115-120

23 K. A. Z. e. al., *Pure Appl. Chem.*, 1993, 65, 1745

24 L. Camargo Dias, R. Custodio and F. B. T. Pessine, *Chem. Phys. Lett.*, 1999, 302, 505-510

25 M. J. Frisch, G. W. Trucks, H. B. Schlegel, G. E. Scuseria, M. A. Robb, J. R. Cheeseman, J. A. Montgomery, T. V. Jr., K. N. Kudin, J. C. Burant, J. M. Millam, S. S. Iyengar, J. Tomasi, V. Barone, B. Mennucci, M. Cossi, G. Scalmani, N. Rega, G. A. Petersson, H. Nakatsuji, M. Hada, M. Ehara, K. Toyota, R. Fukuda, J. Hasegawa, M. Ishida, T. Nakajima, Y. Honda, O. Kitao, H. Nakai, M. Klene, X. Li, J. E. Knox, H. P. Hratchian, J. B. Cross, V. Bakken, C. Adamo, J. Jaramillo, R. Gomperts, R. E. Stratmann, O. Yazyev, A. J. Austin, R. Cammi, C. Pomelli, J. W. Ochterski, P. Y. Ayala, K. Morokuma, G. A. Voth, P. Salvador, J. J. Dannenberg, V. G. Zakrzewski, S. Dapprich, A. D. Daniels, M. C. Strain, O. Farkas, D. K. Malick, A. D. Rabuck, K. Raghavachari, J. B. Foresman, J. V. Ortiz, Q. Cui, A. G. Baboul, S. Clifford, J. Cioslowski, B. B. Stefanov, G. Liu, A. Liashenko, P. Piskorz, I. Komaromi, R. L.

Martin, D. J. Fox, T. Keith, M. A. Al-Laham, C. Y. Peng, A. Nanayakkara, M. Challacombe, P. M. W. Gill, B. Johnson, W. Chen, M. W. Wong, C. Gonzalez and a. J. A. Pople, Gaussian 03 (Revision D.01), Gaussian, Inc., Wallingford, CT, 2004

26 A. D. Becke, *Phys. Rev., A* 1988, 38, 3098- 3100

27 C. Lee, W. Yang and R. G. Parr, *Phys. Rev., B*, 1988, 37, 785- 789

28 R. Ditchfield, W. J. Hehre and J. A. Pople, *J. Chem. Phys.*, 1970, 52, 5001-5007

29 J. B. Foresman, M. Head-Gordon, J. A. Pople and M. J. Frisch, *J. Phys. Chem.*, 1992, 96, 135-149

30 S. Mierts, E. Scrocco and J. Tomasi, *Chem. Phys.*, 1981, 55, 117-129

31 M. S. Chauhan, K. Sharma and S. Chauhan, in *Data extract from Landolt-Börnstein IV/17: Static Dielectric Constants of Pure Liquids and Binary Liquid Mixtures,*ed. S. B. Heidelberg, Springer Berlin Heidelberg, 2001,Vol. 17,pp. 854-855

32 A. Dreuw and M. Head-Gordon, *Chem. Rev.*, 2005, 105, 4009-4037

33 J. Preat, P. F. Loos, X. Assfeld, D. Jacquemin and E. A. Perpete, *Int. J. Quant. Chem.*, 2007, 107, 574-585

34 K. Iida, D. Yokogawa, H. Sato and S. Sakaki, *Chem. Phys. Lett.*, 2007, 443, 264-268

35 R. R. Contreras and A. J. Aizman, *Int. J. Quant. Chem.*, 1990, 89-96

36 E. S. Marcos, J. Maraver, M. F. Ruizlopez and J. Bertran, *Can. J. Chem.*, 1986, 64, 2353-2358

37 K. Iida, D. Yokogawa, H. Sato and S. Sakaki, *J. Chem. Phys.*, 2009, 130,

38 A. Krishtal, P. Senet and C. Van Alsenoy, *J. Chem. Theory Comput.*, 2008, 4, 2122-2129

Chapter 4

POLARITY OF NILE RED IN BINARY MIXTURES CONTAINING ACETONITRILE

4.1 Introduction

Nile Red (Figure 4-1) is a lipophilic fluorescent dye that possesses absorption and emission bands that are highly sensitive to its physical and chemical environment. For this reason, Nile Red (NR) has been used as a stain in fluorescence microscopy,[1] a laser dye,[2] and in forensics.[3] NR has also been used as a probe in the microenvironment of polymers,[4,5] ionic liquids,[6,7] proteins and substrates,[8,9] pesticides on vegetables,[10] and as a sensor for organic vapours.[11] Recently, it has helped elucidate the mechanism of protein kinase inhibition for the synthesis of anti-cancer drugs.[12] The sensitive nature of NR is attributed to a large increase in dipole moment magnitude when going from the ground to excited state. The origin and future potential for the application of NR is thus lies in its ground and excited state dipole moment values.

Figure 4-1: Molecular Structure of Nile Red

Experimental determination of the ground and first excited state dipole moment can be obtained with high accuracy using fluorescence polarization, electric dichroism and Stark spectroscopy; however these techniques demand extensive amounts of equipment and have never been used for Nile Red. It is more popular and economical to use a method which measures the absorption and emission band shift as a function of solvent polarity (solvatochromic) or temperature (thermochromic). Both solvatochromic

68

and thermochromic methods plot the Stokes shift (energy difference between the emission and absorption bands) to solvent polarity and temperature respectively, and thus measuring Stokes shift is important. These methods have been used to determine the change in dipole moment of NR. Dutt et al. (1990) first reported a change of 1 D in alcohol-water mixtures.[13] Ohta et al. (1995) reported a change in dipole of 6.8 D for NR in a collection of non-polar and polar solvents.[5] Ghoneim (1999) conducted a thermochromic study of NR in methyl-tetrahydrofuran and 1-butanol and found a change in dipole moment of 7.5 D and 10 D respectively.[14] Most recently, Kawksi and co-workers reported NR dipole moment values using both methods, obtaining change in dipole moment values of 1.8 D $\pm$ 1 D (solvatochromic)[15] and 1.75 D $\pm$ 0.5 D (thermochromic).[16] The large discrepancy from literature values was attributed to poor solvent selection or the assumption that the polarizability of NR is zero. Our previous theoretical investigation[17] of NR predicted a $\Delta\mu$ of 0.99 D in benzene and 2.24 D in acetonitrile in agreement Kawksi et al. values. However, the techniques used (HF and CIS) were shown to overestimate excitation energies and in addition, the predicted HF ground state dipole moment was significantly less than that predicted by density functional theory. For this reason we chose to continue pursuing the $\Delta\mu$ of Nile Red with experimental techniques.

The excitation and emission bands of NR are still of interest and are similar to the donor-acceptor molecule 4-(N,N)-dimethylaminobenzonitrile (DMABN). Both possess a dialkylamino donor group and two maxima in the emission band.[18] This dual fluorescence in NR has been attributed to two minima on the first excited state

69

potential energy surface separated by a large geometry change and accompanied by charge transfer (CT).[19] Proposed geometry changes include a twist of the donor functional group (TICT),[20,21] planarization of the donor (PICT),[22] Pseudo-Jahn-Teller effect[22] and rehybridization of the acceptor (RICT).[23]

The absorption band of NR is also structured but has been given less attention. Ohta et al. who first reported two peaks in the absorption band, monitored the excitation spectra and lifetimes from the emission peak and concluded that they are from the same electronic state, which suggested that vibronics are responsible.[5] Boldrini et al. reported that the inhomogeneous band structure of the absorption and emission spectra can be reproduced by using a two-state electronic model coupled to internal vibrations consistent with Ohta et al., but little information on the geometry change associated with the vibration was given.[24] Yablon et al. also made note of dual absorption and emission peaks for NR in alkanes and olefins which varied as a function of refractive index.[25] However, although they found only the second emission peak to red-shift linearly with the refractive index, both absorption bands can be seen red-shifting in their report, but which absorption maximum to use is not discussed.

Common practice for measuring the Stokes shift is to take the difference of the band maxima (cm^{-1}). For structured spectra of molecules that undergo large geometric changes in the excited state , this approach can result in poor correlation with the solvent descriptor.[26] In this communication, the change in dipole moment $\Delta\mu$ is determined in binary solvent mixtures by plotting the Stokes shift as a function of the

solvent polarity parameter E_T^N. It is well known that preferential solvation in binary mixtures occurs for both Betaine 30[27-31] and Nile Red,[14] and we address its implications in each case. The selection of absorption peak to use in a structured absorption band and its implications on Stokes shift is explored.

In this study, the solvent polarity parameter is derived from the transition energy of the solvent sensitive dye (I): 4-[2,4,6-tri(phenyl)pyridinium-1-yl]-2,6-di(phenyl)phenolate, commonly known as Betaine 30. Details on Betaine 30 have been previously given in a monograph[32] and reviewed;[33] and only a brief presentation is given here. The polarity parameter is represented by the transition energy $E_T(30)$, obtained from the measurement of the maximum absorption wavelength of Betaine 30 in a solvent from where polarity is to be measured. The polarities of a large number of solvents have been determined using the λ_{max} values of the CT $\pi^* \leftarrow \pi$ absorption band of betaine dye and converted into the polarity parameter known as $E_T(30)$ (kcal/mol) using equation (4-1) (where h, c, and N_A are Planck's constant, velocity of light, and Avogadro's number, respectively).

$$E_T(30) = hcN_A\tilde{v} = 28591\frac{1}{\lambda_{max}} \tag{4-1}$$

In order to avoid conversion of the E_T (30) values between the non-SI unit (kcal/mol) and the SI-unit (kJ/mol) and to facilitate fitting of experimental data to a given model, the dimensionless, or normalized, polarity parameter E_T^N is calculated according to equation (4-2), where E_T^N is the normalized polarity parameter whose values for water (E_T^N =1.0000) and tetramethyl silane (E_T^N = 0.0000) are based on

numerical values E_T (30) of 63.1 kcal/mol and 30.7 kcal/mol for water and TMS, respectively.

$$E_T^N = \frac{[E_T(30)_{solvent} - E_T(30)_{TMS}]}{[E_T(30)_{water} - E_T(30)_{TMS}]} = \frac{[E_T(30)_{solvent} - 30.7]}{32.4} \qquad (4\text{-}2)$$

Due to the limited solubility of Betaine 30 in some non-polar solvents and mixtures, the lipophilic Betaine 45, which possesses tert-butyl groups substituted on the peripheral phenyl groups in the 4- positions, is used. Its solvent polarity parameter, E_T (45), can be converted to E_T(30) using equation (3).[33]

$$E_T(30) = \frac{[E_T(45) - 1.808]}{0.9424} \qquad (4\text{-}3)$$

The change in dipole moment $\Delta\mu$ can be obtained from the slope of the line when plotting the Stokes shift against the solvent polarity parameter E_T^N,[32] according to equation (4-4).

$$\tilde{v}_{abs} - \tilde{v}_{fluo}(cm^{-1}) = 11307.6 \times \left[\left(\frac{\Delta\mu}{\Delta\mu_B}\right)^2 \left(\frac{a_B}{a}\right)^3 \right] E_T^N + \text{constant} \qquad (4\text{-}4)$$

Where $\tilde{v}_{abs}$ and $\tilde{v}_{fluo}$ are the absorption and emission maxima, and $\Delta\mu$ is the change in dipole moment for Nile Red (NR). $\Delta\mu_B$ (9 D) is the change in dipole moment for Betaine 30 determined from Stark spectroscopy[34] and a_B (6.2 Å) is the Onsager cavity radius for Betaine 30.[35] The Onsager cavity radius for NR is denoted "a" and is estimated from Van der Waals volumes. However, different models can be employed for calculating the volume and this is has been the case for Nile Red. Ohta and coworkers

have used determined the radius to be 5Å,[5] while Kawski used the same cavity radius of 4.1Å, originally used by Dutt.[13] We chose to use the value of Ohta (5Å), although there is little consequence in having a poor approximation for the cavity size to the E_T^N method. This is because any error in the estimation of the radius is overcome by taking a ratio of the cavity volumes of Betaine 30 and Nile Red. Thus the plot of the Stokes shift, LHS of equation (4-4), against E_T^N yields a straight line whose slope is used in the determination $\Delta\mu$ for each set of binary solvent mixtures.

It is worth mentioning that the Stokes shift has been found to correlate better to E_T^N than previous formulations of solvent polarity.[35] This is because the E_T^N method, as developed by Ravi and co-workers, eliminates the error associated with a poor cavity radius approximation as discussed, and also accounts for solute polarizability, and dielectric enrichment.[35] The E_T^N method does not assume the polarizability of the solute to be zero, as due the formulation derived from the F_1 and F_2 parameters, since the solvent is characterized by the Betaine 30 dye which can partially account for the polarizability of the solvent. In binary mixtures, dielectric enrichment (DE) may occur and a disproportionate amount (relative to the bulk of the mixture) of the more polar solvent may accumulate in the solvent shells around the solute molecule. In this study, the degree of DE occurring for both Nile Red and Betaine 30 is assessed through the plotting of their spectral data vs. the mole fraction of the more polar solvent.

4.2 Experimental

NR was purchased from Sigma-Aldrich and was used without further purification. The solvents used were acetonitrile, ethyl acetate, benzene, fluorobenzene, chlorobenzene, bromobenzene and iodobenzene which were obtained from Sigma-Aldrich. They were dried with molecular sieves for at least 72 hours before use. Betaine dye and its tert-butyl substitute were a gift from Prof. Dr. Christian Reichardt (Marburg, Germany) and were used as received.

Binary mixtures of each solvent with acetonitrile were prepared. The concentration of stock solution of NR in each solvent was 1.97×10^{-5} M. One mL of stock solution was added to various amounts of solvent and each was made up to 25 mL with acetonitrile. The spectra of betaine in mixtures and fluorescent spectra of each mixture were recorded with Perkin Elmer Lambda 11 UV/VIS spectrometer and Perkin Elmer LS 50B luminescence spectrophotometer, respectively.

4.3 Results and Discussion

4.3.1 Band structure and its Implications

The absorption bands of Nile Red in AcN / EtOAc are shown in figure 4-2(a). It can be seen that in neat ethyl acetate, the absorption band is comprised of 2 maxima at 523 nm and 535 nm with the former being the absolute maximum. However, with increasing solvent polarity (increasing the mole fraction of AcN), the peak at 523 nm does not change by more than 2 nm, while the peak at 535 nm red-shifts toward 549nm in neat acetonitrile. The intensity of the two absorption peaks also change with increasing
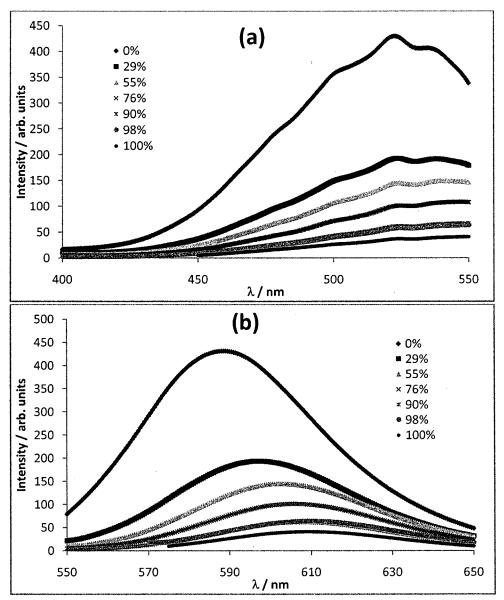
Figure 4-2: (a) Absorption and (b) Emission Spectra of Nile Red in ethyl acetate, acetonitrile, and ethyl acetate/binary mixtures comprised of different mole fractions of acetonitrile.

solvent polarity, as the red-shifting peak becomes the absolute maximum with increased AcN composition. For determining the dipole moment of Nile Red, only one absorption peak should be selected for all mixtures to avoid a discontinuity in the linear plot of equation (4-4). In the thermochromic analysis reported by Kawski, Nile Red in EtOAc was shown to have two peaks in the absorption band at room temperature, however at high temperature, only the more red-shifted peak is observed and thus only one absorption peak can be used to obtain the Stokes shift. Yet the significance of the absorption maximum at 523 nm that disappeared at higher temperatures was never discussed, and it may be of vibronic, electronic or conformational origins.

From our previous unpublished work using cyclohexane / ethyl acetate solvent mixtures, it was found that using the peak at 520-525 nm provided good correlation (r^2=0.9828), whereas the red-shifting peak maximum was not always present so that a Stokes shift measurement could be taken. In cyclohexane / nitrobenzene mixtures, the red-shifting peak was present in all six mixtures investigated, but the plot of Stokes shift vs. E_T^N resulted in a poor linear regression. In this report, it is shown that for the AcN/ substituted benzene series, two sets of Stokes shifts values (per solvent mixture) can be obtained and both correlate well with the solvent parameter E_T^N, and result in two different values for the change in dipole moment.

In the following sections both sets of Stokes shifts are plotted against a common solvent polarity parameter E_T^N: the first set uses the absorption maxima that is not

sensitive to solvent polarity (~523 nm) and is designated as Set 1, while Set 2 uses the absorption maximum that red-shifts from approximately 530 nm to 550 nm.

The emission bands of Acetonitrile (AcN) / Ethyl acetate (EtOAc) are shown in Figure 4-2(b). It can be seen that in neat ethyl acetate, the emission maximum is at 588 nm. Increasing the mole fraction of acetonitrile resulted in a red-shift of the emission maximum from 588 nm to 610 nm. In all solvents (both neat and binary), only an emission peak with charge transfer nature was found. Thus the Stokes shift can be taken from one set of emission peaks.

4.3.2 Acetonitrile / Ethyl Acetate Mixtures

The plot of Stokes shift vs. E_T^N is shown in Figure 4-3(a). Set 1 (Stokes shift obtained using the stationary absorbance peak) yields a plot that gives good correlation (r^2=0.9842) and a slope of 2241.7. The change in dipole moment was found to be 2.90 D and an error of 1.27 D, which were calculated from the slope and standard deviation of the slope, respectively.

Set 2 (Stokes shift obtained using the red-shifting absorption maximum) yields a plot that has poor linear correlation (0.0729) and a slope of 205.2. The change in dipole moment obtained from the second set was found to be 0.88 D with an error of 0.74 D. For Set 1, no literature has ever been reported using this absorption maximum. However, it is the most reliable, as will be evident in further sections, because it is always present as a maximum in neat non-polar, neat polar solvents and the mixtures
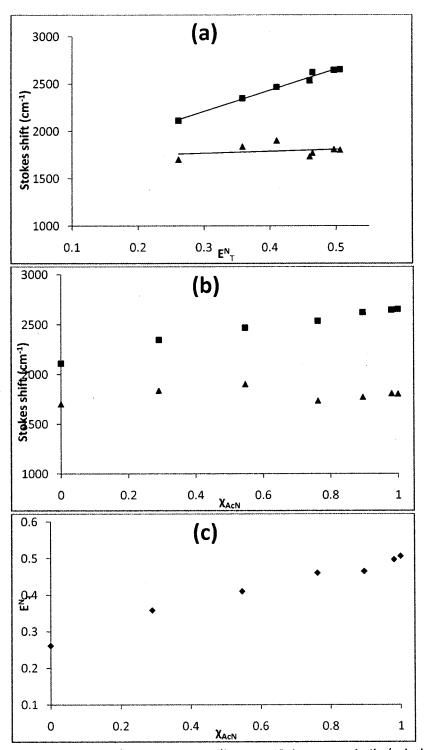
Figure 4-3: Plots corresponding to NR in acetonitrile/ethyl acetate binary mixtures:
(a) solvatochromic plot of Stokes shift vs. solvent polarity parameter E_T^N: ■ Set 1 and ◆ Set 2, (b) Plot of Stokes shift vs. mole fraction of acetonitrile for: ■ Set 1 and ◆ Set 2, (c) Plot of the solvent polarity parameter E_T^N vs. mole fraction of acetonitrile.

presented in this study. The change in dipole moment from Set 1 is in agreement with the work by Kawski et al, who reported values of 1.8 D from a solvatochromic technique in neat solvents.[15] Perhaps of more interest, Kawski also found a $\Delta\mu$ of 1.9 D in Ethyl acetate and 1.6 D in 1, 2-Dichloroethane (average of 1.75 D) from a thermochromic study.[16] If Kawski had used the same Onsager cavity Radii for NR (5Å), his average value would be 2.35 D. This value is only different from our reported value by 0.55 D. Kawski also mentioned that assuming the polarizability of NR to be zero can result in overestimation of $\Delta\mu$ (5-11 D), which several authors did.[5,36,37] However, Kawski and co-workers used the absorption band corresponding to Set 2 in which we obtained a lower $\Delta\mu$ (0.88 D) and a very poor regression coefficient (r^2=0.0729). Comparing to our theoretical investigation of NR by *ab initio* methods, we found a change in dipole moment from between 1.0 D in benzene and 2.2 D in acetonitrile.[17] The work of Yablon and coworkers found the absorption peak of NR in non-polar solvents (heptanes, dodecane and poly-alpha olefins) to have the red-shifting peak as the absolute maximum at about 490 nm, but it is not discussed as to why it is only a local maximum in the higher polar solvents.[25]

Set 2, which uses the red-shifting peak to obtain Stokes shift values, appears to have a linear relationship for the first three data points, but a sudden decrease in Stokes Shift from 1904 cm^{-1} to 1735 cm^{-1} occurs and little sensitivity after a E_T^N value of 0.4105 is observed. This non-linearity makes the plot unreliable for attaining a change in dipole moment since there will be a large error associated with its calculation.

Since preferential solvation can occur for NR, Betaine 30, or both, we have plotted both Stokes shift and E_T^N vs. mole fraction of AcN and they are shown in Figures 4-3(b) and 4-3(c), respectively. These plots assess non-ideal increases of each variable with the mole fraction of AcN because of dielectric enrichment. In Figure 4-3(b), Set 1 is shown to have a slight deviation as the Stokes shift is greater than ideality. However, the plot of E_T^N vs. χ_{AcN} is also shown to deviate from ideality, indicating that a higher χ_{AcN} ratio is present in the solvent shell than the bulk of the mixture, especially at small fractions. This however has little impact on the plot of Stokes shift vs. E_T^N plot since no curvature is observed.

4.3.3 Acetonitrile / Benzene

The plot of Stokes shift vs. E_T^N for Nile Red in AcN/benzene is shown in Figure 4-4(a). It can be seen that using either set of Stokes shifts produced a linear plots. The line of best fit for Set 1 was found to have a slope of 2790.4 and an r^2=0.9732. The slope of the line of best fit for Set 2 was found to be 1673. 8 and the regression coefficient was r^2=0.9474. The change in dipole moment obtained from Set 1 was found to be 3.24 D $\pm$ 0.94 D, while for Set 2 the change in dipole moment was 2.51 D $\pm$ 0.81 D. The discrepancy between the two slopes is large and it originates from the absorption bands used, since the two sets use common E_T^N and emission maxima values. $\Delta\mu$ of Set 2 is in better agreement with the values of Kawski, being different from his thermochromic $\Delta\mu$ values by 0.15 D, possibly due to Set 2 being the more correct pairing of excitation/emission maxima. Set 2 corresponds to the absorption band that experiences a red-shift upon increasing solvent polarity, which is also the case for the one emission
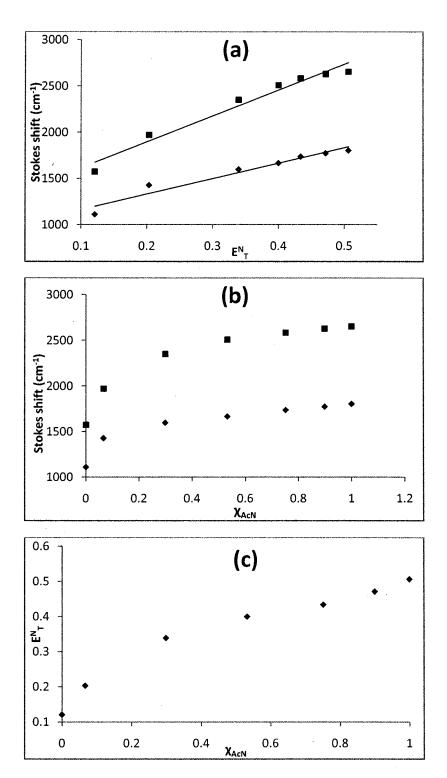
Figure 4-4: Plots corresponding to NR in acetonitrile/benzene binary mixtures: **(a)** solvatochromic plot of Stokes shift vs. solvent polarity parameter E_T^N: ■ Set 1 and ◆ Set 2, **(b)** Plot of Stokes shift vs. mole fraction of acetonitrile for: ■ Set 1 and ◆ Set 2, **(c)** Plot of the solvent polarity parameter E_T^N vs. mole fraction of acetonitrile.

maximum used. In contrast, the usage of Stokes shifts from Set 1 has been shown to be effective in every case, and for this reason each set remains valuable.

The effect of dielectric enrichment (DE) around NR is shown in Figure 4-4(b), while the effect of DE around Betaine 30 is shown in Figure 4-4(c). AcN/benzene mixtures have been known to behave in a non-ideal way, however, it was necessary to investigate whether DE would occur around both solutes.[38] It can be seen that NR has an affinity for the more polar solvent AcN, since both Set 1 and Set 2 exhibit a rapid increase in Stokes shift while the χ_{AcN} is low. Betaine 30 also experiences DE and has an affinity for AcN, since a rapid increase in E_T^N is observed after just a small increase in χ_{AcN}. DE occurs more around NR than for Betaine 30. This is evident in the solvatochromic plot in Figure 4-4(a), in which both Sets 1 and 2 experience curvatures with downwards inflections. Hypothetically, in the event that DE would occur more for Betaine 30 than NR, a curvature of upwards inflection would be observed. The consequence of any curvature is a slope with a larger associated error. In the sections 3.4 through 3.7, it is shown that Set 1 appears to continue this trend of having the DE of NR being greater than the DE of Betaine 30, however for Set 2 the opposite is true.

4.3.4 Acetonitrile / Fluorobenzene

The plot of Stokes shift vs. E_T^N for Nile Red in AcN/fluorobenzene is shown in Figure 4-5(a). For Set 1, the line of best fit was found to have a slope of 2358.7 and a regression coefficient of r^2=0.9642. The resulting $\Delta\mu$ was then found to be 2.98 D with an error of 0.92 D. For Set 2, the line of best fit was found to have a slope of 1144.5 and
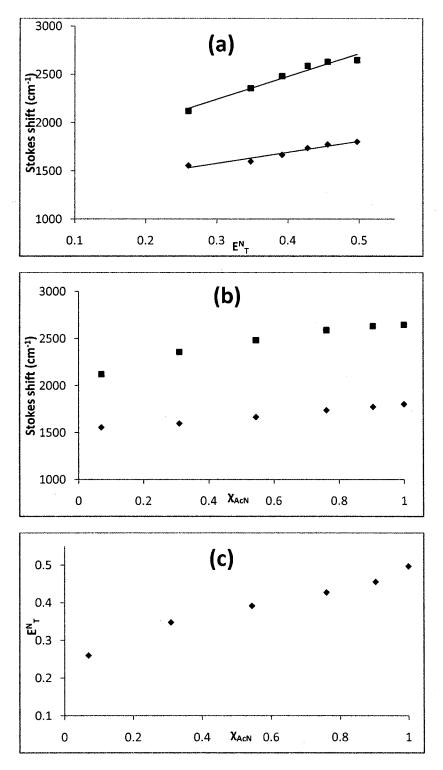
Figure 4-5: Plots corresponding to NR in acetonitrile/fluorobenzene binary mixtures: **(a)** solvatochromic plot of Stokes shift vs. solvent polarity parameter E_T^N: ■ Set 1 and ◆ Set 2, **(b)** Plot of Stokes shift vs. mole fraction of acetonitrile for: ■ Set 1 and ◆ Set 2, **(c)** Plot of the solvent polarity parameter E_T^N vs. mole fraction of acetonitrile.

a regression coefficient of r^2=0.9485. The resulting $\Delta\mu$ is then 2.07 with an error of 0.71 D. Similar to that of the AcN/benzene mixtures, the slope determined from Set1 was found to be larger than that found for Set 2. However, they are in poorer agreement with each other, differing by 0.9 D.

The large discrepancy is due to a lower value of $\Delta\mu$ from Set 1 and an even lower value of $\Delta\mu$ from Set 2. As mentioned in sections 4.3.2 and 4.3.3, the $\Delta\mu$ obtained from Set 1 may be overestimated due to the error brought on by dielectric enrichment (DE) which occurs more for Nile Red than for Betaine 30. This results in curvature with a downwards inflection in the solvatochromic plot of Stokes shift vs. E_T^N and thus a larger associated error. The evidence of DE can be seen in Figures 4-5(b) and 4-5(c), where Figure 5-4(b) is the plot of Stokes shift vs. χ_{AcN} and Figure 4-5(c) is the plot of the solvent polarity parameter E_T^N vs. χ_{AcN}. Figure 4-5(b) shows that Set 1 shows some deviation from ideality, and that Nile Red experiences some DE upon increasing χ_{AcN}. The DE is considerable less for NR in AcN/fluorobenzene mixtures than the DE that occurred in AcN/Benzene mixtures, which is expected because fluorobenzene possesses a static dipole moment, while benzene does not.

For Set 2, the $\Delta\mu$ obtained in AcN/fluorobenzene has decreased from 2.51 D to 2.07 D relative to the AcN/benzene mixtures. It was found that the Stokes shift of Set 2 followed ideality. DE did occur around Betaine 30 and this lead to a curvature with an upwards inflection in the solvatochromic plot of Set 2,which is evident in Figure 4-5(a),

84

but deviation from non-ideality is less than what was found for AcN/benzene mixtures. This curvature will also lead to an increase in error associated with $\Delta\mu$.

4.3.5 Acetonitrile / Chlorobenzene

The solvatochromic plot of Stokes shift vs. E_T^N for Nile Red in AcN/chlorobenzene is shown in Figure 4-6(a). For Set 1 the line of best fit possessed a slope of 2164.1 and a regression coefficient of $r^2=0.9549$. The calculated $\Delta\mu$ was determined to be 2.85 D with an error of 0.94 D. This value is in agreement with the $\Delta\mu$ obtained from Set 1 for NR in AcN/EtOAc (2.90 D ± 1.27 D) and AcN/fluorobenzene (2.98 D ± 0.92 D) mixtures. In Figure 4-6(b), which is the plot of Stokes shift vs. χ_{AcN}, it can be seen again that DE occurs for the absorption band of Set 1. Betaine 30 experiences very little DE, which is evident in the near-ideal plot of Figure 4-6(c). The consequence of only NR experiencing DE results in a slight curvature, and the correlation coefficient of the solvatochromic plot (Figure 4-6(a)) is fairly good ($r^2=0.9549$). For Set 2, the line of best fit possessed a slope of 1359.6 $\Delta\mu$ was found to be 2.26 D ± 0.54 D, which is between that obtained for NR in AcN/fluorobenzene (2.07 D) and AcN/benzene (2.51 D) mixtures.

Figure 4-6(b) is the plot of Stokes shift vs. χ_{AcN} and it shows, for Set 2, DE around NR is minimal and can be considered ideal whereas for Set 1 some DE occurs. DE of Betaine 30 in chlorobenzene/AcN mixtures is also observed and thus curvature in the solvatochromic plot 4-6(a) is noted. Despite this, the curvature was minimal as the regression coefficient for Set 2 ($r^2=0.9864$) is quite good.
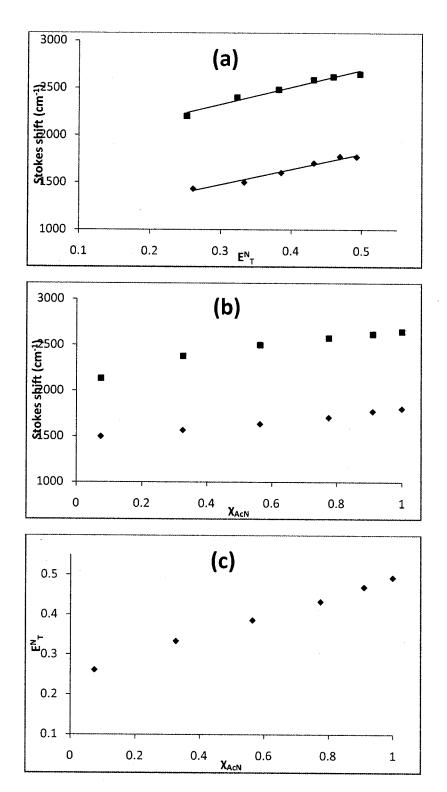
Figure 4-6: Plots corresponding to NR in acetonitrile/chlorobenzene binary mixtures:
(a) solvatochromic plot of Stokes shift vs. solvent polarity parameter E_T^N: ■ Set 1 and ◆
Set 2, (b) Plot of Stokes shift vs. mole fraction of acetonitrile for: ■ Set 1 and ◆ Set 2,
(c) Plot of the solvent polarity parameter E_T^N vs. mole fraction of acetonitrile.

4.3.6 Acetonitrile / Bromobenzene

The solvatochromic plot of Stokes shift vs. E_T^N for Nile Red in AcN/bromobenzene is shown in Figure 4-7(a). For Set 1 the line of best fit possesses a slope of 1820.1 and a regression coefficient of $r^2=0.9701$. The calculated $\Delta\mu$ was 2.62 D with an error of 0.94 D. Again, this value is slightly lower than the values of AcN/fluoro- (2.98 D) and AcN/chloro- (2.85D) benzenes but there is fairly good agreement. In Set 2, the line of best fit possessed a slope of 1551.7 and the calculated $\Delta\mu$ was then determined to be 2.41 D with an error of 0.73 D. This value is comparable to the values found in chloro- and fluoro- substituted benzenes as well as benzene itself.

The analysis of DE is also comparable to the other two substituted benzenes analyzed. The plot of the Stokes shift vs. χ_{AcN} is shown in Figure 4-7(b). It can be seen that minimal DE occurs to in AcN/bromobenzene mixtures. In Figure 4-7(c), it can be seen that the DE of Betaine 30 is also similar to that found in the fluoro- and chloro-substituted benzenes. The result again is a solvatochromic plot (Figure 4-7(a)) with downwards curvature but does not affect the linearity of the Stokes shift vs. E_T^N, since the regression coefficient of $r^2=0.9681$ shows a good linear relationship. The effect of substitution for the increasing order of $\Delta\mu$ was now found to be Br<Cl~F<H, which suggests that $\Delta\mu$ of NR is dependent on substituent (atomic) size or polarizability for the halogenated benzene used. If the polarizability is responsible for the lowering of the calculated $\Delta\mu$, then it would be fair to assume that investigating NR in a highly polarizable solvent will give lower Set 1 $\Delta\mu$ values than for a solvent that is not polarizable.

Figure 4-7: Plots corresponding to NR in acetonitrile/bromobenzene binary mixtures: (a) solvatochromic plot of Stokes shift vs. solvent polarity parameter E_T^N: ■ Set 1 and ♦ Set 2, (b) Plot of Stokes shift vs. mole fraction of acetonitrile for: ■ Set 1 and ♦ Set 2, (c) Plot of the solvent polarity parameter E_T^N vs. mole fraction of acetonitrile.

The analysis of DE is also comparable to the other two substituted benzenes analyzed. The plot of the Stokes shift vs. χ_{AcN} is shown in Figure 4-7(b). It can be seen that minimal DE occurs to in AcN/bromobenzene mixtures. In Figure 4-7(c), it can be seen that the DE of Betaine 30 is also similar to that found in the fluoro- and chloro-substituted benzenes. The result again is a solvatochromic plot (Figure 4-7(a)) with downwards curvature but does not affect the linearity of the Stokes shift vs. E_T^N, since the regression coefficient of r^2=0.9681 shows a good linear relationship. The effect of substitution for the increasing order of $\Delta\mu$ was now found to be Br<Cl~F<H, which suggests that $\Delta\mu$ of NR is dependent on substituent (atomic) size or polarizability for the halogenated benzene used. If the polarizability is responsible for the lowering of the calculated $\Delta\mu$, then it would be fair to assume that investigating NR in a highly polarizable solvent will give lower Set 1 $\Delta\mu$ values than for a solvent that is not polarizable.

The order of increasing Set 2 $\Delta\mu$ for the series of substituted benzene solvents is F<Cl<Br<H. Thus far, the order indicates that there is a relationship between the polarity range of solvents which one investigates NR and the calculated $\Delta\mu$. The $\Delta\mu$ may be dependent on the polarity range that Nile Red is being investigated, because the benzene (-H) would evaluate the Stokes shift of NR in a significantly larger polarity range (E_T^N=0.12 to E_T^N=0.51), while chlorobenzene and fluorobenzene evaluates NR in a smaller polarity range (E_T^N=0.26 to E_T^N=0.51). Our unpublished results of NR in cyclohexane/EtOAc binary mixtures supports this speculation, since we found a NR $\Delta\mu$ value of 4.77 D, which analyzes NR in the non-polar to moderately polar solvent region

(E_T^N=0.04 to E_T^N=0.26). It is hypothesized that Δμ is dependent on the polarity range because the ground state dipole moment (μ$_g$) increases dramatically to the external field of the solvent and the E_T^N method measures the change of the induced dipole moments. Supporting this is our DFT study of Nile Red in which the gas phase Δμ$_g$ (9.28 D) was significantly lower than Δμ$_g$ in acetonitrile (15.11 D). This means that polarizability of NR must be taken into consideration. Kawski was first to point out that NR should not be assumed to have a polarizability of zero, however the validity and impact of their assumption that 2α/a$_0$ = 1 is a fix to accounting for the polarizability of NR also needs to be questioned.

4.3.7 Acetonitrile / Iodobenzene

The solvatochromic plot of Stokes shift vs. E_T^N for Nile Red in AcN/iodobenzene is shown in Figure 4-8(a). For Set 1 the line of best fit possesses a slope of 1450.4 and the change in dipole moment was found to be 2.33 D ± 0.89 D. The Δμ determined is considerably less than that found in previous mixtures using Set 1. The trend of increasing Δμ as an effect of halo-substitution is I<Br<Cl<F<H, confirming that the variability in Δμ is dependaent on the polarizability of the solvent.

The effect of dielectric enrichment of NR in iodobenzene/AcN mixtures can be seen in Figure 4-8(b). It can be seen that there is considerably more DE occurring in this mixture than the other substituted benzene systems. However in Figure 4-8(c), which shows the DE of Betaine 30 in iodobenzene/AcN mixtures, solvation of Betaine 30 is also of non-ideality. The combination of DE occurring to both solvent shells of NR and

90
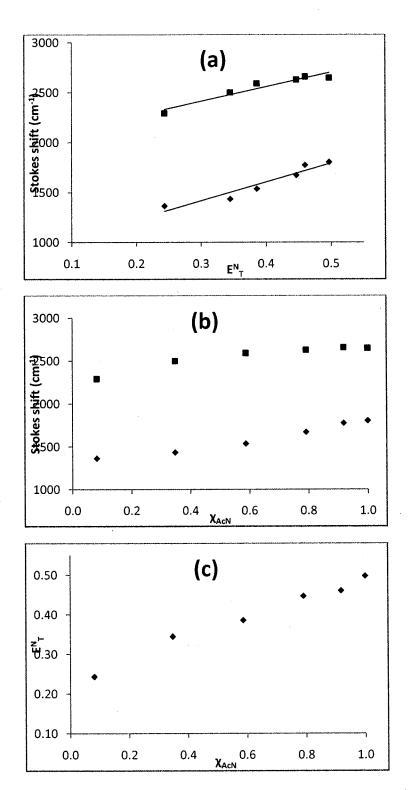
Figure 4-8: Plots corresponding to NR in acetonitrile/iodobenzene binary mixtures: (a) solvatochromic plot of Stokes shift vs. solvent polarity parameter E_T^N: ■ Set 1 and ◆ Set 2, (b) Plot of Stokes shift vs. mole fraction of acetonitrile for: ■ Set 1 and ◆ Set 2, (c) Plot of the solvent polarity parameter E_T^N vs. mole fraction of acetonitrile.

Betaine 30 may be the reason for the poorer correlation (r^2=0.9208) in the solvatochromic plot of Set 1.

For Set 2, the line of best fit has a slope of 1875.8 and the change in dipole moment was 2.65 D ± 0.89 D. What is striking is that the calculated $\Delta\mu$ for Set 2 is larger than the $\Delta\mu$ for Set 1, which was not the case for any other solvent mixture. The DE occurred for Nile Red in a way that did not occur for all other solvent systems. In Figure 4-8(b), it can be seen that the plot of Stokes shift against χ_{AcN} produced a non-linear plot with upwards curvature. This upwards curvature is indicative that the local χ_{AcN} NR is smaller than the bulk χ_{AcN}, meaning NR has a greater affinity for iodobenzene over acetonitrile. However, as seen in Figure 4-8(c), the local χ_{AcN} around the solvent shell of Betaine 30 remains larger than the bulk χ_{AcN}, and the resulting solvatochromic plot of the Stokes shift vs. E_T^N has an upwards point of inflection.

4.4 Conclusions

Plotting of the Stokes shift of NR against the solvent polarity parameter E_T^N were successful; however the presence of two absorption maxima required that two sets of Stokes shift be plotted against solvent polarity. The two sets of Stokes shifts (Set 1 and Set 2) were found to yield different values for the $\Delta\mu$ of NR (A summary is given in Table 4-1). For Set 1, the variability of $\Delta\mu$ was found to follow the polarizability of the halobenzene solvent, in agreement with Kawski's caution that a polarizable solvent will affect $\Delta\mu$. For Set 2, the variability in $\Delta\mu$ was dependent on the polarity range for which NR was investigated, which is related to the non-zero polarizability of NR. It also agrees with the cautions put forth by Kawski. However, the $\Delta\mu$ values of NR in polarizable

binary mixtures remain in good agreement with Kawski's values and our theoretical study, thus their impact is minimal.[15,16,17] Although, the usage of the absorption peak that red-shifted (Set 2) appeared to be the more logical one to pair with the emission peak since both red-shifted with increasing solvent polarity, it was found there was no linear plot of using Set 2 in AcN/EtOAc binary mixtures and thus was not reliable. However, the absorption peak corresponding to Set 1 was a stationary peak (solvent insensitive) and was found to reliably produce a linear plot in all solvent mixtures. The average values of the $\Delta\mu$ obtained from Set 1 and Set 2 (AcN/EtOAc excluded because of poor correlation) was found to be 2.81 D ± 0.96 D and 2.38 D ± 0.76 D respectively. Set 1 was found to be in good agreement with the $\Delta\mu$ of Kawski and co-workers, who report a $\Delta\mu$ of 2.35 D when using an Onsager cavity radius of 5 Å for NR. We chose not to report a $\Delta\mu$ that is an average from Set 1 and 2, because there was insufficient evidence to suggest that they come from the same electronic band. One set of Stokes shifts may involve an excitation to an excited state surface from which the emission does not take place.

Table 4-1: Change in dipole moments for Sets 1 and 2 in Acetonitrile/co-solvent binary mixtures. The slopes, y-intercepts and correlation coefficients (r^2) of the line of best fit for the plot Stokes shift vs. E_T^N also are tabulated.

Co-solvent	Set	(slope)	y-intercept	r^2	$\Delta\mu$ (D)*
Ethyl acetate	1	2241.7	1538.7	0.9842	2.90±1.27
	2[†]	205.17	1708.7	0.0729[†]	0.88±0.74
Benzene	1	2790.4	1340	0.9732	3.24±0.94
	2	1673.8	998.4	0.9474	2.51±0.81
Fluorobenzene	1	2358.7	1537.8	0.9641	2.98±0.92
	2	1144.5	1237.2	0.9485	2.07±0.71
Chlorobenzene	1	2164.1	1619.5	0.9549	2.85±0.94
	2	1359.6	1126.8	0.9864	2.26±0.54
Bromobenzene	1	1820.1	1779.7	0.9701	2.62±0.78
	2	1551.7	1025.3	0.9681	2.41±0.73
Iodobenzene	1	1450.4	1980	0.9208	2.33±0.89
	2	1875.8	856.3	0.9198	2.65±1.02

*Error determined from the standard deviation of the slope of the regression line.

[†]non-linear plot

4.5 References

1 D. L. Sacket, J. R. Knutson and J. Wolff, *J. Biol. Chem.*, 1990, 265, 14899-14906

2 D. Basting, D. Ouw and F. P. Schäfer, *Opt. Commun.*, 1976, 18, 260-262

3 E. Navarro, A. Castello, J. A. Lopez-Alfaro and F. Verdu, *J. Forensic. Leg. Med.*, 2007, 14, 340-342

4 A. K. Dutta, K. Kamada and K. Ohta, *J. Photochem. Photobiol., A*, 1996, 93, 57-64

5 A. K. Dutta, K. Kamada and K. Ohta, *Chem. Phys. Lett.*, 1996, 258, 369-375

6 S. V. Dzyuba and R. A. Bartsch, *Tetrahedron Lett.*, 2002, 43, 4657-4659

7 H. Tajalli, A. G. Gilani, M. S. Zakerhamidi and P. Tajalli, *Dyes Pigm.*, 2008, 78, 15-24

8 D. L. Sackett and J. Wolff, *Anal. Biochem.*, 1987, 167, 228-234

9 A. Nath, C. Fernández, J. N. Lampe and W. M. Atkins, *Arch. Biochim. Biophys.*, 2008, 474, 198-204

10 S. Hassoon and I. Schechter, *Anal. Chim. Acta*, 1998, 368, 77-82

11 D. Li, C. A. Mills and J. M. Cooper, *Sens. Actuators, B,* 2003, 92, 73-80

12 S. L. Black, W. A. Stanley, F. V. Filipp, M. Bhairo, A. Verma, O. Wichmann, M. Sattler, M. Wilmanns and C. Schultz, *Bioorg. Med. Chem.,* 2008, 16, 1162-1173

13 G. B. Dutt, S. Doraiswamy and N. Periasamy, *J. Chem. Phys.*, 1991, 94, 5360-5368

14 N. Ghoneim, *Spectrochim. Acta., A,* 2000, 56, 1003-101

15 A. Kawski, P. Bojarski and B. Kuklinski, *Chem. Phys. Lett.*, 2008, 463, 410-412

16 A. Kawski, B. Kuklinski and P. Bojarski, *Chem. Phys.*, 2009, 359, 58-64

17 P. O. Tuck, R. C. Mawhinney and M. Rappon, *Phys. Chem. Chem. Phys.*, 2009, 4471-4480

18 E. Lippert, W. Luder and H. Boos, Adv. Mol. Spectrosc., Pergamon Press, Oxford, 1962

19 Z. R. Grabowski, K. Rotkiewicz and W. Rettig, *Chem. Rev.*, 2003, 103, 3899-4032

20 W. Rettig and V. Bonacic-Koutecký, *Chem. Phys. Lett.*, 1979, 62, 115-120

21 W. Rettig and E. Lippert, J. Mol. Structure: THEOCHEM, 1980, 80, 17

22 G. Berden, J. vanRooy, W. L. Meerts and K. A. Zachariasse, *Chem. Phys. Lett.*, 1997, 278, 373-379

23 N. Chattopadhyay, C. Serpa, M. M. Pereira, J. S. de Melo, L. G. Arnaut and S. J. Formosinho, *J. Phys. Chem., A,* 2001, 105, 10025-10030

24 B. Boldrini, E. Cavalli, A. Painelli and F. Terenziani, *J. Phys. Chem. A*, 2002, 106, 6286-6294

25 D. G. Yablon and A. M. Schilowitz, *Appl. Spectrosc.*, 2004, 58, 843-847

26 P. Suppan and N. Ghoneim, *Solvatochromism*, Royal Society of Chemistry, Cambridge, 1997

27 N. Ray, R. Pramanik, P. Kumar Das and S. Bagchi, *Chem. Phys. Lett.*, 2001, 341, 255-262

28 N. Ghoneim, *Spectrochim. Acta, A*, 2001, 57, 1877-1884

29 N. Ray and S. Bagchi, *Chem. Phys. Lett.*, 2002, 364, 621-627

30 A. Maitra and S. Bagchi, *J. Mol. Liq.*, 2008, 137, 131-137

31 M. Rappon and S. Gillson, *J. Mol. Liq.*, 2006, 128, 108-114

32 C. Reichardt, *Solvents and Solvent Effects in Organic Chemistry*, WILEY-WCH, Weinheim, 2003

33 C. Reichardt, *Pure Appl. Chem.*, 2008, 80, 1415-1432

34 W. Liptay, B. Dumbache and H. Wesenbe, Z. *Naturforsch., A: Phys. Sci.*, 1968, A23, 601

35 M. Ravi, A. Samanta and T. P. Radhakrishnan, *J. Phys. Chem.*, 1994, 98, 9133-9136

36 N. Sarkar, K. Das, D. N. Nath and K. Bhattacharyya, *Langmuir*, 1994, 10, 326-329

37 C. M. Golini, B. W. Williams and J. B. Foresman, *J. Fluoresc.*, 1998, 8, 395-404

38 M. S. Chauhan, K. Sharma and S. Chauhan, in *Data extract from Landolt-Börnstein IV/17: Static Dielectric Constants of Pure Liquids and Binary Liquid Mixtures*,ed. S. B. Heidelberg, Springer Berlin Heidelberg, 2001,Vol. 17,pp. 854-855

Chapter 5

Predicting Solvent Polarity by use of TD-DFT: Betaine 30

5.1 Introduction

Betaine 30 (4-[2,4,6-tri(phenyl)pyridinium-1-yl]-2,6-di(phenyl)phenolate) is a dye that possesses a solvent polarity sensitive UV/VIS absorption spectrum. The $S_0 \rightarrow S_1$ absorption is a $\pi^* \leftarrow \pi$ transition accompanied by a large charge transfer from the phenolate ring to the pyridinium moiety (Figure 5-1). This large charge transfer has been extensively studied[1-4] and the difference between the ground (15 D) and excited state (-6 D) dipole moments is the reason for its sensitivity towards solvent polarity.[5] With a change in dipole of 9 D, it has been found useful in the characterization of solvent polarity. This has led to the popular E_T^N solvent polarity scale, which is derived from the transition energy of the dye in solution.[6] Since originally employed as a polarity scale, Betaine 30 has been used to characterize the polarity of alcohols,[3, 7, 8] ionic liquids[9, 10] and polymer solids.[11, 12]

Figure 5-1: Zwitterionic structures of solvent polarity probes Betaine 30 (R=H) and Betaine 45 (R=tert-butyl) before and after excitation.

The E_T^N solvent polarity parameter is dimensionless and is obtained from the transition energy of Betaine 30. The molar transition energy $E_T(30)$ of Betaine 30 in kcal/mol is given by equation 5-1:

$$E_T(30) = hcN_A \tilde{v} = 28591 \frac{1}{\lambda_{max}}$$ (5-1)

where h is Planck's constant, c is the speed of light, N_A is Avogadro's number, and $\tilde{v}$ is the wavenumber of the transition for Betaine 30 in cm^{-1}.

$E_T(30)$ values are then normalized, following equation (5-2), so that tetramethylsilane (TMS) is 0 (least polar) and water is 1 (most polar):

$$E_T^N = \frac{[E_T(30)_{solvent} - E_T(30)_{TMS}]}{[E_T(30)_{water} - E_T(30)_{TMS}]}$$ (5-2)

Since Betaine 30 is not soluble in all solvents, Betaine 45, a tert-butyl substituted derivative, is used to obtain secondary $E_T(30)$ values for more non-polar solvents. A conversion of $E_T(45)$ to $E_T(30)$ was formulated from a correlation equation (r^2=0.999) using 16 solvents that can solvate both betaine dyes.[13]

$E_T(30) = (E_T(45) - 1.808)/0.9424$ (5-3)

Although Betaine 30 has been well studied since its synthesis and in its application as a solvent polarity scale, theoretical investigations reported are limited to lower levels of theory (semi-empirical) or smaller derivatives (without peripheral phenyl groups) due to its size (72 atoms). The most recent study was done in 2007 by Bartkowiak et al., who conducted a HF and MP2 study of Pyridinium-N-Phenolates (a

small fragment of Betaine 30) to study the effects of the inclusion of electron correlation on the geometries of para-, meta- and ortho- isomers.[14] In 2006 Mennucci et al. conducted a semi-empirical ZINDO-PCM study of Betaine 30 in several solvents, both non-polar and polar.[15] Their study showed that by changing the scaling factor (α_O), a parameter which dictates the radius of oxygen atom for making the solute cavity, helped attain absorption energies closer to experimental. In 2001, Jasien and Weber reported a CIS study of the solvent effects on the absorption spectra of Betaine 30.[16] Their work optimized structures at the HF level of theory in addition to using the Onsager cavity model of solvation. In 1999, Maroncelli and Mente explored the basis of the $E_T(30)$ by Monte Carlo simulations of Betaine 30 in 12 solvents using a rigid all-atom model optimized with AM1.[17]

This communication explores the basis of the $E_T(30)$ scale, however using Density Functional Theory (DFT) for geometry optimization and Time-Dependent Density Functional Theory (TD-DFT) for the assessment of absorption energies, which to our knowledge has not yet been done. A correlation plot of Experimental vs. Theoretical E_T^N is presented, for the purpose of generating secondary E_T^N values from computational methods.

5.2 Methods

All calculations were carried out using the Gaussian 09 program.[18] Betaine 30 and Betaine 45 were optimized using Density Functional Theory (DFT) in the gas phase and in solution using the Polarizable Continuum Model (PCM). The hybrid DFT functional

used throughout this paper was the Becke 3-parameter exchange functional[19] combined with the Lee Yang and Parr correlation functional.[20] A split valence 6-31+G(d) basis set was used, with polarization and diffuse functions added to allow for asymmetry and a better description of electron density far away from the nuclei.[21] Time Dependent-Density Functional Theory using the B3LYP functional (referred to throughout as TD-B3LYP) was employed for absorption energies using B3LYP optimized ground state geometries.

The Polarized Continuum Model (PCM) was used to simulate non-specific solvation of Betaine 30 and Betaine 45.[22] The solute cavity was created as a sum of the interlocking UFF radii with a default scaling factor of 1.1. Since this model only accounts for the electrostatic interaction between the solvent and solute molecules, explicit solvation also was included for highly coordinating solvents like water and alcohols. The explicit solvation was carried out by coordinating one solvent molecule to the phenolate oxygen in the Betaine 30 molecule. In the case of water, the coordination of one or two water molecules was investigated. The second water molecule while initially coordinated directly to the Betaine 30 molecule, optimized to the hind side of the first water molecule in a chain like fashion (Figure 5-2, structure D).

5.3 Results and Discussion

The geometry optimizations of Betaine 30 at the B3LYP/6-31+G(d) level of theory was successful at reproducing the geometries in the past literature. For the gas phase geometry, the twist angle between the pyridinium and phenolate rings was 55.4° (not

shown), which is comparable to that found in the works of Caricato et al.[15] and Mente et al.,[17] who reported twist angles of 49° and 48° respectively. Our value is likely larger because of the higher level of theory (DFT), since our previous work on the solvatochromic dye Nile Red had also showed a larger twist angle for B3LYP/6-31+G(d) than with HF/6-31+G(d).[23] Optimized Betaine 30 geometries with one molecule of ethanol, methanol and water coordinated to the phenoxide oxygen are shown in Figure 5-2 and have oxygen-oxygen distances of 2.72 Å, 2.71 Å and 2.70 Å respectively. Also shown in Figure 5-2 is the optimized structure of Betaine 30 with two water molecules and the water oxygen-phenoxide oxygen distance becomes 2.65 Å. These oxygen-oxygen distances are very similar to literature values. The ethanol, methanol and water oxygen-oxygen distances are in agreement with the HF/3-21G optimized structures reported by Jasien and Weber, who reported the same values of 2.65 Å, 2.66 Å and 2.72 Å respectively.[16] An experimental x-ray crystal structure value for the ethanol oxygen-phenolate oxygen bond distance was reported as 2.71 Å, which is different by only 0.01Å.[24]

The absorption spectrum of Betaine 30 was found to be a HOMO→LUMO transition in all cases. Figure 5-3 shows the general blue shift occurring as an effect of the solvent polarity. The absorption band is broad and homogeneous, resembling that of experiment.
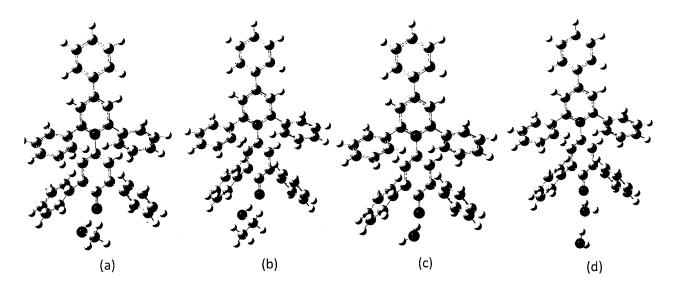
Figure 5-2: B3LYP/6-31+G(d) optimized structures of Betaine 30 with solvent molecules coordinated to the phenolate oxygen. (a) Methanol (b) Ethanol (c) Water (d) Two waters coordinated in a chain.
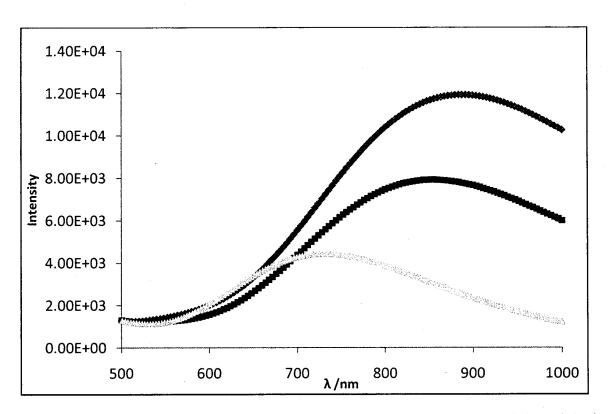
Figure 5-3: Absorption spectra of uncoordinated Betaine 30 in Tetramethylsilane (Blue), Diethyl ether (red) and Water (green).

Table 5-1: Experimental and theoretical values of λ_{max} and E_T^N for Betaine 30 and Betaine 45 (in brackets)

Solvent ([b])	Experimental[a]		rB3LYP/6-31G+(d)			
	λ_{max} /nm	E_T^N	λ_{max} /nm	E_T^N	LOBF E_T^N ([d])	LOBF E_T^N ([e])
Tetramethylsilane	[1054[c]]	0.000	891 [920[c]]	0.000	0.029	-0.012
Heptane	[1040[c]]	0.012	891 [920[c]]	-0.001	0.018	-0.012
Cyclohexane	[1047[c]]	0.006	895 [920[c]]	-0.001	0.029	-0.012
Benzene	834	0.111	899	0.059	0.023	0.054
Toluene	843	0.099	893	0.078	0.008	0.039
Diethyl Ether	829	0.117	856	0.191	0.126	0.151
Nitromethane	618	0.481	745	0.598	0.244	0.262
Acetone	647	0.417	762	0.528	0.283	0.299
Tetrahydrofuran	764	0.207	817	0.321	0.498	0.502
Dimethyl Formamide	662	0.386	744	0.602	0.431	0.439
Dichloromethane	702	0.309	805	0.363	0.510	0.513
Acetonitrile	627	0.460	745	0.598	0.495	0.499
Dimethyl Sulfoxide	634	0.444	741	0.615	0.495	0.499
Ethanol	551	0.654	755	0.556	-	-
Methanol	516	0.762	747	0.590	-	-
Water	453	1.000	732	0.655	-	-
Water (1)	453	1.000	677	0.913	-	-
Ethanol (1)	551	0.654	699	0.804	0.682	0.675
Methanol (1)	516	0.762	687	0.863	0.735	0.725
Water (2)	453	1.000	660	1.000	0.861	0.844

[a]Experimental values were obtained from "Solvent and Solvent Effects in Organic Chemistry" by Christian Reichardt.

[b]Because of the poor solubility of Betaine 30 in non-polar solvents, tert-butyl substituted Betaine 45 was used [reported in square brackets] and $E_T(45)$ was converted to $E_T(30)$ by equation (5-2).

[c]Values in (round brackets) correspond to the number of explicit solvent molecules coordinated to the Betaine-30 molecule.

[d] E_T^N parameters using the line of best fit equation without using Betaine 45 to obtain the ET(30) values in Tetramethylsilane, cyclohexane and heptane.

[e] E_T^N parameters using the line of best fit equation by converting TD-DFT Betaine 45 values to obtain the ET(30) values in Tetramethylsilane, cyclohexane and heptane.

Table 5-1 presents the TD-B3LYP absorption maxima of Betaine 30 and Betaine 45 in solvents simulated with the PCM model along with the experimental results of Betaine 30 reported by Reichardt.[6] Since the overall goal was to develop a technique for determining E_T^N for any solvent, the anchor points E_T(TMS) and E_T(Water) are discussed first. The E_T(30) for TMS was found to be 32.1 kcal/mol, which is only 1.4 kcal/mol more than experimental. The value is also higher in energy than the E_T(30) values for Betaine 30 in heptane and cyclohexane which are 32.1 kcal/mol and 32.0 kcal/mol, respectively, and contrary to experiment. The discrepancy in order between theory and experiment for these E_T(30) values is likely because the PCM model poorly accounts for weak dispersion interactions that dominate non-polar solvent systems. The experimental values reported by Reichardt were determined using Betaine 45 because in normal experimental conditions, Betaine 30 is insoluble in these solvents. For the E_T(30) of water, the discrepancy between theory and experiment is considerably larger. The theoretical value for E_T(30) water is 20.9 kcal/mol less than the experimental value of 63.1 kcal/mol. This large difference is most likely due to the hydrogen-bonding nature of water.

For the Betaine in the other solvents, absorption energies were generally underestimated in energy. The transition energy of Benzene was underestimated by 2.5kcal/mol, and this underestimation increases with polarity (6.5kcal/mol in DMSO). This poor estimation of energy may be because TD-DFT poorly describes excitations involving charge transfer,[25] however the use of hybrid functionals can sufficiently control the charge-transfer dilemma.[26]

To improve the values of $E_T(TMS)$, the indirect calculation (equation 5-3) of $E_T(30)$ for TMS, heptane and cyclohexane was performed from the TD-DFT energies of Betaine 45. The indirect $E_T(30)$ was found to be a 1.0kcal/mol less in energy from directly obtaining $E_T(30)$ from the TDDFT of Betaine 30, and only 0.4kcal/mol more than the experimental value. For the improvement of protic solvents water, methanol and ethanol, coordination of explicit solvent molecules to the phenoxide improved the $E_T(30)$ values by 3-3.3kcal/mol. A second water coordinated to first (in a chain) was found to further improve the $E_T(30)$ of water by another 0.75kcal/mol. However, the discrepancy between experimental $E_T(30)$ and theoretical $E_T(30)$ was still quite substantial, ranging from 11.0kcal/mol (EtOH) to 19.8kcal/mol (water). It has been well known that the phenolate oxygen is capable of behaving as a hydrogen bonding acceptor. Menucci et al. improved absorption maxima by adjusting the scaling factor of the phenolate oxygen[15] according to the five classes of solvents by Kamlet and Taft.[27]

Several lines of best fit from the plot Experimental E_T^N vs. Theoretical E_T^N were obtained and tabled in Table 5-2, since all combinations of including/excluding Betaine 45 and including/excluding explicit solvation was examined such that the best regression (r^2) could be found. The visualization all possible plots can be seen in Figure 5-4. In Figure 5-4, the blue markers represent the most current values of theoretical E_T^N with the addition of explicit solvent molecules to improve the linear relationship, while the non-blue colored markers do not contribute to the line of best fit but are there for comparison. Without any improvements, the line of best fit would be y=0.603x + 0.304 with an r^2 of 0.765. The first improvement proposed earlier was to calculate the $E_T(30)$

values from the TD-DFT energies of Betaine 45, and then converting it using equation 5-3. However, it can be seen that including this correction only improves the r^2 slightly in the range of -0.001 to 0.004. This would indicate that it is not crucial to use TD-DFT energies of Betaine 45 to obtain accurate values of E_T^N for non-polar solvents. For this reason, only lines of best fit that did not use Betaine 45 will be discussed further.

Table 5-2: Equations of lines of best fit with their respective r^2 coefficient for all combinations of including/excluding Betaine 45 and including/excluding explicit solvation for the plot of Experimental E_T^N vs. Theoretical E_T^N.

	Without Explicit Alcohol Coordination					
	Without Betaine 45			With Betaine 45		
	No Explicit water	1 Explicit Water	2 Explicit Water	No Explicit water	1 Explicit Water	2 Explicit Water
slope	0.603	0.840	0.896	0.637	0.861	0.917
intercept	0.034	0.031	0.036	-0.009	-0.013	-0.007
r^2	0.765	0.867	0.881	0.766	0.867	0.883

	With Explicit Alcohol Coordination					
	Without Betaine 45			With Betaine 45		
	No Explicit water	1 Explicit Water	2 Explicit Water	No Explicit water	1 Explicit Water	2 Explicit Water
slope	0.530	0.767	0.832	0.570	0.795	0.856
intercept	0.041	0.027	0.029	0.000	-0.014	-0.012
r^2	0.812	0.932	0.954	0.816	0.931	0.954
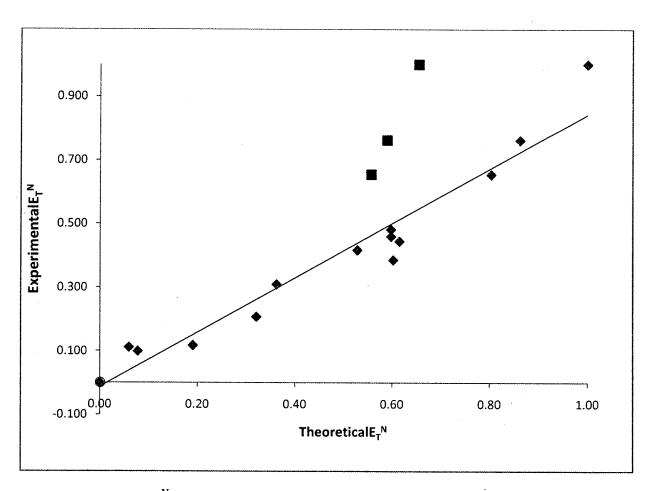
Figure 5-4: E_T^N values obtained with explicit solvation; the $E_T(30)_{water}$ corresponding to Betaine 30 with two coordinating water molecules was used to for equation (5-2) ; the red markers signify E_T^N values for ethanol, methanol and water without coordinating any explicit solvent molecule to the solute. The green marker signifies the E_T^N value which corresponds to a single water molecule coordinating the Betaine 30 molecule. The $E_T(30)$ values of TMS, heptane and cyclohexane were obtained indirectly from the TD-DFT energies of Betaine 45. The orange markers signify the $E_T(30)$ values of TMS, heptane and cyclohexane directly calculated from the TD-DFT energies of Betaine 30.

The inclusion of explicit solvent molecules improved the r^2 coefficient dramatically. Without explicitly solvating the alcohols MeOH and EtOH, the inclusion of one explicit water molecule improved the r^2 coefficient from 0.765 to 0.867. A second water molecule improved the r^2 slightly more to $r^2=0.881$. The majority of the remaining error is due to having not accounting for the hydrogen-bonding that takes place in the alcohols MeOH and EtOH. With the inclusion of explicit solvation for these two solvents, the r^2 is considerably better with a value of 0.954 for the equation is $E_{T\,Experimental}^{N} =$ (0.832) $E_{T\,Theoretical}^{N} + 0.029$.

5.4 Conclusions

The TD-B3LYP study of Betaine 30 was successful at predicting the trend in blue shift as a function of solvent polarity with and without the inclusion of explicit solvation. Although the blue shift was smaller in magnitude than that of experiment, a conversion plot was made with decent correlation. Initially, the line of best fit had a modest correlation coefficient of $r^2=0.7556$, and the inclusion of using both TD-DFT Betaine 45 energy values for non-polar solvents and explicit solvation was explored. Using Betaine 45 improved the $E_T(30)$ values for TMS, Heptane and cyclohexane to with 0.3kcal/mol of their experimental values, however they did not improve the r^2 coefficient for the conversion plot of Experimental vs. Theoretical E_T^N. Coordinating explicit solvent molecules to the phenoxide oxygen of Betaine 30 improved the $E_T(30)$ values from 3-3.3kcal/mol closer to their respective experimental values, but the explicit solvation allowed for a conversion plot with very good correlation to be made ($E_{T\,Experimental}^{N} =$

(0.832) $E_T^N{}_{\text{Theoretical}}$ $+ 0.029$, $r^2 = 0.954$). Rationally changing the scaling factor on the phenoxide oxygen may help attain better values for the non-protic, polarizable solvents such as benzene, toluene and acetonitrile in which non-electrostatic interactions (dispersion) may play a large role around the non-polar regions of Betaine 30.

5.5 References

1 B. C. Perng, M. D. Newton, F. O. Raineri and H. L. Friedman, *Journal of Chemical Physics*, 1996, 104, 7177-7204

2 C. Fuchs and M. Schreiber, *Journal of Chemical Physics*, 1996, 105, 1023-1028

3 P. J. Reid and P. F. Barbara, *Journal of Physical Chemistry*, 1995, 99, 3554-3565

4 P. J. Reid, S. Alex, W. Jarzeba, R. E. Schlief, A. E. Johnson and P. F. Barbara, *Chemical Physics Letters*, 1994, 229, 93-100

5 E. Lippert, *Z. Naturforschung*, 1955, 10A, 541

6 C. Reichardt, *Solvents and Solvent Effects in Organic Chemistry*, WILEY-WCH, Weinheim, 2003

7 X. H. Zhao, F. J. Knorr and J. L. McHale, *Chemical Physics Letters*, 2002, 356, 214-220

8 X. H. Zhao, J. A. Burt and J. L. McHale, *Journal of Chemical Physics*, 2004, 121, 11195-11201

9 V. Znamenskiy and M. N. Kobrak, *Journal of Physical Chemistry B*, 2004, 108, 1072-1079

10 Y. Wu, T. Sasaki, K. Kazushi, T. Seo and K. Sakurai, *J. Phys. Chem. B*, 2008, 112, 7530-7536

11 S. Nishiyama, M. Tajima and Y. Yoshida, *Molecular Crystals and Liquid Crystals*, 2008, 492, 130-138

12 S. Nishiyama, S. Aikawa, Y. Yoshida and M. Tajima, *Molecular Crystals and Liquid Crystals*, 2007, 462, 257-265

13 C. Laurence, P. Nicolet and C. Reichardt, *Bull. Soc. Chim. France*, 1987, 1001

14 W. Bartkowiak, W. Niewodniczanski, T. Misiaszek and R. Zalesny, *Chemical Physics Letters*, 2005, 411, 8-13

15 M. Caricato, B. Mennucci and J. Tomasi, *Molecular Physics*, 2006, 104, 875-887

16 P. G. Jasien and L. L. Weber, *Journal of Molecular Structure-Theochem*, 2001, 572, 203-212

17 S. R. Mente and M. Maroncelli, *Journal of Physical Chemistry B*, 1999, 103, 7704-7719

18 M. J. Frisch, G. W. Trucks, H. B. Schlegel, G. E. Scuseria, M. A. Robb, J. R. Cheeseman, J. A. Montgomery, T. V. Jr., K. N. Kudin, J. C. Burant, J. M. Millam, S. S. Iyengar, J. Tomasi, V. Barone, B. Mennucci, M. Cossi, G. Scalmani, N. Rega, G. A. Petersson, H. Nakatsuji, M. Hada, M. Ehara, K. Toyota, R. Fukuda, J. Hasegawa, M. Ishida, T. Nakajima, Y. Honda, O. Kitao, H. Nakai, M. Klene, X. Li, J. E. Knox, H. P. Hratchian, J. B. Cross, V. Bakken, C. Adamo, J. Jaramillo, R. Gomperts, R. E. Stratmann, O. Yazyev, A. J. Austin, R. Cammi, C. Pomelli, J. W. Ochterski, P. Y. Ayala, K. Morokuma, G. A. Voth, P. Salvador, J. J. Dannenberg, V. G. Zakrzewski, S. Dapprich, A. D. Daniels, M. C. Strain, O. Farkas, D. K. Malick, A. D. Rabuck, K. Raghavachari, J. B. Foresman, J. V. Ortiz, Q. Cui, A. G. Baboul, S. Clifford, J. Cioslowski, B. B. Stefanov, G. Liu, A. Liashenko, P. Piskorz, I. Komaromi, R. L. Martin, D. J. Fox, T. Keith, M. A. Al-Laham, C. Y. Peng, A. Nanayakkara, M. Challacombe, P. M. W. Gill, B. Johnson, W. Chen, M. W. Wong, C. Gonzalez and a. J. A. Pople, Gaussian 03 (Revision D.01), Gaussian, Inc., Wallingford, CT, 2004

19 A. D. Becke, *Physical Review A*, 1988, 38, 3098-3100

20 C. Lee, W. Yang and R. G. Parr, *Physical Review B*, 1988, 37, 785-789

21 R. Ditchfield, W. J. Hehre and J. A. Pople, *The Journal of Chemical Physics*, 1970, 52, 5001-5007

22 S. Mierts, E. Scrocco and J. Tomasi, *Chemical Physics*, 1981, 55, 117-129

23 P. O. Tuck, R. C. Mawhinney and M. Rappon, *PCCP*, 2009, 11, 4471-4480

24 R. Allmann, *Z. Kristallogr.*, 1969, 128, 115

25 A. Dreuw and M. Head-Gordon, *Chemical Reviews*, 2005, 105, 4009-4037

26 C. Jamorski, Jodicke and H. P. Luthi, *J. Am. Chem. Soc.*, 2003, 125, 252

112

27 R. W. Taft, M. J. Kamlet, J.-L. M. Abboud and M. H. Abraham, *J. Organic Chemistry*, 1983, 48, 2877

Chapter 6

What are the origins of dual fluorescence?

A comparative study of DMABN, ABN, DMABE and DMABFE

6.1 Introduction

Anomalous dual fluorescence was first observed in 4-(N, N) dimethylaminobenzonitrile (DMABN) by Lippert in 1959.[1] It is dubbed anomalous since it breaks Kasha's rule[2] that only one fluorescence band will be observed because all excitations should relax and fluoresce from the lowest lying singlet excited state. However, DMABN was found to have two emission bands, one a broad and more red-shifted peak was dubbed the L_A band (for anomalous) while the normal fluorescence band was dubbed the L_B band. The L_A band is solvent polarity sensitive due to its charge-transfer (CT) nature and becomes predominant in more polar media such as acetonitrile. Lippert's initial proposal was that fluorescence occurred from two excited state surfaces (L_A and L_B) and that the L_A band became the lowest lying excited state in the more polar solvent.[1] However, when other CT molecules also were found to possess dual emission bands, unexplainable exceptions were found and a new model was necessary.[3,4]

Numerous models to explain the dual fluorescence of DMABN have been put forth in the literature. These include excimer formation,[5] solute-solvent exciplex formation,[6] a solvent-induced pseudo-Jahn-Teller mechanism,[7] and intramolecular charge transfer accompanied by a large geometry change.[8-14] The latter was found to be in better agreement with observation, but what the actual geometric change associated with the intramolecular charge transfer (ICT) is still being debated. Rehybridrization of the acceptor (RICT), pyramidalization of the donor (WICT), planarization of the donor (PICT) and twisting of the donor (TICT) are all models.[14] However, the TICT model has been the

most robust model, with a few molecules in favor of the PICT model[15]. Recently, the development of improved spectroscopic[16,17] and theoretical techniques[18] have allowed new findings regarding the nature of the excited state of DMABN. Another interesting observation is that DMABN possesses two fluorescence bands[19] while the isoelectronic analog DMABE (4-dimethylamino benzoethyne) and the non-methyl substituted ABN (4-aminobenzonitrile) do not. It has been attributed in the literature to the CT excited state of these similar molecules by much higher in energy than the lowest lying excited state, thus resulting in only one fluorescence band.[20] This lowest lying excited state has been characterized as having an excited state dipole moment close in magnitude to the ground state and has been named the local excited state (LE state). Nile Red, a laser dye with a diethyl amino donor moiety, has also been reported to exhibit dual fluorescence in non-polar alkanes and water-ethanol binary mixtures,[21,22] but only one emission band is observed between the two extremes of solvent polarity.

Rappoport and Furche have reported the nature of the LE and ICT excited states in DMABN using TD-DFT excited state geometry optimization.[18] They confirmed that the ICT state was a minimum at a twist angle (between dimethylamino and benzene ring groups) of 90°. However, the nature of the LE state was also interesting. The LE state was found to have 2 minima at twist angles of 33° and 90° with an energy barrier between the two of only 0.09 eV, which has never been reported previously. They reported the energy barrier to be less than the accuracy of the method, and so characterizing the geometry of the LE state to have antiquinoidal character remains uncertain. A later report criticized the excited state surfaces reported by Rappoport and

Furche, suggesting that the energy is highly underestimated when twisting the dimethylamino group, since the surfaces collapse toward the ground state with decreasing orbital overlap between the donor and acceptor moieties.[23]   Lim and coworkers have recently suggested a πσ*-mediated ICT mechanism for the emission of DMABN in a spectroscopic study, in which they report a third excited state which corresponds to the promotion of an electron from the aromatic π-system to a σ* orbital localized on the accepting nitrile group.[17]
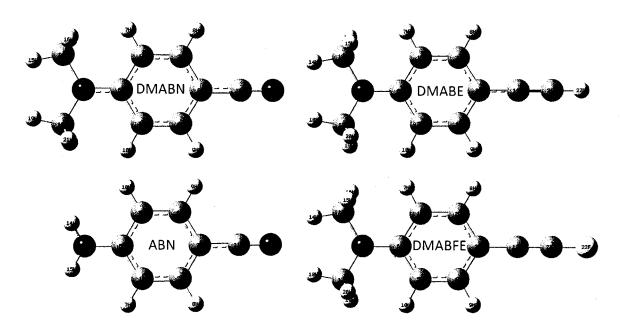
Figure 6-1: Molecular Structures of four donor-acceptor molecules, 4-Dimethylaminobenzonitrile (DMABN), 4-aminobenzonitrile (ABN), 4-dimethylaminobenzoacetylene (DMABA) and 4-dimethylaminobenzofluoroacetylene (DMABFA).

We carry out a TD-DFT study on the nature of the transitions for the first three transitions of the donor-acceptor molecules (Figure 6-1) DMABN, ABN, DMABE and

DMABFE (4-dimethylamino benzofluoroethyne and compare them. In addition, we follow the same technique of monitoring the change in excitation energy as a consequence of solvent polarity and solvent-induced geometry change that we have employed in our previous work on Nile Red.[24] Finally, since our motive for this investigation was to gain insight regarding the excited states of Nile Red, we compare the nature of these transitions to those found for Nile Red in our previous work.

6.2 Methods

Calculations were carried out using the Gaussian 09 program.[25] Gas phase optimized geometries were first obtained using Density Functional Theory. The hybrid density functional used throughout this paper was the Becke-3 parameter exchange functional[26] with the Lee yang and Parr correlation functional.[27] A split valence 6-31+G(d) basis set was used and appeared to be an adequate size of basis set.[28] The polarization and diffuse functions were added to allow for more asymmetry and a better description of the electron density far from the nuclei. A larger split valence triple-zeta 6-311++G(d,p) basis set has also been used but the results were not included since the change in the excitation energies was minimal and no difference in the types of transitions were observed.

The excitation energies of DMABN, DMABE, ABN and FDMABE (p-(N,N)Dimethylamino benzofluoroethyne) were determined using Time-Dependent Density functional theory (TD-DFT). These four molecules were chosen to study the effects of substitution on the transition types. The functional used was the same as that used for the geometry optimizations (TD-B3LYP) along with the same basis set to ensure

a vertical transition was obtained. TD-DFT excitations were also carried out using acetonitrile and cyclohexane from the gas phase geometries to determine the change in excitation energy as an effect of solvent polarity. Similarly, gas phase TD-B3LYP energy calculations from the optimized geometries of cyclohexane and acetonitrile were obtained to isolate the effect of geometry change on the excitation energy. The excitation energies of Nile red were taken from our previous study and are used to evaluate the similarities of Nile red to DMABN.[24]

6.3 Results and Discussion

6.3.1 DMABN

The important geometrical parameters namely donor-phenyl bond length (C6-N13), phenyl-acceptor bond length (C3-C11), the twist angle and pyramidalization are reported for DMABN in Table 6-1(a). The twist angle and pyramidalization were both defined arbitrarily, where the twist angle is the average of the dihedrals D(C1,C6,N13,C14) and D(C5,C6,N13,C18) and pyramidalization is 180 minus the dihedral D(C6,N13,C14,C18). These geometries were selected to see whether any subtle changes in ground state geometry could be the reason for the large difference in emission spectra of DMABN.

The C6-N13 bond length for DMABN was found to be 1.378 Å, 1.373 Å and 1.369 Å in the gas phase, cyclohexane and acetonitrile respectively. These values along with the C3-C11 bond lengths, twist angles and pyramidalizations are the same as those reported in the work by Scalmani and coworkers.[29] For this reason these geometries will not be

119

discussed except in relation to the other three molecules ABN, DMABE and DMABFE which have not been reported at the B3LYP/6-31+G(d) level.

Table 6-1: Important Geometry descriptors in the gas phase, cyclohexane and acetonitrile for 4-dimethylaminobenzonitrile (DMABN), 4-aminobenzonitrile (ABN), 4-dimethylamino benzoethyne (DMABE) and 4-dimethylamino benzofluoroethyne (DMABFE)

(DMABN)

Geometry descriptor	Gas Phase	Cyclohexane	Acetonitrile
C6-N13 /Å	1.378	1.373	1.368
C3-C11/Å	1.430	1.428	1.425
Pyramidalization*	7.1	0.2	0.2
Twist Angle†	0.0	0.0	0.0

(ABN)

Geometry descriptor	Gas Phase	Cyclohexane	Acetonitrile
C6-N13 /Å	1.387	1.383	1.378
C3-C11/Å	1.431	1.429	1.426
Pyramidalization*	39.0	37.9	36.8
Twist Angle†	0.0	0.0	0.0

(DMABE)

Geometry descriptor	Gas Phase	Cyclohexane	Acetonitrile
C6-N13 /Å	1.388	1.385	1.381
C3-C11/Å	1.428	1.428	1.428
Pyramidalization*	19.2	17.5	15.1
Twist Angle†	0.1	0.1	0.0

(DMABFE)

Geometry descriptor	Gas Phase	Cyclohexane	Acetonitrile
C6-N13 /Å	1.388	1.385	1.381
C3-C11/Å	1.431	1.432	1.432
Pyramidalization*	20.1	19.1	17.7
Twist Angle†	0.0	0.1	0.0

* Pyramidalization is defined as the 180 - dihedral D(C6,N13,C14,C18) for DMABN and ABN, and 180 - dihedral D(C6,N12,C14,C18) for DMABE and DMABFE
† Twist angle is defined as the average of the dihedrals D(C1,C6,N13,C14) and D(C5,C6,N13,C18) for DMABN, D(C1,C6,N13,H15) and D(C5,C6,N13,H14) for ABN, and (C1,C6,N12,C13) and D(C5,C6,N12,C17) for DMABE and DMABFE.
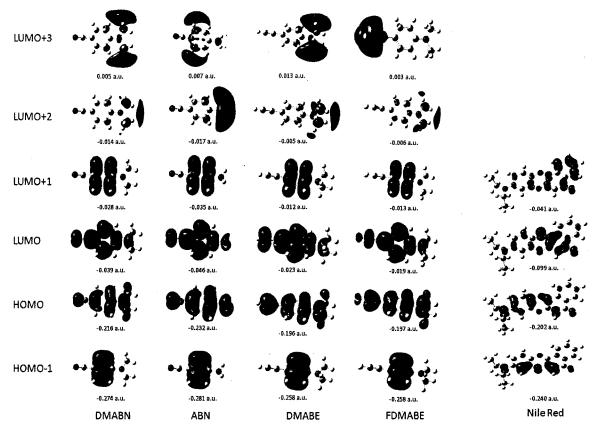
Figure 6-2: Molecular orbitals and energies for -Dimethylaminobenzonitrile (DMABN), 4-aminobenzonitrile (ABN), 4-dimethylaminobenzoacetylene (DMABA) and 4-dimethylaminobenzofluoroacetylene (DMABFA). Four molecular orbitals of NR are included for comparison.

The vertical TD-B3LYP excitation energies of DMABN are reported in Table 6-2(a) while the visualization of the gas phase molecular orbitals and their respective energies are shown in Figure 6-2. In the gas phase, it can be seen that the first transition of DMABN corresponds to an excitation of mixed nature at 280 nm. The transition is a combination of a HOMO-1→LUMO and a HOMO→LUMO+1. In Figure 6-2, the HOMO-1 and HOMO are similar in appearance to the π_3 and π_2 e_{2u} bonding MOs of benzene, respectively. Since the HOMO (π_2 e_{2u}) can interact with the substituents while the HOMO-1 (π_3 e_{2u}) cannot, it is no longer degenerate. The LUMO and LUMO+1 are similar to the π_4 and π_5 e_{2u} orbitals of benzene and also are no longer degenerate because the LUMO can interact with substituents while the the LUMO+1 is isolated.[30] The energies are in agreement with the work of Foresman and co-workers, who reported the lowest energy excitation corresponding to a HOMO→LUMO+1 transition at TD-B3LYP/6-31+G(d)//B3LYP/6-31G+(d) level of theory.[20] This level of theory is identical to our work, however we extend their results to ABN, DMABE and DMABFE in later sections which have not yet been reported. They assign this transition as the promotion to the excited state surface corresponding to the locally excited (LE) state since it possesses an oscillator strength of 0.03 and little change in excitation maxima as a result of solvent. The oscillator strength reported here is also in agreement with their value of 0.03. The second excitation in the gas phase is at 268 nm and corresponds to a HOMO→LUMO transition. The oscillator strength is large (0.70) and has been assigned as the transition corresponding to a promotion to the CT excited state surface. The third excitation corresponds to a HOMO→LUMO and HOMO→LUMO+2 transitions, but is not discussed

in detail since it lies much higher in energy than the first two. Upon solvation to the more polar solvent acetonitrile, it was found that CT state becomes the lower lying excited state. It has been rationalized in the past by Foresman and co-workers that this is an explanation as to why CT fluorescence band becomes the more predominant band in polar solvents. It is now lower in energy than the LE excited state.[20]

The non-vertical excitations of DMABN are reported in Table 6-1(b). From the gas phase geometry, the first excitation corresponding to a HOMO-1→LUMO and HOMO→LUMO+1 transition of DMABN in cyclohexane and acetonitrile was found to be 283 nm and 285 nm respectively. The vertical excitation in the gas phase was 280 nm, and thus a solvent shift of 5 nm is observed. The HOMO→LUMO excitation (ICT) was found to have a red-shift from 268 nm to 285 nm (17 nm difference). This implies that the majority of the red-shift in the absorption spectra of DMABN is due to solvent polarity on the excitation process and not geometry change. This is confirmed with the results of the non-vertical TD-B3LYP gas phase excitation of DMABN from the acetonitrile optimized geometry. The difference between the vertical gas phase excitation and the gas phase excitation using the acetonitrile geometry is only 1 nm for the LE state and no observed change for the CT state. This is similar to what we found for Nile Red (NR). Our recent work on NR was successful at showing that most of the red-shift in its first excitation was due to the effect solvent polarity on the excitation process, rather than a red shift as a consequence of solvent induced geometry change.[24]

Table 6-2: (a) Nature of the three lowest energy transitions (vertical) of 4-dimethylaminobenzonitrile (DMABN) in the gas phase, cyclohexane and acetonitrile. (b) Nature of three non vertical transitions of DMABN: excitations in cyclohexane from the gas phase optimized geometry, in acetonitrile from gas phase optimized geometry, and in the gas phase from the acetonitrile optimized geometry.

(a)

DMABN	λ_{max}/nm	f (osc. strength)	Transition Character
Gas Phase			
S0-->S1	280	0.0327 (LE)	HOMO-1 to LUMO, HOMO to LUMO+1
S0-->S2	268	0.5256 (CT)	HOMO-1 to LUMO+1, HOMO to LUMO, HOMO to LUMO+2
S0-->S3	261	0.0386	HOMO to LUMO, HOMO to LUMO+2
Cyclohexane			
S0-->S1	283	0.045 (LE)	HOMO-1 to LUMO, HOMO to LUMO+1
S0-->S2	279	0.7003 (CT)	HOMO to LUMO
S0-->S3	256	0.0259	HOMO to LUMO+2
Acetonitrile			
S0-->S1	285	0.7054 (CT)	HOMO to LUMO
S0-->S2	285	0.0392 (LE)	HOMO-1 to LUMO, HOMO to LUMO+1
S0-->S3	249	0.0234	HOMO to LUMO+2

(b)

DMABN	λ_{max}/nm	f (osc. strength)	Transition Character
TD-B3LYP in cyclohexane, gas phase geometry			
S0-->S1	283	0.0434	HOMO-1 to LUMO, HOMO to LUMO+1
S0-->S2	279	0.692	HOMO to LUMO
S0-->S3	255	0.0278	HOMO to LUMO+2
TD-B3LYP in acetonitrile, gas phase geometry			
S0-->S1	285	0.0368	HOMO to LUMO
S0-->S2	285	0.6892	HOMO-1 to LUMO, HOMO to LUMO+1
S0-->S3	248	0.0242	HOMO to LUMO+2
TD-B3LYP in gas phase, acetonitrile geometry			
S0-->S1	281	0.0347	HOMO-1 to LUMO, HOMO to LUMO+1
S0-->S2	268	0.5547	HOMO to LUMO, HOMO-1 to LUMO+1
S0-->S3	263	0.0201	HOMO to LUMO+2

Table 6-3: (a) Three lowest energy vertical transitions for Nile Red in the gas phase, cyclohexane and acetonitrile. (b) Nature of three non vertical transitions of Nile Red: excitations in cyclohexane from the gas phase optimized geometry, in acetonitrile from gas phase optimized geometry, and in the gas phase from the acetonitrile optimized geometry.

(a)

Nile Red	λ_{max}/nm	f (osc. strength)	Transition Character
Gas Phase			
S0-->S1	463	0.7392 (CT)	HOMO to LUMO
S0-->S2	426	0	HOMO-2 to LUMO, HOMO-2 to LUMO+1
S0-->S3	384	0.0032	HOMO-4 to LUMO, HOMO-1 to LUMO
Benzene			
S0-->S1	502	0.9468 (CT)	HOMO to LUMO
S0-->S2	409	0	HOMO-2 to LUMO, HOMO-2 to LUMO+1
S0-->S3	393	0.0016	HOMO-4 to LUMO, HOMO-1 to LUMO
Acetonitrile			
S0-->S1	516	0.9332 (CT)	HOMO to LUMO
S0-->S2	403	0.008	HOMO-4 to LUMO, HOMO-1 to LUMO
S0-->S3	386	0	HOMO-2 to LUMO, HOMO-2 to LUMO+1

(b)

Nile Red	λ_{max}/nm	f (osc. strength)	Transition Character
TD-B3LYP in benzene, gas phase geometry			
S0-->S1	464	0.6083	HOMO to LUMO
S0-->S2	432	0.000	HOMO-2 to LUMO, HOMO-2 to LUMO+1
S0-->S3	386	0.0053	HOMO-4 to LUMO, HOMO-1 to LUMO
TD-B3LYP in acetonitrile, gas phase geometry			
S0-->S1	468	0.6029	HOMO to LUMO
S0-->S2	444	0.000	HOMO-2 to LUMO, HOMO-2 to LUMO+1
S0-->S3	389	0.0114	HOMO-4 to LUMO, HOMO-1 to LUMO
TD-B3LYP in gas phase, acetonitrile geometry			
S0-->S1	514	0.8891	HOMO to LUMO
S0-->S2	399	0.0164	HOMO-4 to LUMO, HOMO-2 to LUMO, HOMO-1 to LUMO
S0-->S3	389	0.000	HOMO-3 to LUMO, HOMO-3 to LUMO+1

125

For Nile Red (Table 6-3(a)), the lowest energy excitation corresponds to a HOMO→LUMO transition. The HOMO and LUMO are dissimilar from the HOMO and LUMOs observed for the other four donor-acceptor molecules. This transition is of charge transfer character, since the HOMO is localized on the left side of the molecule while the LUMO is localized on the right side. This contrasts with DMABN, in which the CT excited state was the second lowest surface and was capable of relaxing to the LE state. The difference in gas phase excitation energy between the two transitions was found to be 0.17 eV for DMABN. For Nile Red, the difference begins at 0.23 eV and increases upon increasing solvent polarity. Yet, Nile Red has been reported to exhibit dual fluorescence in non-polar solvents[22] and in water-methanol binary mixtures.[21] This finding challenges the idea that dual fluorescence can be explained simply by a visual description of the ground state molecular orbitals and their energies. Nile Red has only one near lying virtual orbital (LUMO) in the gas phase and is of charge transfer character so solvent polarity was found to stabilize it even more. This implies that only one emission band should be visible, which contradicts experiment.

6.3.2 ABN

The ground state optimized geometries of ABN are reported in Table 6-1(b). The C6-N13 and C3-C11 bond lengths in the gas phase were found to be 1.387 Å and 1.431 Å respectively. These values are different by only 0.001 Å from the bond lengths of DMABN, which is within error. The twist angle of ABN was also similar to DMABN (0.0°), however, the pyramidalization of the amino group was considerably greater. It was found to be 39.0 in the gas phase and decreased slightly to 36.8 in acetonitrile.

The vertical excitation energies of ABN are tabulated in Table 6-4(a), while the non-vertical excitations of ABN are tabulated in 6-4(b). The first vertical excitation energies of ABN in the gas phase, cyclohexane and acetonitrile were found to be 268 nm, 268 nm and 269 nm respectively. The lowest energy excitations in gas phase, cyclohexane and acetonitrile all possessed a low oscillator strength of 0.03 and involved the transitionsHOMO-1→LUMO and HOMO→LUMO+1, making them similar to the LE excitation for DMABN. The second transitions in gas phase, cyclohexane and acetonitrile were found to have excitation energies of 254 nm, 262 nm and 266 nm respectively. The transitions were a combination of HOMO-1→LUMO+1, HOMO→LUMO which is the same as DMABN but the configuration HOMO→LUMO+2 was also found to contribute to the transition. The LE excited state was found to be the lowest lying state in all solvents and is the suggested explanation as to why only one emission band is observed experimentally.[31,32] The excitation of ABN is dissimilar to that of Nile Red since its lowest excitation energy corresponds to a promotion to the ICT excited state surface.

For the non-vertical transitions (Table 6-4(b)), ABN was found to have first excitation energies of 269 nm and 268 nm in acetonitrile and cyclohexane respectively, using the gas phase geometry. This is a minute difference of only 1 nm from the vertical transition in the gas phase geometry, suggesting that this excited state is not sensitive to solvent polarity. This is in agreement with experimental absorption spectra of ABN, where only a little red-shift is observed upon increasing solvent polarity. The gas phase TD-B3LYP excitation from the acetonitrile geometry was found to be 270nm, only 2 nm more than the gas phase TD-B3LYP excitation energy.

Table 6-4: (a) Nature of the three lowest energy vertical transitions of 4-aminobenzonitrile (ABN) in the gas phase, cyclohexane and acetonitrile. (b) Nature of three non vertical transitions of ABN: excitations in cyclohexane from the gas phase optimized geometry, in acetonitrile from gas phase optimized geometry, and in the gas phase from the acetonitrile optimized geometry.

(a)

ABN	λ_{max}/nm	f (osc. strength)	Transition Character
Gas Phase			
S0-->S1	268	0.0201 (LE)	HOMO-1 to LUMO, HOMO to LUMO+1
S0-->S2	254	0.3375 (CT)	HOMO-1 to LUMO+1, HOMO to LUMO, HOMO to LUMO+2
S0-->S3	247	0.0796	HOMO to LUMO, HOMO to LUMO+2
Cyclohexane			
S0-->S1	269	0.0282 (LE)	HOMO-1 to LUMO, HOMO to LUMO+1
S0-->S2	262	0.561 (CT)	HOMO to LUMO, HOMO-1 to LUMO+1
S0-->S3	241	0.0049	HOMO to LUMO+2
Acetonitrile			
S0-->S1	269	0.0245	HOMO-1 to LUMO, HOMO to LUMO+1
S0-->S2	266	0.5775	HOMO to LUMO, HOMO-1 to LUMO+1
S0-->S3	232	0.0001	HOMO to LUMO+2

(b)

ABN	λ_{max}/nm	f (osc. strength)	Transition Character
TD-B3LYP in cyclohexane, gas phase geometry			
S0-->S1	269	0.0272	HOMO-1 to LUMO, HOMO to LUMO+1
S0-->S2	261	0.5578	HOMO to LUMO, HOMO-1 to LUMO+1
S0-->S3	240	0.0049	HOMO to LUMO+2
TD-B3LYP in acetonitrile, gas phase geometry			
S0-->S1	268	0.0224	HOMO-1 to LUMO, HOMO to LUMO+1
S0-->S2	264	0.5681	HOMO to LUMO, HOMO-1 to LUMO+1
S0-->S3	230	0.0002	HOMO to LUMO+2, HOMO to LUMO+3
TD-B3LYP in gas phase, acetonitrile geometry			
S0-->S1	270	0.0216	HOMO-1 to LUMO, HOMO to LUMO+1
S0-->S2	256	0.3214	HOMO to LUMO, HOMO-1 to LUMO+1, HOMO to LUMO+2
S0-->S3	249	0.1027	HOMO to LUMO, HOMO to LUMO+2

This implies that the LE state is insensitive to solvent polarity (the dipole moment is similar to that of the ground state) and to solvent-induced geometry change. For the second excitation, which possesses HOMO→LUMO character along with two others (HOMO-1→LUMO+1 and HOMO→LUMO+2), sensitivity to solvent polarity was observed. ABN in cyclohexane and acetonitrile at the gas phase geometries were found to have excitation maxima of 261 nm and 264 nm respectively. This shows a difference of 10 nm red-shifted from the gas phase to acetonitrile. Solvent-induced geometry change was observed to be minimal. However, the difference between the vertical gas phase excitation of ABN (254 nm) to gas phase excitation in the acetonitrile geometry (256 nm) was only 2 nm.

6.3.4 DMABE

The optimized ground state geometries are tabulated in Table 6-1(c). The C6-N13 and C3-C11 gas phase bond lengths were found to be 1.388 Å and 1.428 Å respectively. Once again, these bond lengths are very close to those found for DMABN, being different by only 0.002 Å. The twist angle was 0.1° in the gas phase and cyclohexane, while in acetonitrile it was found to be 0.0□, which is slightly different that found for DMABN. Another interesting feature was the pyramidalization of DMABE which was between that of DMABN and ABN. In the gas phase the pyramidalization was 19.2 and slightly planarized to 15.1 in acetonitrile. The lowering of both twist angle and pyramidalization in acetonitrile suggests that more overlap may be occurring between the donor and phenyl group as solvent polarity is increased.

The vertical excitation spectra of DMABE (4-dimethylamino benzoethyne) in the gas phase, cyclohexane and acetonitrile are shown in Table 6-5(a) while the molecular orbitals are visualized in Figure 6-2 along with their respective energies. The first excitation is of low oscillator strength (~0.03) which involve the HOMO-1→LUMO and HOMO→LUMO+1 transitions, which is the same as for the LE excitations in DMABN and ABN. The excitation energies in the gas phase, cyclohexane and acetonitrile are 286 nm, 290 nm and 293 nm respectively. This red-shift of 7 nm is significantly larger than those found for DMABN and ABN (5 nm and 1 nm respectively). This is an interesting observation since it is generally stated that the LE state possesses a dipole moment similar to the ground state. The second excitation which was of the HOMO→LUMO character was found to be sensitive to solvation. The excitation energies in the gas phase, cyclohexane and acetonitrile were found to be 279 nm, 286 nm and 289 nm respectively. The excitation to the CT surface never becomes lower in energy than the LE excitation and again, is a possible explanation for the absence of dual fluorescence for DMABE in both experimental and theoretical work.[33-35]

The non-vertical transitions of DMABE are shown in table 6-5(b). Using the gas phase optimized geometry, the first excitations energies of DMABE are 289 nm and 292 nm in cyclohexane and acetonitrile respectively. The gas phase vertical excitation was 286nm, and so a red-shift of 6 nm as a consequence of solvent polarity is observed. This is similar to that of DMABN, where a 5 nm shift was observed as a consequence of solvent polarity. The gas phase excitation from the acetonitrile optimized geometry of DMABE was found to be 287nm, different from the vertical gas phase excitation by only 1 nm.

Table 6-5: (a) Nature of the three lowest energy vertical transitions of 4-dimethylaminobenzoethyne (DMABE) in the gas phase, cyclohexane and acetonitrile. (b) Nature of three non vertical transitions of DMABE: excitations in cyclohexane from the gas phase optimized geometry, in acetonitrile from gas phase optimized geometry, and in the gas phase from the acetonitrile optimized geometry.

a)

DMABE	λ_{max}/nm	f (osc. strength)	Transition Character
Gas Phase			
S0-->S1	286	0.0333 (LE)	HOMO-1 to LUMO, HOMO to LUMO+1
S0-->S2	279	0.3276 (CT)	HOMO to LUMO, HOMO to LUMO+2
S0-->S3	272	0.3026	HOMO to LUMO, HOMO to LUMO+2
Cyclohexane			
S0-->S1	290	0.0477 (LE)	HOMO-1 to LUMO, HOMO to LUMO+1
S0-->S2	286	0.7397 (CT)	HOMO to LUMO, HOMO to LUMO+2
S0-->S3	269	0.0543	HOMO to LUMO+2
Acetonitrile			
S0-->S1	293	0.0444 (LE)	HOMO-1 to LUMO, HOMO to LUMO+1
S0-->S2	289	0.7487 (CT)	HOMO to LUMO
S0-->S3	262	0.0328	HOMO to LUMO+2

(b)

DMABE	λ_{max}/nm	f (osc. strength)	Transition Character
TD-B3LYP in cyclohexane, gas phase geometry			
S0-->S1	289	0.0465	HOMO-1 to LUMO, HOMO to LUMO+1
S0-->S2	286	0.734	HOMO to LUMO, HOMO to LUMO+2
S0-->S3	268	0.0553	HOMO to LUMO+2
TD-B3LYP in acetonitrile, gas phase geometry			
S0-->S1	292	0.0417	HOMO-1 to LUMO, HOMO to LUMO+1
S0-->S2	288	0.7337	HOMO to LUMO
S0-->S3	260	0.0348	HOMO to LUMO+2
TD-B3LYP in gas phase, acetonitrile geometry			
S0-->S1	292	0.0417	HOMO-1 to LUMO, HOMO to LUMO+1
S0-->S2	288	0.7337	HOMO to LUMO
S0-->S3	260	0.0348	HOMO to LUMO+2

131

This is similar to what was found DMABN and ABN, that the LE state is insensitive to solvent-induced geometry change. The gas phase excitation of DMABE from the acetonitrile geometry yielded an excitation maximum of 288 nm, which is only 2 nm more than the gas phase vertical excitation. However, the second excitation of the DMABE is somewhat sensitive to solvent polarity chance, since a red shift from 279 nm (vertical gas phase excitation) to 286 nm was found.

6.3.5 DMABFE

The important geometrical features of DMABFE are tabulated in Table 6-1(d). The C6-N13 bond length is the same as that of DMABE (1.388 Å), while the C3-C11 bond length is elongated by 0.003 Å, due to the substitution of the fluorine atom at the end of the ethyne moiety. The twist angles for DMABFE were 0.0° in gas phase and acetonitrile and 0.1□ for DMABFE in cyclohexane, which can be considered planar. However, the pyramidalization on the amino group was found to be 20.1 in the gas phase, and 17.7 in acetonitrile which is slightly more pyramidal than DMABE. It appears that pyramidalization which was found to vary greatly from DMABN to DMABFE, does not change the framework of the benzene ring.

The nature of the first three vertical excitations of DMABFE (4-dimethylamino Benzofluoroethyne) is shown in Table 6-6(a) while visualization of the gas phase molecular orbitals can be seen in Figure 6-2. The first excitation in the gas phase was of HOMO-1→LUMO and HOMO→LUMO+1 character which are the same as that found in the gas phase for DMABN, ABN and DMABE. The oscillator strength of the first excitation is also low (0.04) and is LE state. The excitation energies for the first excitation

Table 6-6 (a) Nature of the three lowest energy vertical transitions of 4-dimethylamino benzofluoroethyne (DMABFE) in the gas phase, cyclohexane and acetonitrile. (b) Nature of three non vertical transitions of DMABFE: excitations in cyclohexane from the gas phase optimized geometry, in acetonitrile from gas phase optimized geometry, and in the gas phase from the acetonitrile optimized geometry.

(a)

DMABFE	λ_{max}/nm	f (osc. strength)	Transition Character
Gas Phase			
S0-->S1	287	0.0353	HOMO-1 to LUMO, HOMO to LUMO+1
S0-->S2	278	0.0998	HOMO to LUMO, HOMO to LUMO+2
S0-->S3	266	0.4734	HOMO to LUMO, HOMO-1 to LUMO+2, HOMO to LUMO+3
Cyclohexane			
S0-->S1	290	0.0499	HOMO-1 to LUMO, HOMO to LUMO+1
S0-->S2	278	0.5372	HOMO to LUMO, HOMO-1 to LUMO+2, HOMO to LUMO+3
S0-->S3	270	0.1783	HOMO to LUMO, HOMO to LUMO+2
Acetonitrile			
S0-->S1	294	0.0464	HOMO-1 to LUMO, HOMO to LUMO+1
S0-->S2	279	0.6509	HOMO to LUMO, HOMO-1 to LUMO+2, HOMO to LUMO+3
S0-->S3	272	0.0422	HOMO to LUMO, HOMO to LUMO+2

(b)

DMABFE	λ_{max}/nm	f (osc. strength)	Transition Character
TD-B3LYP in cyclohexane, gas phase geometry			
S0-->S1	290	0.0491	HOMO-1 to LUMO, HOMO to LUMO+1
S0-->S2	278	0.5466	HOMO to LUMO, HOMO to LUMO+2, HOMO to LUMO+3
S0-->S3	269	0.1653	HOMO to LUMO, HOMO to LUMO+2
TD-B3LYP in acetonitrile, gas phase geometry			
S0-->S1	293	0.0444	HOMO-1 to LUMO, HOMO to LUMO+1
S0-->S2	278	0.6465	HOMO to LUMO, HOMO to LUMO+2, HOMO to LUMO+3
S0-->S3	271	0.0372	HOMO to LUMO, HOMO to LUMO+2
TD-B3LYP in gas phase, acetonitrile geometry			
S0-->S1	288	0.0369	HOMO-1 to LUMO, HOMO to LUMO+1
S0-->S2	279	0.0751	HOMO to LUMO, HOMO to LUMO+2
S0-->S3	267	0.5045	HOMO-1 to LUMO+1, HOMO to LUMO, HOMO to LUMO+2

of DMABFE in gas phase, cyclohexane and acetonitrile are 287 nm, 290 nm and 294 nm respectively. The second excitation possessed a large oscillator strength, and was found to have excitation energies of 266 nm in the gas phase and 279 nm in acetonitrile, making it sensitive to solvent polarity. The effect of substitution resulted in a blue shift of 13 nm from DMABE to DMABFE in the gas phase. In acetonitrile, the second excitation is 15 nm higher in energy than the excitation to the LE surface. To our knowledge, the excitation and emission spectra of this fluorinated derivative of DMABE have never been reported. Its study provides insight on the effect of having a stronger acceptor group. It can be seen that a stronger acceptor group hinders dual fluorescence since the LE state is the lowest lying excited state by a large margin and thus it is predicted that this molecule would not show dual fluorescence.

The non-vertical transitions of DMABFE are shown in Table 6-6(b). It can be seen that from the gas phase geometry, the first excitations of DMABFE in cyclohexane and acetonitrile were found to be 290 nm and 293 nm respectively. This is a red shift of 6 nm from the vertical gas phase excitation, suggesting that the LE state of DMABFE is slightly sensitive to solvent polarity. However, the second excitation (ICT) was less so, in which the excitation energies in cyclohexane and acetonitrile were found both to be 278nm, identical to the gas phase vertical excitation energy. This is very different from the molecules of DMABN, ABN and DMABE since their excitations which possessed the large oscillator strength all red-shifted as a consequence of solvent polarity. The first excitation energy of DMABFE in the gas phase using the acetonitrile geometry was 288 nm, which corresponded to a transition to the LE state. It was different by only 1 nm

from the gas phase vertical excitation. For the second excitation, the effect of solvent-induced geometry change is also small, with a change of only 1 nm.

6.4 Conclusions

The use of LE and CT excited state surfaces works for the purpose of comparing and explaining why dual fluorescence occurs for DMABN and not for ABN and DMABE. This system also enabled us to predict with confidence that DMABFE would not possess two bands in its fluorescence spectra. In addition, the pictures of the molecular orbitals involved for the first three transitions provided insight as to the character of the LE and CT excited states of these donor-acceptor molecules. However, this system of pairing the LE surface to the transition of the HOMO-1 to LUMO and HOMO to LUMO+1 (low oscillator strength) and the CT surface attained by a HOMO to LUMO transition could not explain the dual fluorescence of Nile Red. Nile Red was found to have a low lying first excitation corresponding to a solvent sensitive peak and visualization of the molecular orbitals showed they were localized on two parts of the molecule, suggesting charge-transfer. However, this CT excited state surface was the lowest lying band as well and increasing solvent polarity would only stabilize it more, suggesting that Nile Red should only possess one fluorescence peak in gas phase and in acetonitrile. More insight could be attained with an excited state optimization of Nile Red and DMABN using a coulombic attenuated functional such as CAM-B3LYP followed by a TD-CAM-B3LYP excitation energy calculation of the excited state geometries, to obtain vertical emission energies.[18,23]

6.5 References

1 E. Lippert, W. Luder and H. Boos, Advances in Molecular Spectroscopy, Pergamon Press, Oxford, 1962

2 M. Kasha, *Faraday Discuss.*, 1950, 9, 14

3 W. Rettig and E. Lippert, J. Mol. Structure., THEOCHEM, 1980, 80, 17

4 W. Rettig, G. Wermuth and E. Lippert, *Ber. Bunsen Ges. Phys. Chem.*, 1979, 83, 692

5 O. S. Khalil, R. H. Hofeldt and S. P. McGlynn, *Chem. Phys. Lett.*, 1972, 17, 479

6 E. A. Chandross, *The Exciplex*, Academic Press, New York, 1975

7 K. A. Zachariasse, T. Vonderhaar, A. Hebecker, U. Leinhos and W. Kuhnle, *Pure Appl. Chem.*, 1993, 65, 1745-1750

8 Z. R. Grabowski, K. Rotkiewicz and W. Rettig, *Chem. Rev.*, 2003, 103, 3899-4031

9 K. A. Zachariasse, M. Grobys, T. vonderHaar, A. Hebecker, Y. V. Ilichev, O. Morawski, I. Ruckert and W. Kuhnle, *J. Photochem., A*, 1997, 105, 373-383

10 W. Sudholt, A. L. Sobolewski and W. Domcke, *Chem. Phys.*, 1999, 240, 9-18

11 K. A. Zachariasse, *Chem. Phys. Lett.*, 2000, 320, 8-13

12 R. Schamschule, A. B. J. Parusel and G. Kohler, *Internet J. Chem.*, 1998, 1, CP1-U31

13 W. Rettig and B. Zietz, *Chem. Phys. Lett.*, 2000, 317, 187-196

14 Z. R. Grabowski, K. Rotkiewicz and W. Rettig, *Chem. Rev.*, 2003, 103, 3899-4032

15 Y. V. Il'ichev, O. Morawski, I. Rucker and W. Kuhnle, *J. Photochem., A*, 1998, 102, 5670

16 T. Gustavsson, P. B. Coto, L. Serrano-Andres, T. Fujiwara and E. C. Lim, *J. Chem. Phys.*, 2009, 131

17 J. K. Lee, T. Fujiwara, W. G. Kofron, M. Z. Zgierski and E. C. Lim, *J. Chem. Phys.*, 2008, 128

18 D. Rappoport and F. Furche, *J. Am. Chem. Soc.*, 2004, 126, 1277-1284

19 S. Cogan, S. Zilberg and Y. Haas, *J. Am. Chem. Soc.*, 2006, 128, 3335-3345

20 Foresman, *J. Chem. Phys.*, 2002, 116, 8761-8771

21 A. K. Dutta, K. Kamada and K. Ohta, *J. Photochem: A,* 1996, 93, 57-64

22 D. G. Yablon and A. M. Schilowitz, *Appl. Spectrosc.*, 2004, 58, 843-847

23 P. Wiggins, J. A. G. Williams and D. J. Tozer, *J. Chem. Phys.*, 2009, 131,

24 P. O. Tuck, R. C. Mawhinney and M. Rappon, *Phys. Chem. Chem. Phys.*, 2009, 11, 4471-4480

25 M. J. Frisch, G. W. Trucks, H. B. Schlegel, G. E. Scuseria, M. A. Robb, J. R. Cheeseman, J. A. Montgomery, T. V. Jr., K. N. Kudin, J. C. Burant, J. M. Millam, S. S. Iyengar, J. Tomasi, V. Barone, B. Mennucci, M. Cossi, G. Scalmani, N. Rega, G. A. Petersson, H. Nakatsuji, M. Hada, M. Ehara, K. Toyota, R. Fukuda, J. Hasegawa, M. Ishida, T. Nakajima, Y. Honda, O. Kitao, H. Nakai, M. Klene, X. Li, J. E. Knox, H. P. Hratchian, J. B. Cross, V. Bakken, C. Adamo, J. Jaramillo, R. Gomperts, R. E. Stratmann, O. Yazyev, A. J. Austin, R. Cammi, C. Pomelli, J. W. Ochterski, P. Y. Ayala, K. Morokuma, G. A. Voth, P. Salvador, J. J. Dannenberg, V. G. Zakrzewski, S. Dapprich, A. D. Daniels, M. C. Strain, O. Farkas, D. K. Malick, A. D. Rabuck, K. Raghavachari, J. B. Foresman, J. V. Ortiz, Q. Cui, A. G. Baboul, S. Clifford, J. Cioslowski, B. B. Stefanov, G. Liu, A. Liashenko, P. Piskorz, I. Komaromi, R. L. Martin, D. J. Fox, T. Keith, M. A. Al-Laham, C. Y. Peng, A. Nanayakkara, M. Challacombe, P. M. W. Gill, B. Johnson, W. Chen, M. W. Wong, C. Gonzalez and a. J. A. Pople, Gaussian 09 (Revision A1), Gaussian, Inc., Wallingford, CT, 2009

26 A. D. Becke, *Phys. Rev., A*, 1988, 38, 3098-3100

27 C. Lee, W. Yang and R. G. Parr, *Phys. Rev., B*, 1988, 37, 785-789

28 R. Ditchfield, W. J. Hehre and J. A. Pople, *J. Chem. Phys.*, 1970, 52, 5001-5007

29 G. Scalmani, M. J. Frisch, B. Mennucci, J. Tomasi, R. Cammi and V. Barone, *J. Chem. Phys.*, 2006, 124, 094107-094115

30 W. H. Brown, C. S. Foote, B. L. Iverson and E. V. Anslyn, *Organic Chemistry*, Brooks/Cole, Belmont, California, 2009

31 A. Kawski, B. Kuklinski and P. Bojarski, *Chem. Phys. Lett.*, 2006, 425, 257-261

32 M. A. Palafox, V. K. Rastogi and J. K. Vats, *J. Raman Spectrosc.*, 2006, 37, 85-99

33 A. L. Sobolewski and W. Domcke, *J. Photochem., A,* 1997, 105, 325-328

34 A. L. Sobolewski, W. Sudholt and W. Domcke, *J Phys. Chem., A*, 1998, 102, 2716-2722

35 N. Chattopadhyay, C. Serpa, M. M. Pereira, J. S. de Melo, L. G. Arnaut and S. J. Formosinho, *J. Phys. Chem., A*, 2001, 105, 10025-10030

Chapter 7

A TD-DFT and pK$_A$ study of N-phenylbenzohydroxamic acids

7.1 Introduction

N-phenylbenzohydroxamic acids (PBHAs) are weak organic acids that have excellent metal chelating abilities.[1-6] They are found naturally in plants and fungi as iron transporting molecules.[7] This chelating ability of PBHAs has found applications in the fields of enzyme inhibition,[8,9] trace-metal detection[2] and mineral extraction.[10] Since chelation is the key to application, characterizing this ability is vital for future design and optimization.

PBHAs take the general form of PhC(=O)N(Ph')OH. Due to the partial double bond character of the C-N bond, rotation is hindered and two stable geometric isomers (*cis* and *trans*) can be observed.[11] Although in its crystalline form only *cis* or *trans* is observed, in solution this is not the case.[7] In solution both *cis* and *trans* may co-exist, but only the *cis* species can behave as a bidentate ligand. This is because the *cis* species has both oxygens in the right geometry to coordinate metals to form stable 5-membered chelate rings.[12,13] It is therefore important to understand solvent effects on the abundance of the *cis* isomer in basic solution. In addition, since it is the deprotonated cis conformer that has the chelating ability, an understanding of the effects of substitution on its acid dissociation constant is also important. The experimental pK_A of the unsubstituted PBHA has been reported to be 9.81 in 50% MeOH/H$_2$O mixtures.

Past theoretical works have examined the effects of substitution and solvation on the conformation of small hydroxamic acids.[14-17] However, N-phenyl substituted hydroxamic acids (PBHAs) cannot undergo tautomerization to oxime- and nitroso- forms

because there is no proton attached to the nitrogen on the hydroxamic functional group. Only a couple of studies have been reported for the larger PBHAs. In 2004, Ciofini reported the MP2/6-31G(d) geometries of the *cis* and *trans* unsubstituted PBHAs in acetone and water, where the percent abundance and pK_A calculations were reported.[18] Dissanayake and co-workers in 2006 used ab initio methods to study *ortho* -N-substituted (OMe, Br, Cl) PBHAs and it was found that the trans deprotonated conformer was always lowest in energy.[19] They also found that the HF/6-31G+(d) optimized cis PBHA conformers predicted pK_A values that were overestimated by at least than 3 units in every case. The DFT functionals B3LYP the CBS-QB3 method using the same basis set predicted even higher values. Experimental studies of the absorption spectra PBHAs have been carried out in micellar phases and in the presence of strong acids[1,20,21]. It was possible to differentiate the effects of deprotonation from the effects of the solvation on the absorption spectra.

In our study, we investigated *para-N*-phenyl-substituted benzohydroxamic acids to elucidate the effects of substitution, solvent effects on the absorption spectra and acid dissociation constant. The TD-DFT excitation energies are valuable because experimental excitation energies are almost never reproduced theoretically. For this reason, identifying the trends that these conformers exhibit upon substitution, solvation, and deprotonation are crucial. pK_A values were obtained from the aqueous deprotonation free energy (ΔG_{aq}) which is the sum of the gas-phase free energy (ΔG_{gas}) and free energy change on solvation ($\Delta\Delta G_{solv}$).[22]

7.2 Methods

Calculations were carried out using the Gaussian 09 program.[23] Gas phase geometries were first obtained using Density Functional Theory. The hybrid functional used throughout is the PBE0 functional by Perdew, Burke and Erzenhof.[24] Two basis sets were used. A split valence 6-31+G(d) basis set was used and reported throughout this paper as the small basis set (sbs).[25] A larger basis set (lbs) was the split valence triple-zeta 6-311++G(df,2p) basis set.

Re-optimization of the gas phase geometries was carried out using the polarized continuum model of Tomasi and co-workers to simulate the non-specific solvation of hydroxamic acids in ethanol and water.[26] Since this model only accounts for the electrostatic interactions between the solute and solvent, single water molecules were explicitly coordinated to the hydroxamic functional group (and the geometry re-optimized) as an improvement in the description of solvation for hydroxamic acids in a protic water environment. Explicit inclusion of a water molecule has been shown to improve the prediction of excitation energies and acid dissociation constants (pK_A) in aqueous media.[27]

Excitation energies were determined using Time-Dependent Density functional theory (TD-DFT) with the same hybrid functional as for geometry optimization, PBE0. The thermodynamic cycle used for assessing pK_A involves the Gibbs free energy for the deprotonation of hydroxamic acids that is similar to the scheme used by Dissanayake and co-workers.[15]

Since the *N*-phenylbenzohydroxamic acids considered in this study have only one acidic hydrogen, the standard dissociation reaction used for the deprotonation of an acid is:

$$AH_{(aq)} \rightarrow A^-_{(aq)} + H^+_{(aq)} \tag{7-1}$$

The deprotonation of an acid in aqueous medium (ΔG_{aq}) also requires the inclusion of the change in Gibbs free energy of solvation which is added to the Gibbs free energy of deprotonation in the gas phase:

$$\Delta G_{aq} = \Delta G_{gas} + \Delta \Delta G_{solv} \tag{7-2}$$

The pK$_a$ of the hydroxamic acid is then calculated according equation (7-3):

$$pK_a = \frac{G_{gas}(A^-) + G_{gas}(H^+) - G_{gas}(HA) + \Delta G_{solv}(A^-) + \Delta G_{solv}(H^+) - \Delta G_{solv}(HA)}{2.303RT} \tag{7-3}$$

where the formation free energy of a proton ($G_{gas}(H^+)$) is -6.28 kcal/mol and its hydration free energy ($\Delta G_{solv}(H^+)$) is -264.61 kcal/mol.[28, 29]

7.3 Results and Discussion

7.3.1 Geometry of *cis* and *trans* isomers

The gas phase optimized structures of PBHAs are illustrated in Figure 7-1, while the bond lengths of the four common bonds [C-N, C=O, N-O and O-H] for gas phase optimized geometries using both small and large basis sets are tabulated in Tables 7-1 and 7-2, respectively. For the unsubstituted PBHAs, the *cis* protonated conformers possess longer C-O bond lengths and shorter C-N bonds than the *trans*, however, little difference is noticed in the N-O bond length. The O-H bond length in the *cis* form is

142
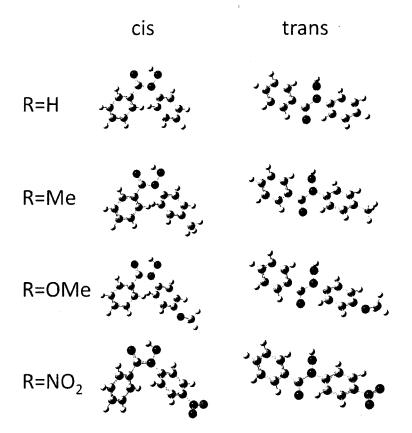
Figure 7-1: gas-phase rB3LYP/6-31+G(d) optimized protonated hydroxamic acids where (R=H, Me, OMe, NO_2). White denotes hydrogen atoms, gray-carbon, red-oxygen, and blue-nitrogen.

Table 7-1: Bond lengths (Å) of hydroxamic acids using (a) small basis [6-31+G(d)] set and (b) large basis set [6-311+G(2df, pd)]. The four bond lengths shown are that of the C-N, C=O, N-O and O-H (protonated only) bonds that make up the HA functional group.

(a)

	H	Me	OMe	NO$_2$
		cis – protonated		
CN	1.360	1.359	1.358	1.371
CO	1.239	1.239	1.239	1.234
NO	1.390	1.390	1.393	1.386
OH	0.989	0.989	0.989	0.989

	H	Me	OMe	NO$_2$
		trans – protonated		
CN	1.389	1.388	1.387	1.399
CO	1.220	1.220	1.221	1.217
NO	1.389	1.390	1.391	1.387
OH	0.971	0.971	0.971	0.971

	H	Me	OMe	NO$_2$
		cis – deprotonated		
CN	1.371	1.369	1.367	N/A[*]
CO	1.240	1.240	1.242	N/A[*]
NO	1.324	1.324	1.325	N/A[*]

	H	Me	OMe	NO$_2$
		trans – deprotonated		
CN	1.367	1.366	1.365	1.385
CO	1.252	1.253	1.253	1.240
NO	1.333	1.333	1.333	1.324

Table 7-1 Continued:

(b)	H	Me	OMe	NO$_2$
		cis – protonated		
CN	1.355	1.354[†]	1.352	1.366
CO	1.231	1.232[†]	1.232	1.226
NO	1.383	1.383[†]	1.385	1.380
OH	0.985	0.985[†]	0.985	0.985

	H	Me	OMe	NO$_2$
		trans – protonated		
CN	1.384	1.383	1.383	1.394
CO	1.211	1.212	1.215	1.209
NO	1.384	1.384	1.385	1.382
OH	0.965	0.965	0.964	0.965

	H	Me	OMe	NO$_2$
		cis – deprotonated		
CN	1.366	1.365	1.362	N/A[*]
CO	1.232	1.232	1.244	N/A[*]
NO	1.318	1.318	1.328	N/A[*]

	H	Me	OMe	NO$_2$
		trans – deprotonated		
CN	1.363	1.362	1.359	1.381
CO	1.243	1.244	1.245	1.231
NO	1.328	1.328	1.328	1.320

[*]after deprotonation, the *cis* conformer relaxed to a *trans* conformation.

[†]Optimized to transition states that corresponds to methyl rotation (imaginary frequency = 6i).

slightly longer (0.018 Å) suggesting that it may possess a proton that is more easily removable than the *trans*. However, the presence of an intramolecular hydrogen bond with the carbonyl oxygen to form a stable five-membered ring has been detected and reported in solution using IR methods.[30] Therefore the acidity of this proton cannot be evaluated simply by the O-H bond length, consideration of the pK_A is necessary.

For the unsubstituted protonated PBHA, it can be seen that the C-N bond is shorter in the *trans* form than the *cis*, likely because of resonance contributions from both phenyl groups, which gives it more double bond character.[31] The longer C-O and N-O bonds are also indicative of bond alternation brought on by increased conjugation.

7.3.2 Effects of substitution on geometry

Three substituents on the *N*-phenyl of the PBHAs were selected and are shown in Tables 7-1 and 7-2 along with their geometries. They were selected to account for all combinations of the resonance and inductive effects on geometry. The substituents – Me, -OMe and -NO_2 are *para*- to the nitrogen side of the hydroxamic (HA) functional group. In the gas phase, the weakly activating methyl substituent does lead to a shortening of the C-N bond by more than 0.001 Å, and the C-O and N-O bonds elongate no more than 0.001 Å. In the solvents ethanol and water, the same trends of C-N bond contraction, C-O and N-O bond elongation are repeated for the protonated *cis* and *trans* species. However, for the anions, the trend shows contraction of the C-N bond by as much as 0.010Å and elongation of the N-O and C-O bonds by as much as 0.003Å. One case that does not follow this trend of C-N bond contraction and N-O and C-O bond elongation is the methyl substituted *cis* deprotonated PBHA in water. Its N-O bond length is in fact shorter than the unsubstituted PBHA by 0.007Å, suggesting that a factor other than solvent is affecting the geometry of the HA functional group. This anomaly also contrasts with geometries reported in the literature. Ventura et al. conducted a study on R(C=O) NHOH hydroxamic acids, and found that the methyl substituted species resulted in a N-O bond elongation, consistent with our results in every other case.[31]

146

For methoxy substitution (-OMe) of the *cis* PBHA in the gas phase, the C-N bond contracted 0.002 Å, the C-O bond remained unchanged and the N-O bond elongated 0.003 Å. In ethanol and water, only the N-O bond length changed with an elongation of 0.004 Å and 0.003 Å respectively. No change in the O-H bond length was observed in the gas phase or with the PCM solvent model. The *trans*-PBHA experienced the same trend as that of the *cis* isomer, with the C-N bond experiencing a contraction in the C-N bond and elongations of the C-O and N-O bonds upon −OMe substitution. For the deprotonated anion, the *cis* and *trans* PBHAs in the gas phase also experienced the same bond length changes as their conjugate acid counterpart.

The nitro (-NO$_2$) substituted PBHA showed opposite effects to the -OMe and -Me substituents. The C-N bond in the *cis* and *trans* PBHA isomers experienced a bond elongation of 0.011 Å and 0.010 Å respectively. Meanwhile, the C-O and N-O bonds experienced bond contractions of about 0.004 Å in the gas phase, opposite to observations for the other two substituents. A rationalization for this is the ambiguity of the HA functional group. Since attached immediately to the hydroxamic nitrogen is a carbon and an oxygen, it seems as though the HA can function as either a resonance donating or withdrawing substituent, depending on the functional group that is attached para- to the hydroxamic acid on the *N*-phenyl. For the cases of −Me and −OMe, the hydroxamic acid group behaved as a resonance withdrawing species, while for the case of −NO$_2$, behaved as a resonance donating species. The −NO$_2$ also removed so much charge from the hydroxamic acid that no *cis* conformation could be optimized upon deprotonation. The *trans* conformation was favorable for the −NO$_2$ PBHA because

the C-phenyl group is able to contribute more electron density through resonance for the deprotonated species, thus stabilizing it.

7.3.3 Effects of increasing basis set on geometry

Contraction of bond lengths was derived on increasing the basis set from PBE0/6-31+G(d) to PBE0/6-311++ G(df,2p). The C-N bond decreased in length in all substituted *cis/trans* PBHAs by a minimum of 0.004 Å while the contraction of the C-O bond was anywhere from 0.006 Å to 0.007 Å. The change in bond length of N-O as a result of increasing basis set was found to be anywhere from 0.003 Å to 0.005 Å. This contraction of bond lengths is not uncommon upon increasing basis set size, since the larger basis set uses more basis functions which will better reproduce the radial decay of electron density when going away from an atomic nucleus. In the case of the -OMe substituted *cis* deprotonated anion, it appears that increasing basis set has increased the N-O bond length, However, deprotonation resulted in the initial *cis* species to relax to a *trans* form (no *cis* deprotonated form was optimized). Although no study of PBHAs have been carried out before using the DFT functional PBE0, Nino et al. reported DFT (B3LYP) and MP2 results for smaller hydroxamic acids.[16] They found that the B3LYP/6-31+G(d) optimized geometries of hydroxamic acids predicted an intramolecular hydrogen bond in the *cis* form while lower levels of theory (semi-empirical AM1) could not. Since a decrease in bond length as a consequence of basis set was evident every time and predictable, only the smaller basis set was used for the investigation of the PBHAs in the PCM solvation model.

7.3.4 Effects of solvent on geometry

The unsubstituted PBHA (-H) was optimized in the gas phase as well as with a polarized continuum model to describe ethanol (Table 7-2B) and water (Table 7-2A). In ethanol, the C-N bond length of the unsubstituted *cis* protonated PBHA contracts from 1.370 Å to 1.360Å. For the substituted PBHAs the contraction of the C-N bond length was 0.009 Å for the methyl and 0.008 Å for both the -OMe and $-NO_2$ substituted PBHAs. The geometry of the unsubstituted PBHAs in water is the same as observed in ethanol, with no change in bond lengths. For the *trans*-protonated species, the geometry change is more significant upon solvation. The C-N bond length contracted anywhere from 0.013 Å ($-NO_2$ substituted) to 0.020 Å (-H and −OMe). For the *cis* and *trans* deprotonated species, a shortening of C-N bond length is also observed. However, the effect of solvent remains uncertain since deprotonation also occurred.

For the protonated PBHAs, the O-H bond elongated less for the *cis* geometry (0.002Å) than for the *trans* (0.011Å) species as a result of solvation in ethanol or water. This is the first indication that the polarity may lower the pK_A of the PBHAs; however, this subject will be discussed later in section 7.3.7. In contrast to the C-N bond, the C-O bond of all HA species (*cis/trans* isomers and substituted) experienced an elongation as a result of solvation. This implies that the polar solvent induces more conjugation between the two phenyl side groups, resulting in a more planar HA species. This concept will be reinforced later in the discussion of TD-DFT and the charge transfer nature of PBHAs.

Table 7-2: Bond lengths of PBHA geometries optimized using the small basis [6-31+G(d)] in (a) water and (b) ethanol. The four bond lengths shown are the C-N, C=O, N-O and O-H (protonated only) bonds that make up the hydroxamic acid functional group.

(a)	H	Me	OMe	NO$_2$
		cis – protonated		
CN	1.350	1.350	1.350	1.363
CO	1.244	1.245	1.244	1.238
NO	1.391	1.391	1.394	1.385
OH	0.991	0.992	0.991	0.992
		trans – protonated		
CN	1.369	1.370	1.366	1.385
CO	1.232	1.232	1.234	1.227
NO	1.383	1.384	1.385	1.380
OH	0.992	0.992	0.992	0.994
		cis – deprotonated		
CN	N/A*	1.344	1.342	1.382
CO	N/A*	1.257	1.258	1.238
NO	N/A*	1.347	1.347	1.338
		trans – deprotonated		
CN	1.354	1.352	1.351	1.382
CO	1.254	1.255	1.257	1.239
NO	1.352	1.352	1.351	1.338

Table 7-2: Continued

(b)	H	Me	OMe	NO$_2$
		cis - protonated		
CN	1.350	1.350	1.350	1.363
CO	1.244	1.244	1.244	1.238
NO	1.390	1.391	1.394	1.385
OH	0.990	0.990	0.990	0.990

	H	Me	OMe	NO$_2$
		trans - protonated		
CN	1.373	1.373[†]	1.369	1.388
CO	1.231	1.231[†]	1.233	1.225
NO	1.384	1.384[†]	1.385	1.381
OH	0.991	0.991[†]	0.990	0.992

	H	Me	OMe	NO$_2$
		cis - deprotonated		
CN	1.346	1.347	1.352	N/A[*]
CO	1.257	1.256	1.257	N/A[*]
NO	1.345	1.345	1.350	N/A[*]

	H	Me	OMe	NO$_2$
		trans - deprotonated		
CN	1.354	1.352	1.352	1.383
CO	1.255	1.256	1.257	1.239
NO	1.350	1.350	1.350	1.337

[†]Optimized to a transition state that corresponds to a methyl rotation (imag. freq. = 12i).

[*]after deprotonation, the *cis* conformer relaxed to a *trans* conformation.

7.3.5 Effects of deprotonation, substitution and solvent on the abundance of *cis* and *trans*

The percent (%) abundance of the *cis* and *trans* conformers of the four PBHAs are shown in Table 7-3. They were obtained from taking the Boltzmann distribution of their energies. The abundance of the unsubstituted *cis* protonated PBHA decreased from 99.9 % in the gas phase to 28.0% in ethanol and 22.6 % in water. Upon deprotonation of the

unsubstituted PBHA, the *cis* conformer has 0.0 % abundance in the gas phase, however in ethanol it increased to 65.7%. In water however, no optimized *cis* geometry could be obtained, as deprotonation and re-optimization led to a relaxation to a *trans* geometry.

Table 7-3: Percent (%) abundance relative to energy of hydroxamic acid isomers in gas phase [small (sbs) and large (lbs) basis set], ethanol and water:

R	Conditions	*Trans*		*cis*	
		protonated	Deprotonated	protonated	deprotonated
H	gas phase (sbs)	0.1	100.0	99.9	0.0
	gas phase (lbs)	0.0	100.0	100.0	0.0
	water (sbs)	77.4	51.0	22.6	N/A[†]
	EtOH (sbs)	72.0	34.3	28.0	65.7
Me	gas phase (sbs)	0.0	100.0	100.0	0.0
	gas phase (lbs)	0.0	100.0	100.0	0.0
	water (sbs)	72.5	11.1	27.5	88.9
	EtOH (sbs)	63.7	31.4	36.3	68.6
OMe	gas phase (sbs)	0.0	100.0	100.0	0.0
	gas phase (lbs)	0.0	100.0	100.0	0.0
	water (sbs)	62.9	8.0	37.1	92.0
	EtOH (sbs)	52.3	26.5	47.7	73.5
NO_2	gas phase (sbs)	0.4	100.0	99.6	N/A[*]
	gas phase (lbs)	0.1	100.0	99.9	N/A[*]
	water (sbs)	97.9	50.3	2.1	N/A[†]
	EtOH (sbs)	97.0	100.0	3.0	N/A[*]

[*]*cis* protonated relaxed to the *trans* isomer upon deprotonation

[†]Relaxed to a minimum that appeared to be of *trans* appearance, but different from the *trans* deprotonated optimized structure in both geometry and energy.

The protonated methyl substituted PBHA, was found to have be 100.0 % *cis* abundant in the gas phase for both small and large basis sets. In ethanol and water the presence of *cis* decreased to 36.3 % and 27.5 % respectively. For the deprotonated species, it is the *cis* conformation that was not present in the gas phase (0.0 %

abundance), while in ethanol and water the *cis* % abundance increased to 68.6 % and 88.9 % respectively. Methyl substitution has increased the presence of the deprotonated *cis* conformation in water. This is ideal as chelation can occur more readily when more PBHA molecules have the correct geometry.

The protonated methoxy (-OMe) substituted PBHA was found to be 100.0 % *cis* in the gas phase for both small and large basis sets. In ethanol and water, the % abundance of the *cis* conformation decreased to 47.7 % and 37.1 % respectively. In comparison to the methyl and unsubstituted cis protonated PBHAs, the presence of the cis conformer remains higher than both, remaining almost equally present in ethanol and water. Upon deprotonation, the *cis* conformer was found to have 0.0 % abundance in the gas phase, while in ethanol and water its presence increased to 73.5 % and 92.0 % respectively. In comparison to the methyl and unsubstituted PBHAs, the *cis* conformation is again more abundant with the −OMe substituent, suggesting more chelation can occur because only the *cis* geometry can bind to metals.

The protonated nitro (-NO$_2$) substituted PBHA was found to have a gas phase *cis* abundance of 99.6 % and 99.9 % using the small basis set and large basis set respectively. In ethanol and water, the cis abundance decreased dramatically to 3.0 % and 2.1 % respectively. In comparison to the other three PBHAs, the *cis* conformation is almost negligible for the −NO$_2$ substituted PBHA and the trend observed is that the cis abundance increases with the activating ability of the functional group *para-* to the hydroxamic acid moiety.

7.3.6 TD-DFT Excitation spectra

TD-PBE0 $S_0 \rightarrow S_1$ excitation maxima of the four optimized PBHAs geometries in the gas phase, ethanol and water are shown in Table 7-4. They are reported and discussed to determine solvatochromic trends in the absorption spectra that may be beneficial in identifying experimental absorption peaks as due to either *cis* or *trans,* and protonated or deprotonated. The excitations reported all possess fairly large oscillator strengths of around f=0.4, indicative of an allowed transition. Increasing the size of basis set was found to change the excitation maximum by no more than 4 nm, which is similar to the effect of basis set in our study of Nile Red[32]. Since an increase in basis set did not affect the excitation maxima significantly, only the small basis set was used to investigate the effects of solvation.

For the protonated species, the unsubstituted *cis* PBHA was found to have a gas phase excitation maximum of 296 nm. This is 18 nm less than the gas phase excitation maxima of the *trans* isomer, which was 278 nm. Methyl (-Me) substitution resulted in little change in the *cis* excitation energy (297 nm) while the *trans* red-shifted to 284 nm. For the methoxy substituted PBHA, the excitation energies for the *cis* and *trans* were both 297 nm. In contrast, the *cis* and *trans* -NO$_2$ substituted PBHA was found to have red-shifted significantly to the other three PBHAs, with excitation maxima of 347 nm and 308 nm respectively.

Table 7-4: TD-DFT excitation energies of protonated and deprotonated hydroxamic acids in gas phase (small and large basis set), ethanol and water (with explicit solvation in brackets).

R	Conditions	Trans /nm		Cis /nm	
		protonated	Deprotonated	protonated	deprotonated
H	small basis set	278	486	296	579
	large basis set	277	494	297	577
	water (explicit)	278 (283)	406 (375)	274 (279)	N/A [†]
	EtOH	281	420	279	386
Me	small basis set	284	487	297	581
	large basis set	283	496	299	595
	Water (explicit)	286 (282)	407 (416)	279 (279)	373 (361)
	EtOH	287	419	279	385
OMe	small basis set	297	481	297	482
	large basis set	296	525	300	494
	water (explicit)	291 (297)	409 (381)	280 (286)	402 (359)
	EtOH	293	408	279	415
NO$_2$	small basis set	308	611	347	No minimum[*]
	large basis set	304	602	341	No minimum[*]
	water (explicit)	352 (352)	575 (525)	378 (367)	N/A[†]
	EtOH	349	583	377	No minimum[*]

[*]cis protonated relaxed to the trans isomer upon deprotonation

[†]Relaxed to a minimum to a trans geometry, but was different from the trans deprotonated geometry and energy.

The trend observed for the effect of substitution of the trans protonated PBHA is a blue-shift upon increasing donating ability of the substituent para- to the HA functional group. However, for the cis geometry, the same trend cannot be observed. The cis excitation maxima experiences little change upon substitution with the exception of the NO$_2$- substituted PBHA. The reason that only the cis –NO$_2$ substituted PBHA experiences a red-shift becomes more evident when inspecting the effects of solvation.

For the *cis* conformers, the excitation maxima of the protonated unsubstituted PBHAs in ethanol and water were found to have blue-shifted from 296 nm to 279 nm and 274 nm respectively. For the protonated *cis* methyl substituted PBHA, the excitation maxima is 279 nm in both ethanol and water, which is a blue shift of 18 nm in relation to the gas phase. The -OMe substituted PBHA also experiences a blue shift upon increasing solvent polarity from 297 nm in the gas phase to 279 nm and 280 nm in ethanol and water. At this point of discussion, it appears that a resonance donating substituent *para-* to the HA functional group will red shift excitation maxima, however, the nitro- substituted group breaks this trend. The cis protonated −NO2 substituted PBHA experiences a red-shift from 347 nm in the gas phase to 277 nm and 378 nm in ethanol and water respectively. As a red-shift is indicative of an increase in the magnitude of the dipole moment from the ground to excited state, a close look of the ground state dipole moment vector were observed (not shown).[33] It was found that for the *cis* -H, -Me and −OMe substituted PBHAs, the dipole moment vector all pointed in the same direction, while for the -NO$_2$ in the dipole moment direction was opposite. This is a possible explanation as to why the −NO2- substituted PBHA does not follow the same trend as the other three. Since the dipole moment vector points opposite for NO2- PBHA, it is indicative that the HA functional group is behaving as the donating group, rather than as an acceptor if the one assumes the PBHAs can be modeled as donor-acceptor molecules.

The protonated *trans* unsubstituted PBHA red-shifts from 278 nm in the gas phase to 281 nm from gas phase to ethanol. However in water, the excitation maximum was

the same as that in the gas phase. The −Me and −OMe substitution resulted in a red-shift to 284 nm and 287 nm respectively for the gas phase (sbs) excitation energies. The −NO$_2$ substitution also resulted in a red shift to 308 nm, 30 nm more than the unsubstituted gas phase excitation energy. The effect of solvation on the excitation energy of the *trans* protonated substituted PBHAs was fairly insignificant for the substituents −Me and -OMe. For the −Me substituted PBHA, the excitation energy red-shifted by 3 nm from the gas phase to ethanol. The −OMe substituted PBHA blue-shifted from 297 nm in the gas phase to 291 nm in water. The Nitro Substituent again experienced a significantly large red shift upon solvation from 308 nm in the gas phase to 352 nm in water. This anomaly again is explained by the dipole moment vector is pointing in the opposite direction for the −NO$_2$ substituted PBHA, and therefore the hydroxamic acid is behaving as a donor in a donor-acceptor molecule.

For the deprotonated *cis* conformers, the excitation energy of the unsubstituted PBHA was found to be 579 nm and 577 nm using the small and large basis sets respectively. It can be seen that deprotonation brings a large red-shift in the spectra by almost 300 nm. This observation is also true for the unsubstituted deprotonated *trans* conformer, in which the excitation energies were found to be 486 nm and 494 nm for the small and large basis sets respectively. The effect of basis set appears to remain insignificant and was studied using the small basis set.

The effect of substitution on the *cis* deprotonated conformer was found to be small for −Me substitution and large for −OMe substitution. In comparison to the unsubstituted PBHA −Me substitution resulted in a small red shift of 2 nm to 581 nm,

while the excitation energy of the –OMe PBHA was blue shifted to 482 nm. The effect of -NO_2 substitution could not be evaluated, since no geometry could be obtained for the cis deprotonated species.

The effect of solvation on the *cis* deprotonated unsubstituted PBHA was a blue-shift upon solvation. The unsubstituted PBHA gas phase excitation energy blue-shifted from 579 nm to 386 nm in ethanol. No excitation energy was found for the *cis* unsubstituted PBHA since upon deprotonation, it relaxed to a *trans* like geometry. The methyl and methoxy substituted PBHAs also red-shifted upon solvation. The –Me PBHA red-shifted from 581 nm in the gas phase to 373 nm in water while the –OMe PBHA red-shifted from 482 nm (gas phase) to 402 nm (water).

For the deprotonated *trans* conformers, the effect of substitution on the excitation maximum was found to be small for –Me and -OMe substitution and large for –NO_2 substitution. The excitation energy of the –Me PBHA (487 nm) was only 1 nm more than the unsubstituted PBHA, while for the –OMe PBHA, the excitation energy blue-shifted to 481 nm. Nitro substitution again resulted in an anomalous red-shift to 611 nm, which was explained earlier to be a consequence of its strong resonance withdrawing character.

The effect of solvation on the *trans* deprotonated conformer was found to be a blue shift upon increasing solvent polarity. The unsubstituted PBHA in the gas phase had an excitation maximum of 486 nm which blue shifted to 420 nm in ethanol and 406 nm in water. This blue shift remained significant for the -Me and -OMe substituted PBHAs as

well, in which blue-shifts of 80 nm and 72 nm were found respectively. The $-NO_2$ substituted PBHA also red-shifted from 611 nm in the gas phase to 575 nm in water.

The effect of solvation was further extended by investigating how explicit solvent water molecules can change the excitation energies. Explicit water molecules were coordinated near the N-O oxygen as a more realistic scenario of the PBHA in a protic aqueous environment followed by re-optimization of the geometry and then a TD-PBE0 energy calculation. The excitation energies of water coordinated PBHAs can be seen in brackets in Table 7-5.

For the cis protonated species, it was found that for the *cis* -H, -Me and −OMe substituted PBHAs, explicit solvation resulted in a slight red-shift of no more than 6 nm, while for the NO_2- substituted PBHA, a blue shift of 21 nm occurs. For the *trans* protonated PBHAs, A slight red-shift was observed for −H (5 nm) and −OMe (6 nm) substituted PBHAs, while a blue-shift of 4 nm was observed for the methyl substituted PBHA and no change in excitation energy was observed for the -NO_2 substituted PBHA. For the cis deprotonated PBHAs, explicit solvation resulted in the −Me and −OMe excitation energies blue-shifting by 14 nm and 43 nm respectively. Finally, the four *trans* deprotonated PBHAs all exhibit blue-shifts upon including a coordinating water. The smallest blue-shift observed was that of the −Me substituted PBHA (9 nm) while the largest blue-shift was experienced by the −NO_2 (50 nm) substituted PBHA. No conclusions were drawn regarding the inclusion of specific water molecules since no clear trend was observed.

7.3.7 Determination of pK_A

pK_A values are listed in Table 7-5 for the four PBHAs in aqueous media, where the inclusion of explicit solvation, a correction factor and both together are shown as potential improvements to our earlier method.

Table 7-5: Relative pK_A values of PBHAs in gas phase and water using the small basis set [6-31+G(d)] and including either or both a explicit solvation and correction factor.

-R	theoretical pK_A		with explicit solvation		with correction factor		explicit solv. & corr. Factor	
	cis	trans	cis	trans	cis	trans	cis	trans
H	N/A*	17.34	N/A*	12.14	N/A*	7.84	N/A*	6.37
Me	17.10	18.03	12.78	9.96	7.75	8.10	6.60	5.60
OMe	17.06	17.82	12.46	12.16	7.73	8.02	6.49	6.38
NO_2	N/A*	13.61	N/A*	9.88	N/A*	6.44	N/A*	4.35

* pK_A values could not be obtained because the *cis* deprotonated geometry could not be optimized.

In Table 7-5, the *cis* pK_A values are reported to be 17.10 and 17.06 for the −Me and −OMe substituted acids, respectively. No pK_A was obtained for the *cis* unsubstituted and −NO_2 PBHAs since deprotonation resulted in and optimized *trans* conformer only. For the *trans* isomer, the pK_A was found to be 17.34, 18.03, 17.82, and 13.61 for the unsubstituted, −Me, −OMe and −NO_2, respectively. These values are most definitely overestimated, since the unsubstituted (mixture of *cis* and *trans*) PBHA acid is reported to have a pK_A of 8.09 ± 0.19.[34] This poor estimation of pK_A using *ab initio* techniques has been previously reported by Dissanayake and Senthilnithy , who showed that using the thermodynamic cycle used here for a series of smaller hydroxamic acids also overestimated pK_A values by about 9 units.[15] Their solution to this problem however

160

could not be used for our purpose; since their work could only be carried out for hydroxamic acids which do not possess *N*-phenyl substituents. This is because they studied a series of hydroxamic acids that are not N-phenyl substituted and a more acidic hydrogen is present on the nitrogen allows for rearrangements to keto-, oxime- and nitroso- type species.

The effects of substitution also show some peculiar results. Although little discussion on the pK_A of the *cis* isomers can be done with respect to the unsubstituted hydroxamic acid, for the *cis* –Me substituted acid the pK_A of 17.10, is a whole pK_A value lower than its *trans* counterpart. Similarly, the –OMe substituted acid (pK_A=17.06) was lower than its *trans* counterpart, which had a pK_A of 17.82. Since the *cis* isomer is expected to form an intramolecular hydrogen-bond,[30] the *trans* conformer should possess the more acidic hydrogen, contrary to what is observed here. However, it is in agreement with the work of Dissanayake and Senthilnithy, in which they reported the pK_A of a formo-substituted hydroxamic acid to be lower for the *cis* isomer.[15]

To improve the pK_A values we have included an explicit water molecule coordinated to the oxylamine oxygen. In the second column of Table 7-5, it is seen that the inclusion of explicit solvation improved the pK_A significantly. The *trans* –NO_2 substituted conformer improved the least from 13.61 to 9.88, which is still 3.77 units less. The *trans* –Me conformer improved the most from 18.03 to 9.96. Another improvement is that the pK_A values of the *cis* conformers are now lower than those of the *trans*. For the *cis* –Me substituted PBHA, the inclusion of a water molecule resulted in a pK_A of 12.78 while

the *trans* was 9.96. Similarly, the *cis* –OMe substituted PBHA with explicit solvation now has a value of 12.46, while the *trans* isomer has a value of 12.16.

The inclusion of a correction factor based on how far our level of theory deviated from experiment was implemented and also helped lower the pK_A values of the hydroxamic acids. The correction factor was obtained by linearly correlating the experimental pK_A of eleven well documented carboxylic acids against theoretical values ($y = 3.6876x - 8.0317$, $r^2=0.98$) that were optimized at the same level of theory (PBE0/6-31+G(d)). The acids included six aliphatic carboxylic acids (methanoic to hexanoic) and four *para*-substituted benzoic acids (R=H, Me, OMe, NO$_2$).

The correction factor lowered the pK_A of the *trans* species from 17.34 to 7.84 for the unsubstituted PBHA, a difference of 9.5. Similar results were found for the other *trans* PBHAs in which an improvement of 7-9.5 pK_A units was observed. The pK_A values are likely closest to experiment now, since hydroxamic acids typically have pK_A values in the range of 8-10. However, the correction factor could not reproduce the trend of a *trans* isomer having the lower pK_A values than its *cis* counterpart.

The final improvement that we attempted was the inclusion of both explicit solvation and a correction factor. A correction factor for the explicitly solvated hydroxamic acids was included, in which the same eleven acids used earlier had explicit water molecules coordinated to them as well ($y = 2.8102x - 5.7708$, $r^2=0.97$) and then optimized using the same level of theory. The predicted pK_A values were found to be far too low. For the unsubstituted *trans* acid, the pK_A was predicted to be 6.37, well below the experimental value of 8.09±0.19[34]. This could be due to the fact that the aliphatic

carboxylic acids should not be coordinated by water molecules the same way was other acids, since they exist most stably as dimers in solution.[35]

The discrepancy between experimental and theoretical pK$_A$ remains a problem and most solutions proposed in the literature is limited to a specific set of molecules.[15] Another way of improving the prediction of pK$_A$ is by scaling the oxylamine oxygen so that the it occupies less space.[27]

7.4 Conclusions

Our work presents four *N*-phenylbenzohydroxamic acids (-H, -Me, -OMe, -NO$_2$) which have had little to no experimental study. This work successfully predicted the *cis* and *trans* presence of each species in the gas phase and solution, and TD-DFT predicted UV/VIS spectra which is beneficial for the purpose of identification. It was found that the methyl and methoxy substituted were optimal for the purpose of increasing the *cis*-presence when deprotonated. In addition, the pK$_A$ of the –Me substituted acid was also found to have the highest pK$_A$ of the latter, giving it selective chelating abilities. Nitro substitution had a negative effect on the abundance of *cis* isomers in solutions and upon deprotonation, no *cis* geometry could be optimized. The inclusion of explicit solvation successfully lowered the pK$_A$ although values remained high. A correction factor also helped lower the pK$_A$, however invoking both explicit solvation and a correction factor lowered the pK$_A$ values too far.

7.5 References

1 R. Senthilnithy, M. D. P. de Costa and H. D. Gunawardhana, *J. Nat. Sci. Found. Sri Lanka*, 2008, 36, 191-198

2 R. Senthilnithy, M. D. P. De Costa and H. D. Gunawardhana, *Lumin.*, 2009, 24, 203-208

3 G. C. Panda and S. P. Bag, *Indian J. Chem.*, A, 1997, 36, 113-114

4 D. Griffith, K. Krot, J. Comiskey, K. B. Nolan and C. J. Marmion, J. Chem. Soc., *Dalton Trans.*, 2008, 137-147

5 K. K. Ghosh and P. Tamrakar, *Indian J. Chem.*, A, 2003, 42, 1081-1085

6 Y. K. Agrawal, *Thermochim. Acta*, 1977, 18, 245-249

7 H. Kehl, *Chemistry and Biology of Hydroxamic Acids*, S. Karger AG, New York, 1982

8 D. A. Brown and M. V. Chidambaram, *Metal Ions in Biological systems*, Marcel Dekker, New York, 1982

9 K. Kobashi, J. Hase and K. Uehara, *Biochem. Biophys. Acta*, 1962, 65, 380

10 D. Hamilton, R. Natarajan and I. Nirdosh, *Ind. Eng. Chem. Res.*, 2009, 48, 5584-5589

11 M. T. Caudle, C. D. Caldwell and A. L. Crumbliss, *Inorg. Chim. Acta*, 1995, 240, 519-525

12 Y. K. Agrawal and S. G. Tandon, *J. Inorg. Nucl. Chem.*, 1972, 34, 1291-1295

13 Y. K. Agrawal and S. G. Tandon, *J. Inorg. Nucl. Chem.*, 1974, 36, 869-873

14 H. Tavakol, *J. Mol. Structure., THEOCHEM*, In Press, Accepted Manuscript

15 D. P. Dissanayake and R. Senthilnithy, *J. Mol. Structure., THEOCHEM*, 2009, 910, 93-98

16 A. Niño, C. Muñoz-Caro and M. L. Senent, *J. Mol. Structure., THEOCHEM*, 2000, 530, 291-300

17 L. J. Yamin, C. A. Ponce, M. R. Estrada and F. T. Vert, *J. Mol. Structure., THEOCHEM*, 1996, 360, 109-117

18 I. Ciofini, *Magn. Reson. Chem.*, 2004, 42, S48-S56

19 R. Senthilnithy, H. D. Gunawardhana, M. D. P. De Costa and D. P. Dissanayake, *J. Mol. Structure., THEOCHEM* 2006, 761, 21-26

20 K. K. Ghosh and S. Roy, *Indian J. Chem.*, B, 1997, 36, 324-328

21 B. Garcia, S. Ibeas, F. J. Hoyuelos, J. M. Leal, F. Secco and M. Venturini, *J. Org. Chem.*, 2001, 66, 7986-7993

22 R. Casasnovas, J. Frau, J. Ortega-Castro, A. Salvà, J. Donoso and F. Muñoz, *J. Mol. Struct., THEOCHEM, The 6th Congress on Electronic Structure: Principles and Applications (ESPA 2008)*, 2009, 912, 5-12

23 M. J. Frisch, G. W. Trucks, H. B. Schlegel, G. E. Scuseria, M. A. Robb, J. R. Cheeseman, J. A. Montgomery, T. V. Jr., K. N. Kudin, J. C. Burant, J. M. Millam, S. S. Iyengar, J. Tomasi, V. Barone, B. Mennucci, M. Cossi, G. Scalmani, N. Rega, G. A. Petersson, H. Nakatsuji, M. Hada, M. Ehara, K. Toyota, R. Fukuda, J. Hasegawa, M. Ishida, T. Nakajima, Y. Honda, O. Kitao, H. Nakai, M. Klene, X. Li, J. E. Knox, H. P. Hratchian, J. B. Cross, V. Bakken, C. Adamo, J. Jaramillo, R. Gomperts, R. E. Stratmann, O. Yazyev, A. J. Austin, R. Cammi, C. Pomelli, J. W. Ochterski, P. Y. Ayala, K. Morokuma, G. A. Voth, P. Salvador, J. J. Dannenberg, V. G. Zakrzewski, S. Dapprich, A. D. Daniels, M. C. Strain, O. Farkas, D. K. Malick, A. D. Rabuck, K. Raghavachari, J. B. Foresman, J. V. Ortiz, Q. Cui, A. G. Baboul, S. Clifford, J. Cioslowski, B. B. Stefanov, G. Liu, A. Liashenko, P. Piskorz, I. Komaromi, R. L. Martin, D. J. Fox, T. Keith, M. A. Al-Laham, C. Y. Peng, A. Nanayakkara, M. Challacombe, P. M. W. Gill, B. Johnson, W. Chen, M. W. Wong, C. Gonzalez and a. J. A. Pople, Gaussian 09 (Revision A1), Gaussian, Inc., Wallingford, CT, 2009

24 J. P. Perdew, K. Burke and Y. Wang, *Phys. Rev., B*, 1996, 54, 16533 -16539

25 R. Ditchfield, W. J. Hehre and J. A. Pople, *J. Chem. Phys.*, 1970, 52, 5001-5007

26 S. Mierts, E. Scrocco and J. Tomasi, *Chem. Phys.*, 1981, 55, 117-129

27 F. Khalili, A. Henni and A. L. L. East, *J. Mol. Struct., THEOCHEM*, In Press, Accepted Manuscript,

28 M. D. Liptak, G. C. Shields, K. C. Gross, P. G. Seybold and S. Feldgus, *J. Am. Chem. Soc.*, 2002, 124, 6421

29 M. D. Liptak and G. C. Shields, *J. Am. Chem. Soc.*, 2001, 123, 7314

30 M. Davies and N. A. Spiers, *Spectrochim. Acta*, 1959, 15, 487

31 J. J. Dannenburg, L. Turi, J. B. Rama and O. N. Ventura, J. Am. Chem. Soc., 1993, 115, 5754-5761

32 P. O. Tuck, R. C. Mawhinney and M. Rappon, Phys. Chem. Chem. Phys., 2009, 4471-4480

33 P. Suppan and N. Ghoneim, Solvatochromism, Royal Society of Chemistry, Cambridge, 1997

34 R. Natarajan, unpublished results

35 C. Reichardt, Solvents and Solvent Effects in Organic Chemistry, WILEY-WCH, Weinheim, 2003

Chapter 8

Effects of Plasticizers on the Rate of Photochromism of 6-NO$_2$-

BIPS in Polymer Media

8.1 Introduction

Photochromism is the term that describes the reversible transformation of two chemical species with at least one pathway initiated by light.[1] Spiropyrans (*Figure 8-1*) were first synthesized by Decker and Fellenberg in 1909[2] and are photochromic compounds that first gained interest when Fischer and Hirschberg proposed them as a photochemical memory device.[3] Since then, spiropyrans have been researched for the potential application of metal[4] and proton[5] sensing, electro-optical storage,[6] magnetic switches,[7] ophthalmic lenses,[8] modulated light filters,[9] logic switches[10] and as an alternative to food preservatives.[11] New spiropyran analogs, such as spiroxazines and benzospiropyrans, have also become of interest due to their increased fatigue resistance.[11-13]

Figure 8-1: Molecular structure of 6-NO2-BIPS in ring-closed form (spiropyran) and ring-open form (merocyanine).

The photochromism of spiropyran originates from its indoline and chromene moieties which are separated by a spiro bond.[14] The spiro C-O bond is elongated (weakened) in the ground state due to lone-pair donation of the indoline nitrogen into the anti-bonding orbital of the C-O bond. When irradiated with UV light (~345nm), the

C-O bond is cleaved and the two moieties become conjugated through a methylene bond, which gives it a violet-blue color. The merocyanine species is zwitterionic with a positive charge localized on the indilino-nitrogen and a negative charge on the chromene oxygen. Upon visible light absorption or heat, the merocyanine species returns to the ring-closed, unconjugated spiropyran structure. The absorption spectrum of merocyanine is sensitive to its surrounding (solvatochromic) and arises from the destabilization of a large charge transfer with increasing polarity of the medium.[15]

For 6-NO$_2$-BIPS to be viable for photochromic applications, it must possess a good quantum yield upon irradiation, fatigue resistance, dispersability, as well as a polarity and photostationary state that are specific to its application. Thus, the understanding of the surrounding media on the spiropyran-merocyanine system is crucial since it may affect all of these properties. Spiropyrans are most often dispersed in polymer media which will affect the photostationary state, rate of coloration and discoloration (by both visible light and heat) and the color of the merocyanine species.

Several works of 6-NO$_2$-BIPS (1',3'-Dihydro-1',3',3'-trimethyl-6-nitrospiro[2H-1-benzopyran-2,2'-(2H)-indole]) and related photochromic dyes in polymer materials have been reported in past literature. A study on the effect of addition of Iron (II) phthalocyanine to spiropyrans in polymer matrices to protect it from laser degradation was shown to be beneficial when laser pulse were at low pulse rates.[16] Fatigue resistance of 6-NO2 was reported by Davis and co-workers that 6-NO$_2$-BIPS linked to the polymeric polymethacrylate backbone possesses mechanoresponsive properties.[17]

Physical stress would cause ring opening and a colour change to the polymer material, and thus indicated that the plastic has been damaged.

Although a proposed mechanism regarding the ring opening of 6-NO$_2$-BIPS has been given,[14] some aspects are still to be elucidated. Recently, Jeng-Shyong Lin studied the kinetics of 6-NO$_2$-BIPS in PMMA, PEMA, P(n-Butyl)MA and SBS.[18,19] He reported that in the more polar polymer, photocoloration occurred faster while decoloration was slower. A polymer with a lower glass transition temperature was found to increase the rate of discoloration. In 2008, Jannakoudakis et al. conducted a kinetic study of 6-NO$_2$-BIPS in PS and polycaprolactone with the addition of UV absorbers.[11] They found that the addition of UVASORB S5 and Irganox 1098 increased the rates of ring opening and closing due to positive plasticization effects.

In this communication, the nitro-substituted spiropyran 6-NO$_2$-BIPS (1',3'-Dihydro-1',3',3'-trimethyl-6-nitrospiro[2H-1-benzopyran-2,2'-(2H)-indole]) is studied in a variety of polymer media. Although the study on 6-NO2-BIPS dispersed in polymers has been studied before, however, the addition of various plasticizers and insight on how they affect the rate of discoloration has not.

8.2 Methods

The polymers polymethyl methacrylate (PMMA), poly n-butyl methacrylate [P(n-B)MA], polystyrene (PS), poly tert-butyl styrene (PTBS), polyvinyl acetate (PVAc) and polycarbonate (PC) were obtained from Polysciences inc. The polymer pairs PMMA/P(n-B)MA and PS/PTBS allowed us to study the effects of the glass transition temperatures

(T_g) and free volume of the polymers while holding the polarity constant. The T_g values

of the polymers are reported in Table 8-1, while no free volume values have been

reported for these polymers of particular chain lengths at room temperature (298K).[20]

The polymers were purified by dissolving them in dichloromethane, precipitating them

in cold methanol, and then desiccated for 48 hours. The photochromic dye 6-NO_2-BIPS

was obtained from Sigma-Aldrich and no further purification was taken. Polycarbonate

was chosen to study the effects of plasticizers because of its good optical and

mechanical properties. Four classes of plasticizers were investigated in polycarbonate.

The first class of plasticizer was the phthalates, which included dimethyl, diethyl,

dibutyl, di- n-octyl, and benzyl butyl phthalates. This class is the most commercially

available plasticizer and thus was studied in more detail. The others included diethyl

adipate (DEA), octanoic and decanoic acid, and 1-octanol. The long chain carboxylic

acids were chosen to study the impact of a protic nature on the rates of decoloration,

while still having a plasticizing ability with their length.

Table 8-1: Glass transition temperatures of polymers investigated in this study

Polymer	T_g (K)
PMMA	378[26]
P(n-B)MA	293[25]
PS	368[26]
PTBS	399[26]
PVAc	307[26]
PC	423[25]

Thin films were made by dispersing the dye into the polymer matrix by solution casting, similar to the method stated in earlier works.[21-24] A 1% dye to polymer ratio by mass was taken to determine the rate of discoloration of 6-NO_2-BIPS in the polymers. The dye was dispersed into the polymer by dissolving both the polymer and dye in dichloromethane and then cast on a quartz slide. The polymer cast slides were then desiccated for 48 hours to remove any remaining traces of solvent. The films were stored under vacuum and in the dark when not used immediately.

For the decoloration kinetics, the polymer films were first irradiated for 3 minutes using a Blak-Ray B100 long range UV lamp with a filter allowing wavelengths greater than 300nm to pass through. This long exposure time was to ensure that the thin film was converted to the merocyanine species. The colored thin film samples were then back-irradiated with a 100W visible-range tungsten lamp. The tungsten lamp was found to have a radiant flux of 1.49 einstein/s, determined by the chemical actinometer Aberchrome 540.[24] Samples were then irradiated with a visible tungsten lamp for time increments of 5-20 seconds and at least 10 measurements were recorded. Absorption methods were recorded on a Perkin Elmer Lambda-11 spectrophotometer using a modified sample holder to support the quarts slides having thin polymer films cast upon them.

The rate of discoloration was determined using the first order kinetic equation:

$$\ln(A_T - A_\infty) = -k_{MC \to SP} t + \ln(A_0 - A_\infty)$$
(8-1)

A linear plot of $\ln(A_T-A_\infty)$ as a function of irradiation time can be then used to find the rate of decoloration and assess the assumption of first order kinetics.

8.3 Results and Discussion

8.3.1 Absorption band shifting and rate of decoloration in neat polymer matrices

Figure 8-2 illustrates the decoloration of irradiated 6-NO2-BIPS dispersed in PS, PTBS, PMMA, Pn-BMA, PVAc and PC. In PS, the ring-open merocyanine (MC) form was found to return to the spiropyran (SP) ring-closed structure in a linear fashion, and the rate constant of decoloration was found to be $0.019 \, s^{-1}$. 6-NO2-BIPS also returned to the ring-closed SP form linearly ($r^2 > 0.99$) in the polymers PTBS, PMMA and PC which had rate constants of decoloration of $0.018 \, s^{-1}$, $0.014 \, s^{-1}$ and $0.009 \, s^{-1}$, respectively. However, $6\text{-NO}_2\text{-BIPS}$ was found to return to the colorless SP form in a non-linear fashion for the polymers PVAc and Pn-BMA. $6\text{-NO}_2\text{-BIPS}$ in PVAc and Pn-BMA were investigated near or above the T_g (307 K and 293 K, respectively[25,26]) of these polymers and the kinetics may not be of first order because molecular motions can take place at this critical temperature. The merocyanine can also take on four conformers, and only when restricted in a polymer matrix above the T_g is the rate of decoloration linear.[27]

This is the case for the other four polymers which were investigated above their T_g, as their rates of decoloration were found to be linear. However, both the local polarity and polymer free volume may also play a role in ring-closure.[28] Above the T_g, the free volume remains constant, however, a minimum free volume is required for the mechanism of ring closure to occur, and this minimum volume is observed. When comparing the rates of decoloration of $6\text{-NO}_2\text{-BIPS}$ in PS and the bulkier PTBS ($0.019 \, s^{-1}$ and $0.018 \, s^{-1}$ respectively), the difference is within experimental error and suggest that both polymers possess this minimum volume required. For $6\text{-NO}_2\text{-BIPS}$ in PC, the rate
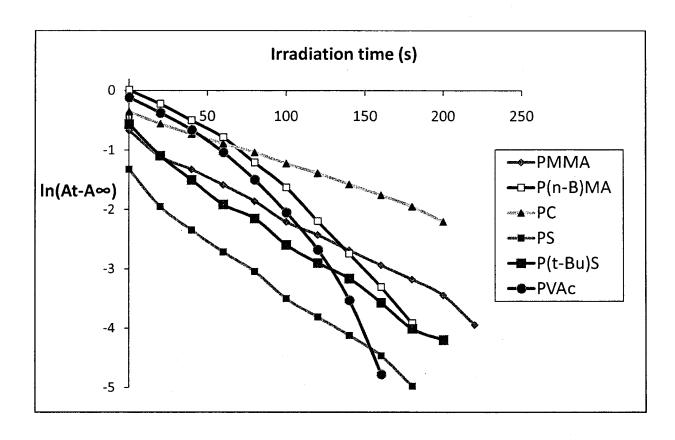
Figure 8-2: Plots of the absorbance (at the λ_{max}) of 6-NO2-BIPS as a function of irradiation time in neat polymer media.
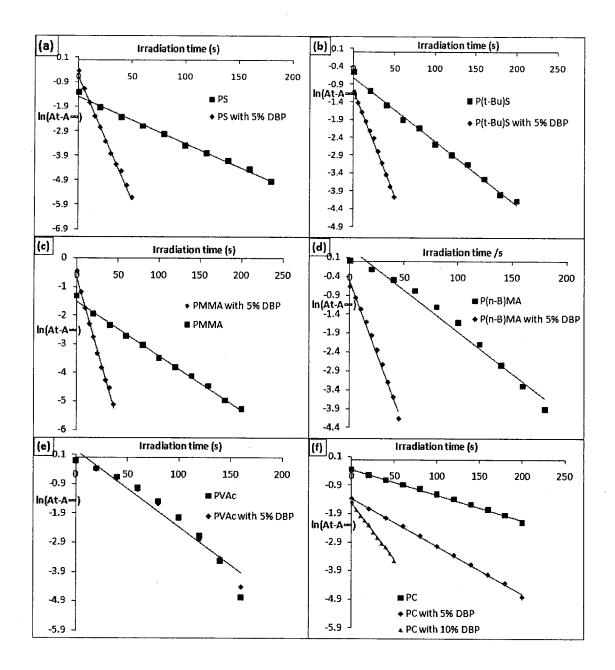
Figure 8-3: 6-NO2-BIPS dispersed in (a) PS (b) PTBS (c) PMMA, (d) Pn-BMA, (e) PVAc and (f) PC with and without the plasticizer dibutyl phthalate.

constant of 0.009 s^{-1} and is well below the rate constants found for 6-NO$_2$-BIPS in the other polymers, and could be because PTBS and PS possess pendant groups that can still undergo motion and facilitate ring-closure even above the T$_g$, while PC does not possess large pendant groups, and thus makes ring-closure rather difficult.

Table 8-2: Decoloration rate constants and absorption maxima for the merocyanine form of 6-NO$_2$-BIPS (in brackets) in polymers with and without the addition of dibutyl phthalate (DBP).

Polymer	Additive (%)	Rate constants of decoloration/ s^{-1} (λ_{max}/nm)
PS	N/A	0.019 (603)
PTBS	N/A	0.018 (593)
PMMA	N/A	0.014 (574)
PnBMA	N/A	0.022 (552)
PVAc	N/A	0.027 (558)
PC	N/A	0.009 (589)
PS	DBP (5%)	0.100 (587)
PTBS	DBP (5%)	0.059 (589)
PMMA	DBP (5%)	0.101 (571)
PnBMA	DBP (5%)	0.077 (549)
PVAc	DBP (5%)	0.027 (565)
PC	DBP (5%)	0.017 (591)

The polarity of the polymer was assessed by observing the absorption maxima of the merocyanine structure, which are tabulated in Table 8-2. The general trend is a blue-shift in the absorption maxima as the polarity of the polymer was increased. This blue shift has been reported both in liquid and polymer environments.[15] The λ_{max} for the merocyanine (MC) form of 6-NO$_2$-BIPS in PS, PTBS, PMMA and PC were found to be 603 nm, 593 nm, 574 nm and 589 nm respectively. The effect of polarity is best illustrated by comparing the value of non-polar PS of 603 nm to that of the more polar PMMA (574

nm). Because MC possesses two full charges (zwitterionic), the blue shift (negative solvatochromism) arises from a non-polar excited state which is destabilized by the more polar polymer. This is in accordance with the findings of Jeng-Shyong Lin, who studied the 6-NO$_2$-BIPS in SBS and PMMA in which he found a blue shift from 600 nm to 575 nm.[18,19] The effect of plasticization also brings a blue-shift in the absorption band of the ring-open MC species. Since both pairs of Pn-BMA/PMMA and PTBS/PS are similar in polarity but differ in T$_g$ and free volume, the effects of plasticization and dye-polymer separation on the absorption maxima can be explained in the absence of solvent polarity. The λ_{max} of 6-NO$_2$-BIPS in P(n-B)MA was found to be 552 nm and considerably more blue shifted than the λ_{max} in PMMA (574 nm). This shows that lowering the T$_g$ resulted in a blue-shift in the absorption maximum and is expected since more molecular motion of the polymer allows for better relaxation of the polymer around the ground state, resulting in a large S$_0$→S$_1$ energy gap. For the pair PTBS and PS, both polymers are above their T$_g$ and thus only free volume should be considered. The absorption maxima of PS (603 nm) and PTBS (593 nm) showed a blue shift of 10 nm. This is considerably smaller than the effects of polarity and T$_g$, however PTBS may have a larger free volume because of its bulkier tert-butyl group and therefore there is more space for the ring-closure of 6-NO$_2$-BIPS.

8.3.2 Addition of dibutyl phthalate (DBP) to polymer matrices

The addition of DBP was to observe the effects of plasticization as well as the potential specific interations between plasticizer and spiropyran, which could in turn affect the kinetics of the bleaching of the thin films to its colorless form. Adding DBP

increased the rate constant of decoloraton in all cases. However, the plasticizer had more influence on some polymer matrices than others. In PS, the rate of decoloration was found to increase 5 fold (0.019 s^{-1} to 0.10 s^{-1}) and a blue shift from 603 nm to 587 nm suggests that the plasticization greatly increased the rate and interaction of the polymer with the 6-NO_2-BIPS MC structure. Similar observations are found in PMMA, PTBS and PC. However, the originally non-linear first-order plot of Pn-BMA was found to become linear with the addition of DBP, with an increased decoloration rate from 0.022 s^{-1} to 0.077 s^{-1} and a blue shift in the absorption maxima of 3 nm was observed upon adding 5% dibutyl phthalate (DBP). The new linear first-order plot suggests specific interactions between the DBP and Pn-BMA may have given a negative plasticization effect (increased T_g). However, the increase of polarity was the stronger factor since the absorption maxima was still blue shifted by 3nm and an increase of decoloration rate by almost four-fold was still observed. A possible explanation for this could be with the addition of the plasticizer, the merocyanine conformer that can undergo ring-closure is preferred to the merocyanine structures that cannot undergo ring-closure. The addition of 5% DBP to the PVAc matrices was found to bring no change to the rate of decoloration (0.027 s^{-1}), however the increase in λ_{max} would suggest the addition of this plasticizer does not prefer one merocyanine conformer over another.

8.3.3 Effects of plasticizers on the rate of decoloration of 6-NO2-BIPS in polycarbonate (PC)

Table 8-3: Rates of decoloration and λ_{max} (in brackets) for the MC form of 6-NO$_2$-BIPS in PC with plasticizing agents (5% by mass) added.

Additive (%)	Rate constants of decolouration/s^{-1} (λ_{max}/nm)
N/A	0.009 (589)
DBP (5%)	0.017 (591)
DEA (5%)	0.0109 (586)
Octanoic Acid (5%)	0.0127 (571)
Decanoic Acid (5%)	0.0156 (570)
1-octanol (5%)	0.0161 (587)
DMP (5%)	0.017 (593)
BzBP (5%)	0.0153 (594)
DEP (5%)	0.0160 (594)
Dn-OP (5%)	0.0163 (595)

The additions of plasticizers to the polymer thin films were added to elucidate the effects of depressing the glass transition temperature on the kinetics of ring closure in 6-NO$_2$-BIPS. In addition, the influence of the addition of these plasticizers on the absorption maxima was also studied. The plasticizers reported include dimethyl phthtalate (DMP), diethyl phthalate (DEP), benzylbutyl phthalate (BzBP), di-(n-octyl) phthalate (D-nOP), diethyl adipate(DEA), octanoic acid, decanoic acid and 1-octanol. Table 8-3 shows the list of plasticizers (5% by mass) and their respective impact on the rate of decoloration. When no additive was present, the rate of decoloration of 6-NO$_2$-BIPS in polycarbonate (PC) was found to be 0.009 s^{-1}. With the addition of dimethyl phthalate (DMP), the rate of decoloration was found to be 0.017 s^{-1}, which is almost an increase of two-fold. PC thin films with 5% by mass DEP, DBP, BzBP and D-nOP showed

similar values with decoloration rates of 0.016 s^{-1} and 0.017 s^{-1}, 0.0153 s^{-1} and 0.0163 s^{-1} respectively. No trends based on the chain length or sterics was evident in this class of plasticizers. The absorption maxima of all the phthalate containing polymer thin films ranged from 591 nm to 595 nm, suggesting that the chain length and bulkiness of the plasticizers was not a contributing factor to the shift in the absorption band of merocyanine. DEA-containing PC thin films showed the smallest change in the rate of decoloration, with a rate constant of only 0.011 s^{-1}. However, the absorption energy of the 6-NO$_2$-BIPS was 586 nm suggesting that the blue-shift was most likely a result of increasing the polarity of the matrix, rather than plasticization effect, since only a small increase in the rate of decoloration was observed. In PC with 5% 1-octanol by mass, 6-NO$_2$-BIPS was found to have an increase in the decoloration constant from 0.009 s^{-1} to 0.016 s^{-1}, comparable to that of DEP and dn-OP. The absorption maxima was further blue-shifted than in PC thin films with phthalate plasticizers, suggesting that the increase in polarity of the plasticizer may be the principal cause of the increasing blue shift.

Both octanoic and decanoic acid blue-shifted the spectra enormously with λ_{max} values of 571 nm and 570 nm respectively. This is the same observation for 6-NO$_2$-BIPS with the plasticizers the due to the increase of polarity of the plasticizers 1-octanol, DEP and dn-OP. The addition of octanoic and decanoic acid also (5% by mass) yielded decoloration rate constants of 0.013 s^{-1} and 0.016 s^{-1} respectively. The rate of decoloration for octanoic acid was less, which is expected since its smaller size would allow it to have more freedom to interact with 6-NO$_2$-BIPS and not be hindered by the

polymer's restriction of motion. A small decrease in the rate constant of decoloration was observed for octanoic acid, since the proton could stabilize the ring-open MC species effectively. However, the same observation does not occur with decanoic acid. $6-NO_2$-BIPS in PC with decanoic acid showed a rate of decoloration similar to thin films with phthalate plasticizers added to them.

8.3 Conclusions

A kinetic study of the ring closure of $6-NO_2$-BIPS was used successfully to show the relationship of polymer environment on the decoloration rate and absorption. The addition of plasticizers tested the idea that increasing the mobility of $6-NO_2$-BIPS in the restricted polymer matrices allowed for faster reactions. These decoloration rates were only found to be of first order if the T_g of the polymer was above the temperature of study (~298K). The inclusion of long chain carboxylic acids showed that plasticization increase the rate of decoloration, but the protic hydrogen had the ability to stabilize the merocyanine species, lowering the enhancing nature of the plasticizer. Work which was not reported included the potential ability of the dye to act as a plasticizer itself, and in turn help its decoloration rates, however by varying the concentration from 1-10% dye:polymer ratio yielded results that suggest the effect was insignificant.

8.5 References

1 H. Durr and H. Bouas-Laurent, *Photochromism: Molecules and Systems*, Elsevier, Amsterdam, 2003

2 H. Decker and H. Fellenberg, *Liebigs Ann. Chem.*, 1909, 364, 1

3 E. Fischer and Y. Hirschberg, *J. Am. Chem. Soc.*, 1952, 4522

4 H. Gorner and A. K. Chibisov, *Chem. Phys.*, 1998, 237, 425-442

5 A. Radu, R. Byrne, N. Alhashimy, M. Fusaro, S. Scarmagnani and D. Diamond, *J. Photochem. Photobiol., A,* 2009, 206, 109-115

6 A. Romani, G. Chidichimo, P. Formoso, S. Manfredi, G. Favaro and U. Mazzucato, *J. Phys. Chem., B,* 2002, 106, 9490-9495

7 Y. Einaga, *J. Photochem. Photobiol., C,* 2006, 7, 69-88

8 N. Nakadzima, A. Kavasima and T. Mogama, Patent 60-103347

9 Ryojiro and M. Takashi, US Patent 5644416

10 K. L. Koompa and R. D. Levine, *Proc. Nat. Acad. Sci.,* 2001, 98, 410

11 A. Samoladas, D. Bikiaris, T. Zorba, K. M. Paraskevopoulos and A. Jannakoudakis, *Dyes Pigm.,* 2008, 76, 386-393

12 S.-H. Kim, C. Yu, C.-J. Shin and M.-S. Choi, *Dyes Pigm.,* 2007, 75, 250-252

13 S.-H. Kim, C.-H. Ahn, S.-R. Keum and K. Koh, *Dyes Pigm.,* 2005, 65, 179-182

14 B. Lukyanov and M. Lukyanova, *Chem. Hetero. Comp.,* 2005, 41, 281-311

15 P. Suppan and N. Ghoneim, *Solvatochromism,* Royal Society of Chemistry, Cambridge, 1997

16 A. Athanassiou, D. Sahinidou, V. Arima, S. Georgiou, R. Cingolani and C. Fotakis, *J. Photochem. Photobiol., A,* 2006, 183, 182-189

17 D. A. Davis, *Nature,* 2009, 459, 68-72

18 J.-S. Lin and H.-T. Chiu, *J. Polym. Res.,* 2003, 10, 105-110

19 J.-S. Lin, *Eur. Polym. J.,* 2003, 39, 1693-1700

20 J. M. G. Cowie, *Polymer Chemistry & Physics of Modern Materials,* International Textbook Company Limited, Aylesbury, 1973

21 M. Rappon, K. M. Ghazalli and S. Rochanakij, *Eur. Polym. J.,* 1995, 33, 1689-1693

22 M. Rappon, A. Chuenarm, A. J. Duggal, H. Gill, O. Bhaovibul and R. T. Syvitski, *Eur. Polym. J.,* 1991, 27, 365-370

23 M. Rappon, R. T. Syvitski and A. Chuenarm, *Eur. Polym. J.,* 1992, 28, 399-403

24 M. Rappon and K. M. Ghazalli, *Eur. Polym. J.,* 1995, 31, 1185-1190

25 *Physical Properties of Polymers Handbook,* AIP Press, Woodbury, NY, 1996

26 *Polymer Handbook,* John Wiley and Sons, Toronto, 1989

27 Y. Futami, M. L. S. Chin, S. Kudoh, M. Takayanagi and M. Nakata, *Chem. Phys. Lett.*, 2003, 370, 460-468

28 A. K. Doolittle, *J. Appl. Phys.*, 1951, 22, 1471-1475

Chapter 9

Summary, Conclusions and Recommendations

9.1 Solvatochromism and Photochromism

Solvatochromism is the effect of solvation on the electronic spectra of solute molecules and is the central theme of this thesis. This is especially important because if one desires to manipulate the physical or chemical properties of a molecule in the condensed phase, one must have an understanding of how the "crowd" can influence the "individual". In this section, we demonstrate that the conclusions drawn from chapters 3-8 provide a qualitative and quantitative definition of solvatochromism, and show its potential to be used in application.

For a molecule to be solvatochromic, its electronic states will be highly stabilized or destabilized because of additional attractive or repulsive interactions between the solute and solvent that would not exist in the gas phase.[1] Common interactions that can greatly influence the energy are electrostatic interactions. These interactions are most easily characterized from the dipole moment, which expresses the non equal distribution of charge over a molecule as a vector. Upon excitation, the charge distribution may be significantly different, resulting in a significantly different dipole moment, and thus the lowering of energy from electrostatic attraction may increase or decrease. For Nile Red its excited state dipole moment is greater, which means the excited state energy surface will be lowered when the solvent polarity is increased. This was demonstrated in chapters 3 and 4 from experimental and *ab initio* approaches, respectively. *Ab initio* studies of DMABN and similar molecules also were shown to have excited state dipole moments that are larger in magnitude, thus exhibiting a red-shift upon increasing solvent polarity. In contrast, Betaine 30 was found to blue-shift upon

185

increasing solvent polarity because its excited state dipole moment was less in magnitude than it ground state, thus there was less stabilization occurring as a result of electrostatic attraction.

This solvent-solute interaction is also taken from a more specific perspective. For example, Nile Red and Betaine 30 possess large ground state dipole moments, and for this reason, even before excitation, there will be a larger mole fraction of acetonitrile present in the near vicinity of NR and Betaine 30 than the bulk solution.[2] This was demonstrated for these two molecules in Chapter 3, where it was shown that the λ_{max} would shift non-linearly upon adding more polar solvent to the mixture.

Solute-solvent interactions can be even more specific, such as hydrogen bonds. Hydrogen bonds destroy the observable linear shift of λ_{max} from increasing solvent polarity, and therefore must be taken into account. The TD-DFT of study Betaine 30 in solvents modeled using a polarizable continuum in chapter 5 was found to correlate well with experimental λ_{max} values when using non-hydrogen bonding solvents. However with alcohols and water, the correlation was poor and inclusion of solvent molecules coordinating the phenoxide oxygen was required to reproduce λ_{max} values.

In order to discuss solvatochromism any further, it is necessary to analyze the energies of states and the associated dipole moments. Our first pursuit of quantifying solvatochromism, was determining the difference in dipole moment between the ground and first excited state for Nile Red in chapter 3. The change in dipole moment was determined by plotting the Stokes shift vs. the solvent polarity parameter E_T^N,

where the slope indicates how much the ground and excited state energies have been stabilized by solvent polarity. It was found that the change in dipole moment of Nile Red was 2.81 D ± 0.96 D or 2.38 D ± 0.76 D, depending on which absorption maxima was used to calculate the Stokes shift, this was a dilemma not foreseen. The first peak (2.38 D) used to determine the Stokes shift was the one that red-shifted upon increasing solvent polarity from 530 nm to 551 nm, while the other peak (2.81D) did not change by more than 5 nm. The peak used by Kawski was the one that red-shifted, and there calculation of the change in dipole moment was 2.35 D, which is in agreement with our change in dipole moment when the red-shifting peak is used. However, at this point in time, no comments in literature have been made regarding the role of the solvent insensitive peak, why it is the absolute maximum in non-polar solvents and why it cannot be used in the determination of Stokes Shift. A possible extension of this work could be to carry out the same method of determining the change of dipole moment of Nile Red, but in a solvent range of very low polarity. This could not be done for this thesis because the solvent polarity parameter E_T^N could not be obtained for neat cyclohexane or low polarity solutions due to the limitations of the UV/VIS spectrometer used(cannot measure beyond 900nm). An *ab initio*, TD-DFT study of the solvatochromism of Nile Red was then carried out in chapter 4, to obtain even more detail regarding the effects of solvation on the energy of the ground and excited states. The change in dipole moment from the ground to first excited state was found to be 2.24 D in acetonitrile, which was comparable to our experimental study.[3] The polarizability was found to be very large for NR and could potentially be a reason as to

why previous authors reported high $\Delta\mu$ values. Finally, we attributed most of the red-shift of NR are a direct consequence of the effect of solvent polarity on the excitation, rather than solvent inducing a geometry change, which in turn affects the excitation energy.

Solvatochromism also brought the dual fluorescence in DMABN and NR to attention. It has been suggested that dual fluorescence originates from the emission from two excited state surfaces, being different from each other in both geometry and charge distribution (i.e. dipole moment)[4]. Experimental research suggests one excited state has a similar charge distribution to the ground state and an excitation to its surface results in no red-shift (LE state), while the second excited state surface does experience a red-shift suggesting that a significant change in charge distribution (CT state) does occur. Our TD-DFT study of DMABN and similar donor-acceptor molecules in chapter 6 confirm excitations to two state surfaces that mirror the solvatochromic observations in experiment. However, we did not obtain any excited state geometries that were significantly different from the ground state. In the gas phase, the most allowed excitation for DMABN was to the second excited state surface, while direct excitation to the lowest excited state surface was forbidden. However, with increasing solvent polarity, the second excited state surface for DMABN was lowered enough in energy such that it surpassed the LE state surface. This inversion of states was not observed in our TD-DFT analysis of ABN, DMABE and DMABFE, and is a proposed reason as to why they do not exhibit dual fluorescence (only emit from their LE band). However, our TD-DFT study of Nile Red in chapter 4 shows that excitation of Nile Red exclusively occurs to

the first excited state surface which is of CT character[3]. This would predict no dual fluorescence for Nile Red, and is in contradiction to experimental observations. To resolve this matter, TD-DFT excited state optimizations could be done with the recent advancement in analytical gradients in the Gaussian 09 software;[5] however, the new version of software did not arrive in time (June 2009) to fully pursue this possibility.

To demonstrate applicability, the studies in chapters 5 and 6-8 are directed at optimizing the function of Betaine 30, PBHAs and 6-NO$_2$-BIPS, all of which are solvatochromic. Due to its large sensitivity to solvent polarity, the transition energy of Betaine 30 has been used to create the solvent polarity parameters, E_T^N, which are reported for over 400 solvents.[6] This solvent polarity scale has allowed chemists to select solvents that will optimize the product yield for a chemical reaction, and is not new. However, we were the first to employ TD-DFT techniques to reproduce the E_T^N scale computationally, which would be desirable since no solvents must be purchased or purified. In chapter 5, the excitation energies of Betaine 30 and 45 were successfully predicted in different solvents mimicked by the polarized continuum model (PCM). It was found that the excitation energies were overestimated in non-polar solvents, while underestimated in moderately polar and polar solvents. However, a linear relationship between solvent polarity and the excitation spectra of Betaine 30 could be reproduced, and this allowed the correlation of experimental and theoretical values. Explicitly coordinating solvent molecules to the phenoxide oxygen of Betaine 30 to reproduce a specific interaction (hydrogen bonding) was found to improve the very poor excitation energies in water, methanol and ethanol. A second water molecule was coordinated to

the first molecule (coordinating to Betaine 30), and the inclusion of two explicit solvent molecules was found to improve the excitation energy further. Although the pyridinium moiety of Betaine 30 has been said in the literature to be inaccessible for hydrogen bonding, it would be interesting to investigate whether a small water molecule could coordinate to it with its oxygen. Betaine 30 has been modified to possess tert-butyl and adamantyl substitituents for better solubility in non-polar solvents. The addition of donor and acceptor groups could be investigated to see whether an even larger charge transfer can occur during excitation.

The *cis/trans* abundance of four *para*-N-phenyl-substituted N-phenylbenzohydroxamic acids was successfully found in the gas phase, ethanol and water. Our main purpose was determining the effects of solvation and substitution on the geometry and pK_A of PBHAs, such that they are selective in their chelating abilities with metals. The effects of substitution, solvent, geometry and deprotonation on the excitation energies were all successfully assessed using TD-DFT. Methyl and methoxy substitution (-Me and -OMe) was found to help make the *cis* the more abundant conformer when deprotonated. -Me and -OMe substitution was found to have raised the pK_A of the *cis* conformers, suggesting that these derivatives have higher selectivity in chelation than the unsubstituted acid. NO_2-substitution had a negative effect on the *cis* abundance and thus lowered the pK_A, but the most peculiar observation was found in its absorption spectra. The effects of solvent polarity showed that the –OMe and –Me substituted PBHAs blue-shifted upon increasing polarity while the –NO_2 substituted PBHA red-shifted. This opposite response to solvent polarity by -NO_2 PBHA was due to it

being a stronger acceptor group than the hydroxamic acid. Therefore the HA functional group behaved as a donor. An extension of this project would be to study the chelation of the *cis* conformer to metals, and whether the effects of solvent could enhance or weaken this ability. Furthermore, identification of chelation with the use TD-DFT and the solvatochromic effects with the PBHA-metal complexes could be characterized.

A kinetic study of the effects of polymer environment on the rate of decoloration of 6-NO_2-BIPS was done, in which both an understanding of photochromism and solvatochromism was necessary. It was found that ring-closure occurred more readily in polymers with lower glass transition temperatures and that the addition of plasticizers (lowers the T_g further) could enhance the rate of decoloration even more. The rate of decoloration was linear in polymers that were studied above their T_g, while non-linear for those studied below their T_g. The ring opening of 6-NO_2-BIPS was not studied since it is known to non-linear. The absorption maximum of 6-NO_2-BIPS was found to blue shift when increasing the polarity of the polymer and when it had more freedom of motion. Plasticizers also caused a blue-shift for 6-NO_2-BIPS, whether it was due to increasing the surrounding polarity rather than increasing the mobility could not be concluded. It would be interesting to investigate whether these plasticizers also increased the rate of ring-opening, and by determining this, the origin of the effect of ring-closing may be solved. If the rate of ring-opening also increases with the addition of plasticizers, it could be due to more polymer mobility (rate of coloration would then increase too), rather than polarity or a specific interaction between the polymer or plasticizer and 6-NO_2-BIPS and that would help initiate the mechanism for ring-closure.

9.2 References

1 P. Suppan and N. Ghoneim, *Solvatochromism*, Royal Society of Chemistry, Cambridge, 1997

2 C. Reichardt, *Pure Appl. Chem.*, 2004, 76, 1903-1919

3 P. O. Tuck, R. C. Mawhinney and M. Rappon, *Phys. Chem. Chem. Phys.*, 2009, 11, 4471-4480

4 Z. R. Grabowski, K. Rotkiewicz and W. Rettig, *Chem. Rev.*, 2003, 103, 3899-4031

5 M. J. Frisch, G. W. Trucks, H. B. Schlegel, G. E. Scuseria, M. A. Robb, J. R. Cheeseman, J. A. Montgomery, T. V. Jr., K. N. Kudin, J. C. Burant, J. M. Millam, S. S. Iyengar, J. Tomasi, V. Barone, B. Mennucci, M. Cossi, G. Scalmani, N. Rega, G. A. Petersson, H. Nakatsuji, M. Hada, M. Ehara, K. Toyota, R. Fukuda, J. Hasegawa, M. Ishida, T. Nakajima, Y. Honda, O. Kitao, H. Nakai, M. Klene, X. Li, J. E. Knox, H. P. Hratchian, J. B. Cross, V. Bakken, C. Adamo, J. Jaramillo, R. Gomperts, R. E. Stratmann, O. Yazyev, A. J. Austin, R. Cammi, C. Pomelli, J. W. Ochterski, P. Y. Ayala, K. Morokuma, G. A. Voth, P. Salvador, J. J. Dannenberg, V. G. Zakrzewski, S. Dapprich, A. D. Daniels, M. C. Strain, O. Farkas, D. K. Malick, A. D. Rabuck, K. Raghavachari, J. B. Foresman, J. V. Ortiz, Q. Cui, A. G. Baboul, S. Clifford, J. Cioslowski, B. B. Stefanov, G. Liu, A. Liashenko, P. Piskorz, I. Komaromi, R. L. Martin, D. J. Fox, T. Keith, M. A. Al-Laham, C. Y. Peng, A. Nanayakkara, M. Challacombe, P. M. W. Gill, B. Johnson, W. Chen, M. W. Wong, C. Gonzalez and a. J. A. Pople, Gaussian 09 (Revision A1), Gaussian, Inc., Wallingford, CT, 2009

6 C. Reichardt, *Solvents and Solvent Effects in Organic Chemistry*, WILEY-WCH, Weinheim, 2003